The Chauffeair
A Thin-Haul Air Taxi

Final Report

Version 2.0
Publication Date: January 29, 2019

by

Group - III
Faculty of Aerospace Engineering

Tutor:	Dr.Ir.Roelof Vos	
Coaches:	Ir.Olaf Stroosma	
	Ir.Gabriel Gonzalez Saiz	
Team members:	Thomas Billet	4210921
	Stan Boekweit	4358740
	Terence Celestina	1524658
	Ruben Forkink	4350146
	Martin Georgiev	4436237
	Pieter Griffioen	4377974
	Sumant Malekar	4374762
	Haroun Saâïd	4292154
	Robel Solomon	4034767
	Roel Thijssen	4439112
	Olivier Witteman	4295579

TU Delft

Executive Summary

The Chauffeair is a hybrid electric thin-haul aircraft which aims to become an important actor in the thin-haul aircraft market. The goal is to have the aircraft certified by 2025. The aircraft will aim to have low operating costs and provide the client with a comfortable flight experience. This is summarized by the following mission need statement (MNS).

"Provide an economically feasible thin-haul transport for operators while ensuring a comfortable passenger experience."

Project Objective

The mission need statement describes how the aircraft must perform and for what purpose it is being designed. The objective of the Design Synthesis Exercise is then best expressed in the following project statement: **"Impress the jury of the symposium and the AIAA with the design of a comfortable and cost-efficient aircraft, that is both innovative and attractive to operators, by 11 students in 10 weeks."**.

Functional Logic Diagrams

A functional flow diagram (FFD) and functional breakdown structure (FBS) have been created in order to obtain a clear understanding of the functions the aircraft must perform and how these will be accomplished. The FFD is a chronological flow of actions whilst the FBS is independent of time and organizes the actions by functionality.

Requirements Analysis

Before designing the aircraft at all, the requirements are analyzed. From these requirements, user requirements can be identified. User requirements have a big influence on the design and are always taken into considerations. Additionally from the requirements, sub-system requirements flow down. These sub-system requirements are noted and displayed.

Risk Assessment

In this section, many different risks are considered, ranging from technical risks to schedule & cost risks. Each of those risks are given a score of likelihood and impact, from one to five. The impact of these risks are analyzed and the critical risks are mitigated. The most critical risks discovered are: "Material selection errors", "Defining incorrect requirements, communications and radio failures" and "Primary engine failure".

Market Analysis

A market analysis is performed in order to obtain knowledge what criteria are to be considered in the design of the aircraft and how important the client deems each aspect. This analysis is performed, assuming a mission range of 135 nautical mile and a ground speed of 180 knots. Aircraft used for similar causes, as the Cirrus SR22 has an average operating cost of $ 375 per flight hour. It is thus desired to make the aircraft design close (or even lower) than this operating cost.

Summary of Trade-off

At the start of the project, many different aircraft designs have been considered. A trade-off has been set up to choose 3 potential designs that have subsequently been analyzed more thoroughly before choosing a final design. The 3 aircraft contestants are: a fully electric design, having a MTOW of 5300 kg, a T-tail and an aspect ratio of 8.5; a fuel design, having a MTOW of 1750 kg, conventional tail, one engine mounted at the fuselage and an aspect ratio of 8.5; a hybrid design, having a MTOW of 2280 kg, a conventional tail, two engines (one on each wing) with 2 secondary engines at the aircrafts wingtips and an effective aspect ratio of 10. According to the project and mission need statements, the hybrid design is deemed most promising and is chosen after an Analytic Hierarchy Process (AHP) trade-off method.

Design Methodology

The method used to create the main design parameters is created, using two different methods, one provided by the supervising professor and one created by the team. The method performs preliminary class I and II weight estimates along with calculations related to the specific design that has been chosen after the trade-off. Iterations are implemented to increase the level of accuracy of the calculations and add consistency to the code architecture. This method extracts a design space and an optimal point, and accordingly, displays the optimal wing area for the design. Furthermore, a serial parallel hybrid electric power train has been chosen. This leads to a MTOW of 1440 kg, a wingspan of 9.8 m, a geometric aspect ratio of 10 and a wing surface area of 9.5 m^2. Subsequently, a sensitivity analysis is performed on the method by changing some inputs. The variables that are most significantly affected are: MTOW, range, C_{D0} and dC_{Lmax}. If the cruise speed is decreased by 10%, for example, the previous values change by: -13%, 36%, 2% and -1% respectively.

Powertrain

The power train is based on the amount of power that is needed to perform the mission of the aircraft. Two main reciprocating engines with counter rotating tip propellers (primary propulsion) are added on the wingtip and a four distributed electric propellers (secondary propulsion) at the leading edge of the wing, in front of the aircraft flaps. The tip mounted reduce lift-induced drag obtained by wing vortices. The reciprocating engines also generate energy for the electric propellers. The secondary propulsion is used for take-off and landing. These distributed propellers improve the aerodynamics on the high-lift devices, to increase the maximum obtainable lift coefficient during these flight phases. The available power at aeropropulsive level is 180 kW, of which 150 kW primary and 30kW secondary

propulsion. The total available energy of the batteries accounts for 20 kWh and the available power of the electromotors, when put in generation mode, equals 5kW per motor, or 20 kW in total. The motor driving the main propellers was chosen to be the Lycoming O-360-series together with the Helix H50V propellers. Regarding the secondary propulsion, the U15 KV100 electromotors with paired motor controller and 40-inch propellers were deemed appropriate.
The aircraft hardware and software architecture contains extended diagrams on the software interfaces, hardware interfaces, electrical connections, data handling and communication flows.

Aerodynamic Design

The aerodynamic design has mainly been analyzed in XFLR5. Different airfoils have been considered, namely: the NACA 2412, NACA 64215 and the NACA 23018. The NACA 2412 has been chosen based on its aerodynamic properties. High lift devices are put on the airfoil, namely trailing edge flaps with a 0.3 flap-to-chord ratio and a 0.55 flap-to-span ratio, to improve the performance of the aircraft at take-off and landing. This provides the lift distribution over the entire wing. These values are crucial for the structural analysis of the aircraft and the determination of the load and moment distributions along the wing box and the fuselage.

Performance

Different performance parameters are analyzed such, as maximum rate of climb and minimum turn radius, which equal 9.5 m/s and 178 m, respectively. These values are consistent and competitive to reference aircraft. The reference mission requirement (flying a range of 250 km in 45 minutes) is exactly met. On the other hand, the sizing mission range is easily reached. The take-off distance is estimated to be 500 m, while the landing distance is 600 m. The service ceiling and absolute ceiling of the aircraft are approximately 3660 m and 3880 m respectively.

Control & Stability

To design for the controllability of the aircraft, control surfaces are sized. Control surfaces like aileron on the wing, the empennage on the fuselage, help with roll, yaw and pitch maneuvers during the flight. The aileron is designed with dynamic equations and a length of 1.09 m is obtained. For the empennage, the horizontal and vertical tail are determined after the 1.5 class estimates. The CG excursion and scissor plots are determined for the sizing of the horizontal tail. The wing position over the fuselage (36 % of fuselage length) and the center of gravity excursions over the mean aerodynamic chord is also determined with the help of those plots. The values obtained are verified by designing the landing gear and seeing if the design would be able function. The vertical stabilizer was sized based on the main requirement of stabilizing the aircraft after an engine failure. A rudder size of 35 % of the vertical tail chord is developed. Finally, the choice for fly-by-wire actuation system is made over the manual mechanical actuation, as it is more advantageous for system mass, redundancy , ease of operation and especially a fully redundant system ready for the future pilotless aircraft. The control derivatives were all obtained using the DATCOM made by the US Air Force. These values were used to analyze the different eigenmotions the aircraft will be exposed to. This gave a half amplitude time of 0.0035, 0.52, 0.02, 0.1, 1.12 for short period, phugoid, aperiodic roll, dutch roll and spiral motions respectively.

	Pilot visibility (angle)	Chair dim (width x length)	Wing span (m)	Fuselage length (m)	Cabin dim (w x h)
Results	17	0.5 x 0.6	9.5	8.7	1.4 x 1.7

	Horizontal tail (m)	Vertical tail (m)	Propellor clearance (\degree)	Scrape angle (\degree)
Results	3.4	2.5	17	15

Aircraft Geometry

Catia models were created for the interior and exterior layout of the aircraft. The cabin layout is also designed with the following configuration : 1 pilot seat in the cockpit and four passengers facing one another in the passenger cabin. The dimensions of the geometry are mentioned in the

Structures

The material of the aircraft was chosen to be Aluminum 6061-T6 because of its low density and high strength properties. The wing box and the fuselage were then structurally analyzed with the idealization (boom) methods. The boom areas and their pitch were assumed constant for both, wingbox and fuselage, while performing structural analysis. The boom areas were supplied by the loads from the aerodynamic loads and stress analysis was determined over the structures. Based on the Von mises failure criteria, the final boom area were altered to satisfy the loads and an average boom area was used through out.

This resulted in determining maximum stresses and failure locations at various different cross-sections along the entire structures and optimize the reinforcement of these sections through the use of ribs, stringers, spars and booms.

Cost

A thorough cost analysis has been made considering all the different costs related to the production and operation of the aircraft. Parameters such as "Man hours", "Certification", "Quality control", "Engineering", were taken into account. An operational cost of $ 282/hour was found with a break-even time of 5 years.

Sustainability

Sustainability analysis is the consideration of multiple aspects contributing to the aircraft's environmental impact, such as the effect of excessive materials, waste, noise and other resources. These aspects have been considered and the aircraft design has, as such, been altered to make it as sustainable as practicably possible.

Aircraft Production and Operations

The manufacturing plan was inspired from the one of a Boeing 777: a U shaped modular assembly line. The main structure will be assembled in one single facility while the smaller components can be manufactured at other factories/locations. A Reliability, Availability Maintainability and Safety (RAMS) analysis was also preformed. Logistics wise, the ground support necessities and operations are defined and analyzed.

Post-DSE activities

The Post DSE activities section describes the steps that will be taken from the symposium all the way up to the end of life of a Chauffeair aircraft. The first phase is the completion of the final design, with CAD drawings and detailed design of all subsystems among others. After that comes the production and distribution phase along with certification. The next phase describes the actual operation of the aircraft and finishes with end of life solutions.

Compliance Matrix

The compliance matrix section includes a table where an overview of all the requirements and their compliance are included.

Conclusion

The aircraft fulfills the mission need statement and all but two requirements. These requirements are not necessarily unattainable, they just have not been investigated properly. **THA-REG-PER-04** and **THA-REG-DEC05** were not analyzed since it is beyond the scope of the conceptual design.

Contents

List of Abbreviations

AIAA	American Institute of Aeronautics and Astronautics
AER	Aerodynamics
AHP	Analytic Hierarchy Process
APU	Auxiliary Power Unit
AvGas	Aviation Gas
AWG	American Wire Gauge
BSc	Bachelor of Science
CAD	Computer Aided Design
CFD	Computational Fluid Dynamics
CFR	Code of Federal Regulations
C.G.	Center of Gravity
CON	Control
CON	Construction
Conv.	Conventional
CST	Cost
DAPCA-IV	Development and Procurement Cost of Aircraft
DC	Direct Current
DEC	Design & Construction
DES	Design Requirement
DSE	Design & Synthesis Exercise
EASA	European Aviation Safety Agency
FAA	Federal Aviation Administration
FBS	Functional Breakdown Structure
FFD	Functional Flow Diagram
FEM	Functional Element Method
GEN	General
HLD	High Lift Devices
HP	High Power
I	Severity of Impact
IATA	International Air Transport Association
ISA	International Standard Atmosphere
L	Likelihood of Occurrence
L/D	Lift-to-Drag Ratio
LE	Leading Edge
LEG	Legal
LOO	Likelihood of Occurrence
MAC	Mean Aerodynamic Chord
MNS	Mission Need Statement
MTOW	Maximum Takeoff Weight
NACA	National Advisory Committee for Aeronautics
OEW	Operational Empty Weight
PID	Proportional Integral Derivative
PER	Flight Performance
PA	Power Available
PR	Power Required
PWR	Power
QDT	Quality Discount Factor
RAMS	Reliability, Availability, Maintainability and Safety
REF	Reference Mission
REG	Regulatory
RIS	Risk
ROC	Rate of Climb
ROD	Rate of Descent
SAF	Safety
SWOT	Strenghts, Weaknesses, Opportunities, Threats
SCH	Schedule
SI	Système international
SIZ	Sizing
SPOF	Single Point of Failure
SPPH	Series Parallel Partial Hybrid
SUB	Subsystem
SUS	Sustainability
STR	Structures
TBD	To Be Determined
TE	Trailing Edge
THA	Thin-Haul Aircraft
TRL	Technological Readiness Level
TU Delft	Delft University of Technology
USA	United States of America
USD	United States Dollars
V-A	Maneuvering Speed
V-C	Design Cruise Speed
V-D	Design Dive Speed
V-S	Stall Speed
VFR	Visual Flight Rules

1 Introduction

The transportation of a small amount of people over a short distance, has been proven in the past to be unprofitable due to a combination of high operating cost and the low demand [1]. Notwithstanding other methods of transportation have mainly become saturated, for example, getting out of Los Angeles by car during peak hour can take quite some time[1]. A market analysis shows that the demand for quick travel over short distances for business travelers and wealthy people is increasing [2]. They do not want to be stuck in traffic for hours, so they can afford to take a small air-taxi to fly over the traffic and save a lot of time. Therefore, the gap in the market is to have a short range aircraft that can carry 2-6 passengers fairly quickly. This small aircraft can bypass the big regional jets, since it can use most airstrips, whilst larger aircraft are limited as they can only land at certain large airports.

This report is preceded by the mid-term report [3] completed to come to one final design concept. Further back in the design process, a market analysis was performed, the requirements were discussed, a work breakdown of the aircraft was developed and an extensive risk analysis was made. This was done to ensure that during the final design phase, discussed in this report, can be done smoothly without running into any problems that could have been avoided.

This report starts with the design concept from the Midterm report [3] and discusses how this was developed to end up at the final design. The report is carefully structured in order to cover the full design process. Chapter 2 first discussed the project objective which is followed by the functional logic diagrams in Chapter 3. Chapter 4 discusses the requirements and Chapter 5 elaborates on the sustainable development strategy. The extensive Risk Assessment from [3] is then extended in Chapter 6 to ensure that new risks are included, analyzed and correctly mitigated. Chapter 7 then discusses the market analysis which was performed after which the trade-off is briefly touched upon in Chapter 8 in order to get to a final design concept. Chapter 9 then discusses how this concept will be further developed to a final design using a code, which is explained in this chapter. Chapters and 11 discuss the vehicle architecture and the powertrain of the aircraft. Chapter 12 will discuss the design's aerodynamic properties and Chapter 13 will elaborate on the aircraft's performance. This is followed by a discussion of the control and stability characteristics in Chapter 14 and the aircraft's geometry in Chapter 15. Chapter 16 contains a structural analysis and a cost analysis is made in Chapter 17. Chapter 18 will explain the aircraft's production and operation aspects. Moreover, Chapter 19 contains a preview of the activities that still have to be completed post DSE. Lastly, a compliance matrix of the design with the requirements is shown in Chapter 20 after which the conclusion is presented in Chapter 21.

[1] BBC News (23 November 2016). In *Thanksgiving traffic jam in Los Angeles is 'most epic'*. Retrieved from `https://www.bbc.com/news/world-us-canada-38083341` Accessed on January 22, 2019

2

Project Objectives

The project statement is stated as follows: **"Impress the jury of the symposium and the AIAA with the design of a comfortable and cost-efficient aircraft, that is both innovative and attractive to operators, by 11 students in 10 weeks."**[4]

This objective can be divided into two parts. Firstly, there is an academic objective: impressing the jury of the symposium and the main stakeholder by demonstrating all project management, systems engineering and aerospace engineering specific skills acquired over the course of the TU Delft Bachelor of Aerospace Engineering. Secondly, there is a specific objective related to the competition: impressing the jury of the AIAA with an innovative design of a thin-haul aircraft that is comfortable for passengers and cost-effective for operators. All the stakeholders needs, at the academic institution, at the AIAA and eventually also at the operator level, must be satisfied.

To achieve this it is important to formulate what the underlying objectives and requirements that will contribute towards the final goal are. The application of the aircraft is novel, in that it serves thin-haul flight routes. In essence, this comes down to a combination of short-haul and low-volume routes. Hence, it does not make much sense to use conventional short-haul aircraft as its size will be too large for the application. Furthermore, most reference aircraft in the light category have a range that substantially exceeds the required range. Hence, for this type of routes it can be concluded that there is a functional deficiency in existing aircraft types and therefore, it's sensible to introduce a new concept. Additionally, there's a market development of growing demand for air taxis. It would be beneficial if the designed aircraft is able to fulfill this function.

Taking more of the requirements into consideration, it can be concluded that there is a stakeholder demand for a relatively quiet aircraft, as it shall comply with relatively strict noise regulations, as well as an emphasis on direct and indirect operational costs and safety.

3

Functional Logic Diagrams

In this chapter the functional logic diagrams will be shown. Section 3.1 and Section 3.2 present the functional flow diagram (FFD) and the functional breakdown structure (FBS) respectively. The layout and the thought process used to create them will be explained in both of the sections.

3.1. Functional Flow Diagram

The FFD describes the flow of functions that system or product should deliver during their cycle life. The FFD did not change much with respect to the base line report [2], as the function of a hybrid electric, conventional or full electric aircraft does not differ much from each other. The functions or regulations they must comply with are very similar. The general flow starts from the manufacturing of the aircraft and then continues to pre-flight operational phase, flight operations phase, post-flight operations phase and lastly the end-of-life phase. The end-of-life phase does not always come right after the post-flight operational phase. This final phase is only initiated if the programmed life cycle of the aircraft is coming to its end. Furthermore, the yellow blocks are used to describe emergency operations, e.g. if the pilot notices significant exterior damage on the aircraft during visual inspection, the aircraft will have to go to a maintenance centre and be repaired. The FFD is shown in Figure 3.1 to Figure 3.7

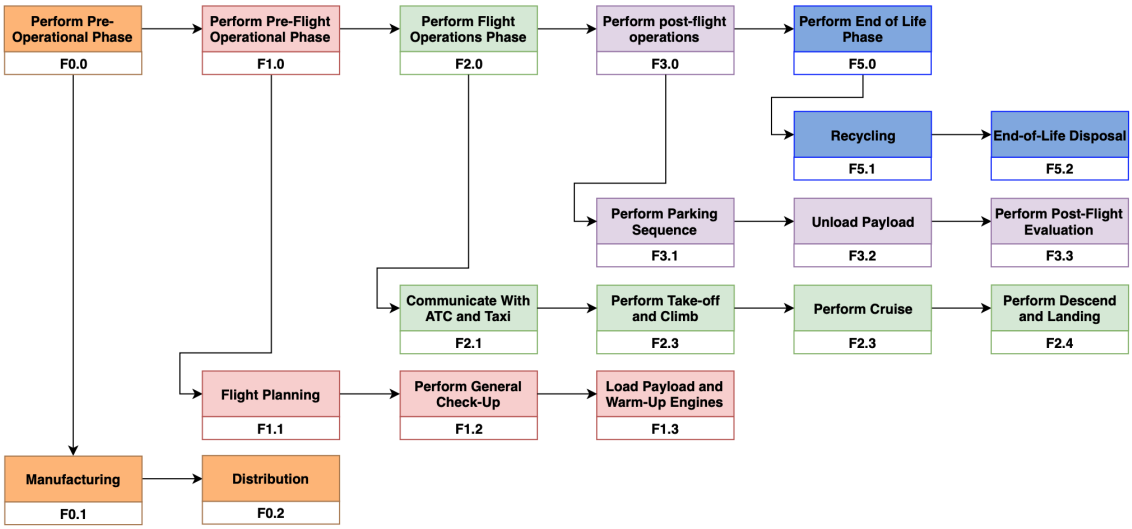

Figure 3.1: The top two levels of the functional flow diagram

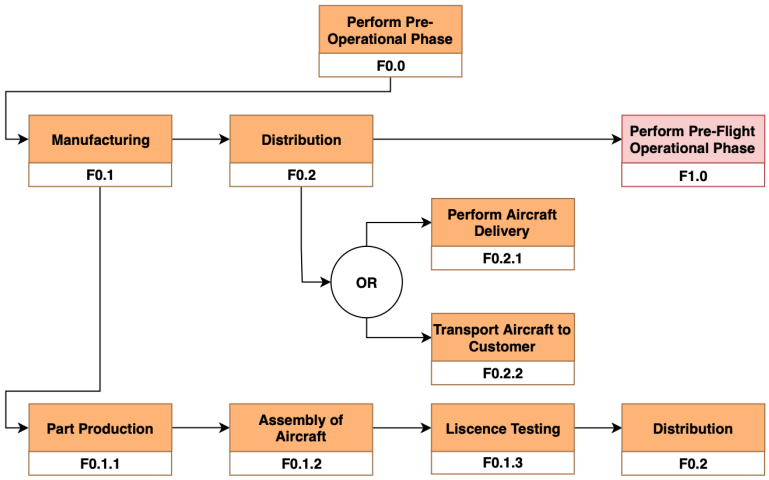

Figure 3.2: Functional flow diagram for phase zero of the five main phases

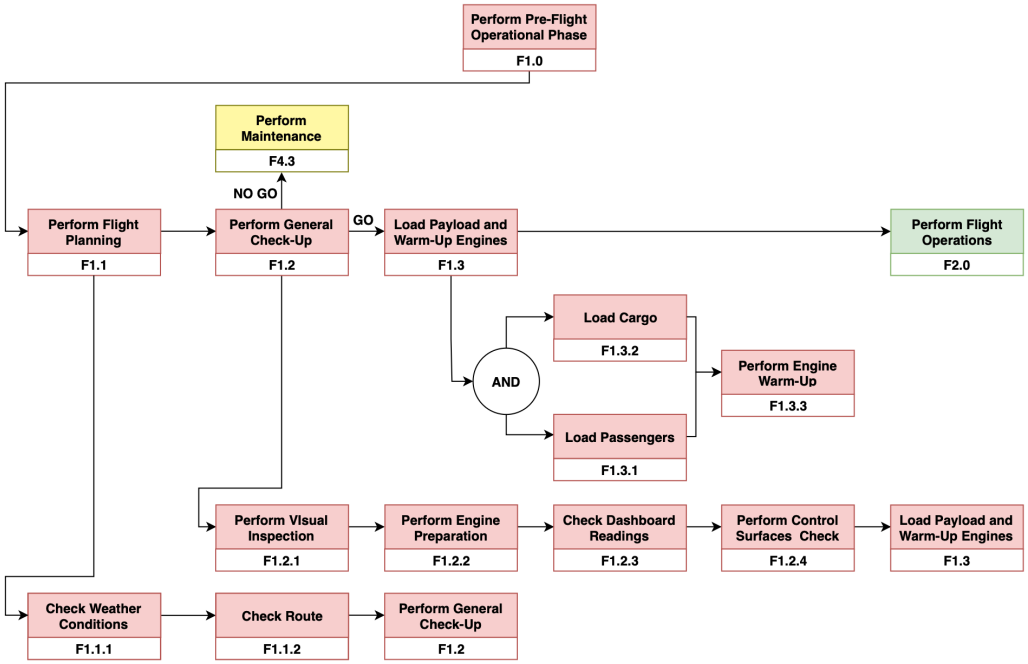

Figure 3.3: Functional flow diagram for phase one of the five main phases

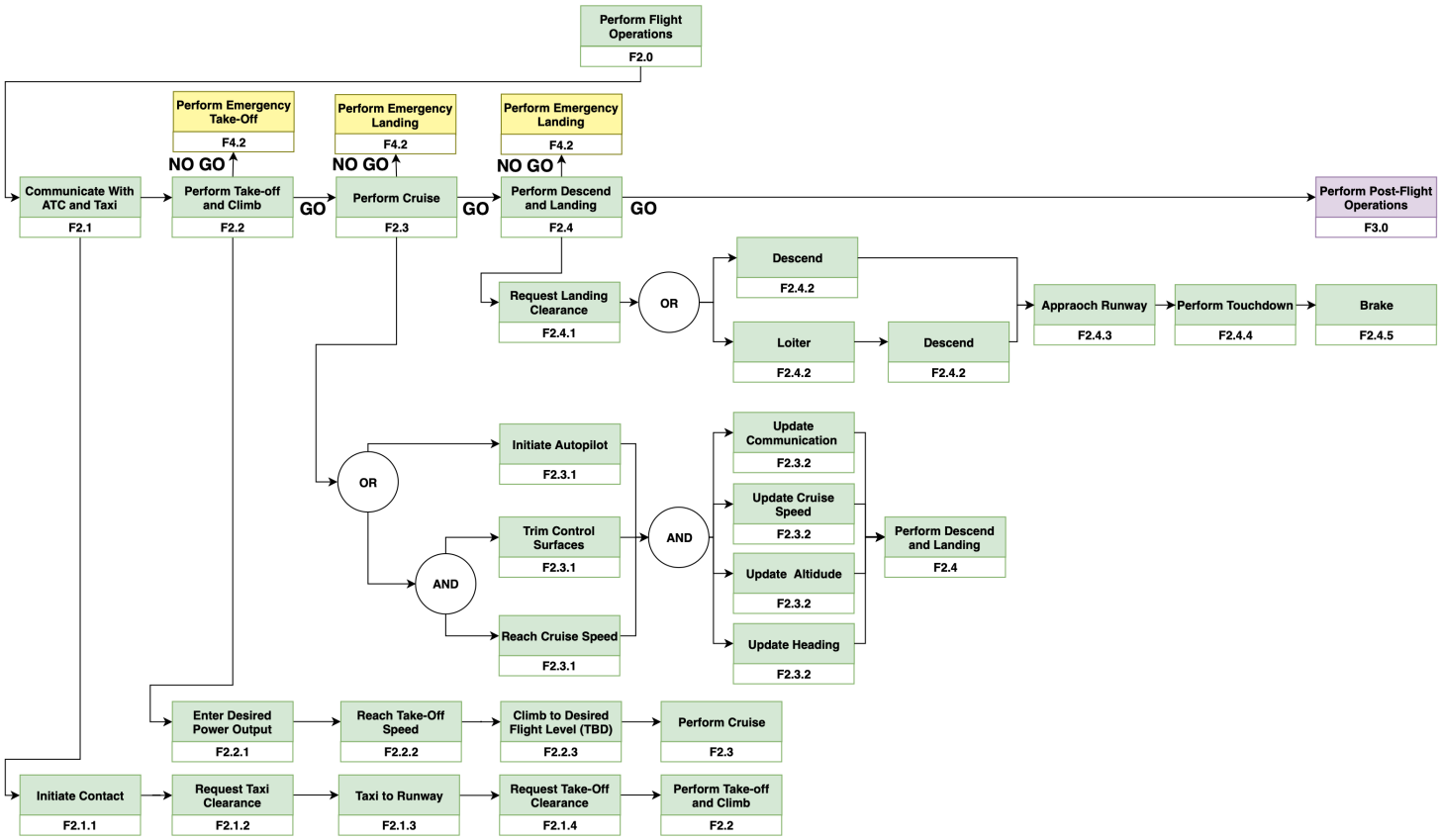

Figure 3.4: Functional flow diagram for phase two of the five main phases

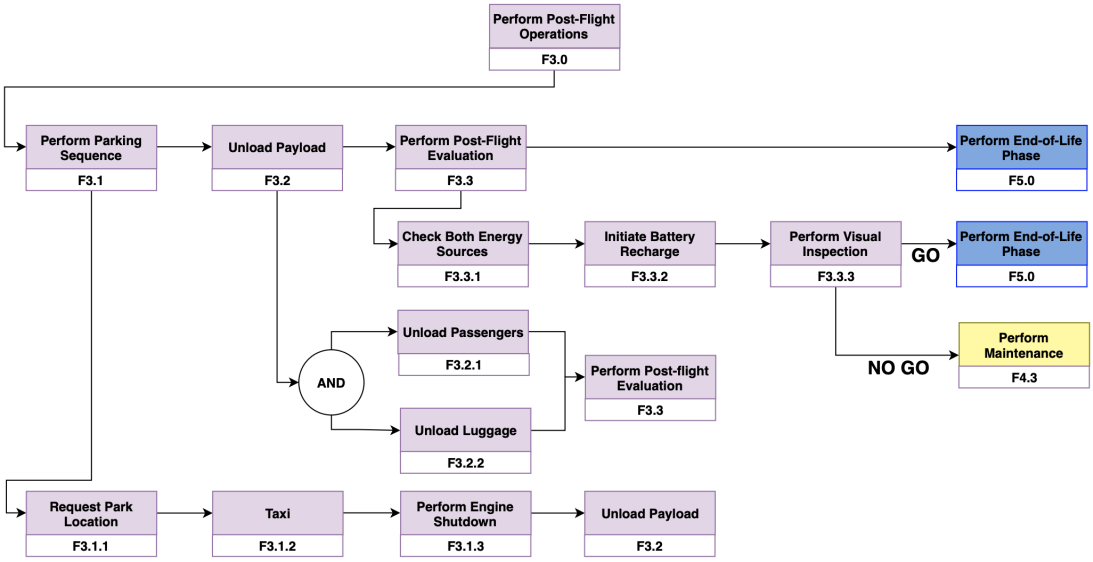

Figure 3.5: Functional flow diagram for phase three of the five main phases

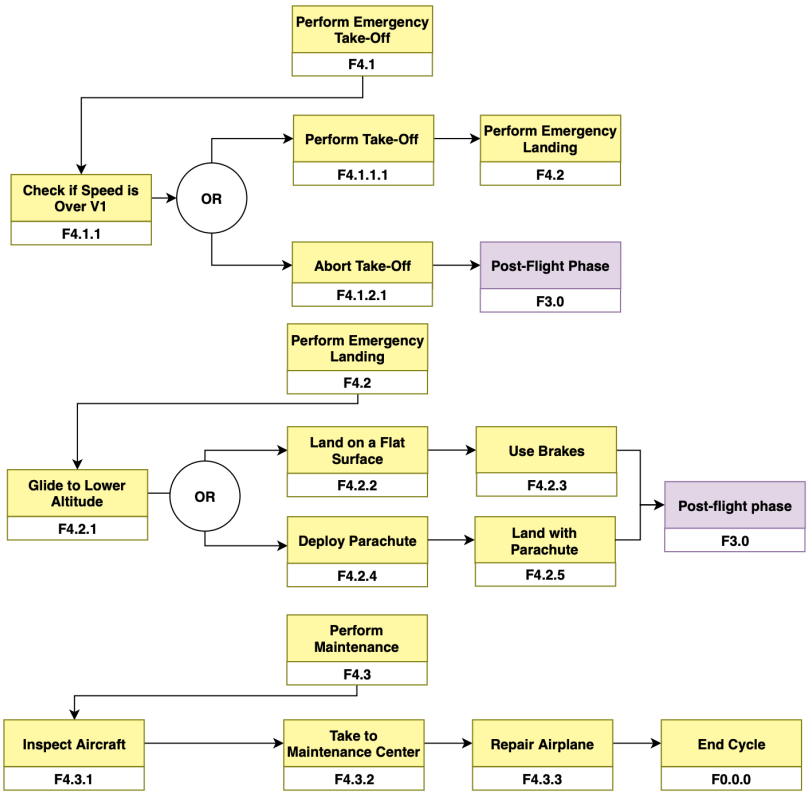

Figure 3.6: Functional Flow Diagram for phase four of the five main phases

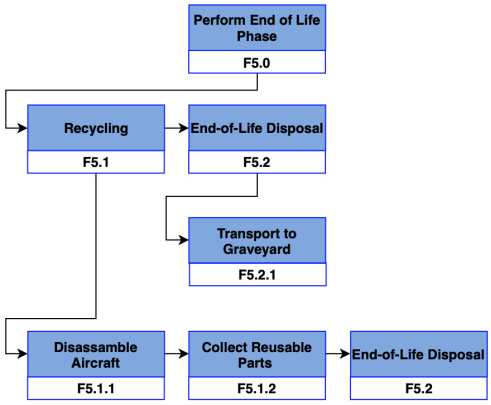

Figure 3.7: Functional Flow Diagram for phase five of the five main phases

3.2. Functional Breakdown Structure

After the FFD, the FBS can be created. The FBS together with the FFD make up the functional logic diagrams. The FFD is expressed chronologically, whilst the FBS describes the breakdown of all the functional blocks. It provides an overview of the actions to be taken by the product. The FBS shown in Figure 3.8 is detailed up to 4 levels deep, while the FFD only goes up to 3. The aircraft shall be providing power from engine start up until engine shut down. The provided power function is indicated at F1.3.3.1, this function remains active during the entirety of the mission. This is also true for functions like lift, control and providing space for payload. Adding generic functions at every phase is considered redundant and therefore not repeated.

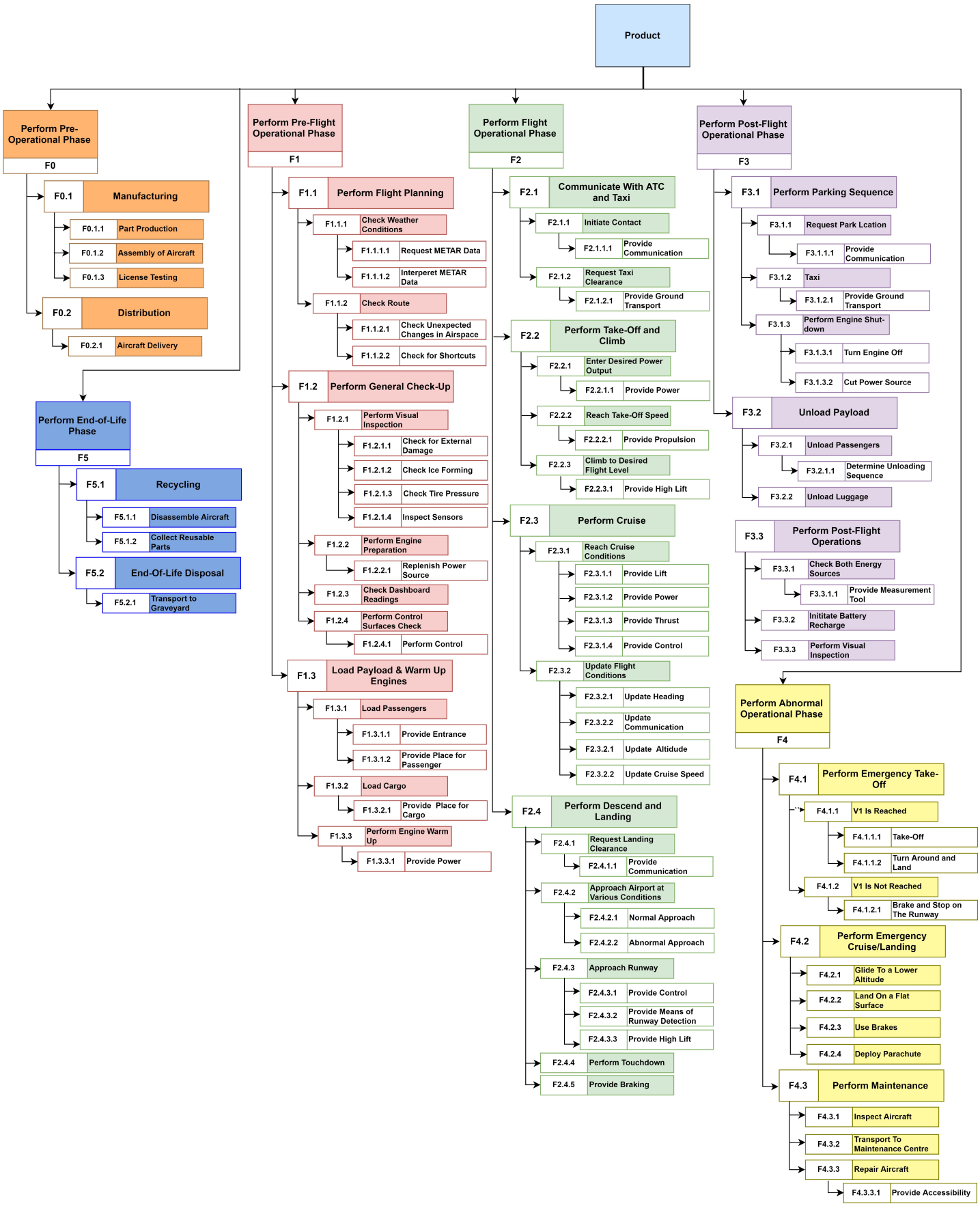

Figure 3.8: Functional breakdown structure of the product

4

Requirements Analysis

This chapter is all about the requirements, it starts with the mission analysis in Section 4.1. Then Section 4.2 and Section 4.3 talk about the user/stakeholders requirements and sub-system requirements.

4.1. Mission Profile

The general mission profile can be found below in Figure 4.1. There are two kinds of mission [1]. The first one concerns the phases climb (3), cruise (4) and descent (5a) and has a range of 135 nmi (250 km) and to do those phases in 45 minutes. This mission is called the reference mission. The reference mission is done at 50% payload.

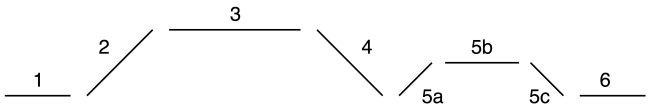

Figure 4.1: Mission Profile overview (1) take off (2) climb (3) cruise (4) descent (5a) diversion climb (5b) diversion cruise (5c) diversion descent and (6) landing

The second mission, the sizing mission, has the same profile as in Figure 4.1, but then with 100% payload and a range of 250 nmi (463 km). For this mission there is no time requirement.

4.2. General Requirements

Table 4.1 until 4.5 are all General requirements of the aircraft with their verification method and their origin. These requirements are from tall the different stakeholders. Which are mainly the AIAA, CFR and the passengers themselves. Some requirements flow down from one another or are taken from the mission analysis (Section 4.1).

Table 4.1: Design requirements

Identifier	Requirement	Verification	Source
THA-DES-GEN-01	The vehicle shall be an aircraft.	Analysis	DSE
THA-DES-GEN-02	The aircraft shall be able to carry a one pilot crew of 82 kg (180 lbs).	Analysis	AIAA
THA-DES-GEN-03	The aircraft shall be capable of loitering for 45 minutes.	Analysis	AIAA
THA-DES-GEN-04	The aircraft shall be able to takeoff within 2500 ft over a 50 ft obstacle.	Analysis	AIAA
THA-DES-GEN-05	The aircraft shall be able to land within 2500 ft over a 50 ft obstacle.	Analysis	AIAA
THA-DES-SIZ-01	The aircraft shall have a sizing range of 250 nmi.	Analysis	AIAA
THA-DES-SIZ-02	The aircraft shall be able to carry a four-passenger payload of 363 kg (800 lbs).	Analysis	AIAA
THA-DES-REF-01	The aircraft shall have a reference range of 135 nautical miles.	Analysis	AIAA
THA-DES-REF-02	The aircraft shall be able to carry a four-passenger payload of 182 kg (400 lbs).	Analysis	AIAA
THA-DES-REF-03	The aircraft shall be capable of cruising at 180 kts ground speed.	Analysis	AIAA

Table 4.2: Non-technical constraints

Identifier	Requirement	Verification	Source
THA-CON-SAF-01	If the aircraft has a single engine, the aircraft shall have a full-aircraft parachute.	Inspection	AIAA
THA-CON-CST-01	The direct and indirect operating costs shall be minimized	Analysis	AIAA
THA-CON-LEG-01	The aircraft shall comply with FAA CFR Title 14 Part 23 (airplanes).	Analysis	AIAA
THA-CON-LEG-02	The aircraft shall comply with FAA CFR Title 14 Part 36 Section 301(c).	Analysis	AIAA
THA-CON-SCH-01	The aircraft shall be developed within 10 weeks.	Demonstration	DSE
THA-CON-SCH-02	The aircraft shall enter into service before 2026.	Demonstration	AIAA
THA-CON-RIS-01	All technologies employed on the aircraft shall meet a Technology Readiness Level (TRL) of 7+.	Inspection	AIAA
THA-CON-SUS-01	The noise level of the airplane, measured and corrected as prescribed, shall not exceed 70 dB(A) for airplanes with a maximum takeoff weight larger than 570 kg. For airplanes with a maximum takeoff weight larger than 570 kg, the noise limit increases with the logarithm of the airplane weight at the rate of 10.75 dB(A) per doubling of weight, until the limit of 85 dB(A).	Analysis	CFR 36

Table 4.3: Performance regulations

Identifier	Requirement	Verification	Source
THA-REG-PER-01	The limits for weights and centers of gravity shall provide safe operation of the airplane.	Analysis	CFR 23
THA-REG-PER-02	Following the sudden critical loss of thrust, the airplane shall remain controllable at the calibrated airspeed (TBD).	Analysis	CFR 23
THA-REG-PER-03	The airplane shall have static longitudinal, lateral and directional stability in normal operations.	Analysis	CFR 23
THA-REG-PER-04	The airplane shall have controllable stall characteristics in straight flight, in turning flight and in accelerated turning flight.	Analysis	CFR 23
THA-REG-PER-05	The airplane shall not have a tendency to inadvertently depart controlled flight.	Analysis	CFR 23
THA-REG-PER-06	The airplane shall have controllable longitudinal and directional handling characteristics during taxi operations, during takeoff operations and during landing operations.	Analysis	CFR 23
THA-REG-PER-07	The aircraft shall be able to climb at a gradient of 8.3% at takeoff thrust at sea level with ISA+0 conditions.	Analysis	CFR 23

Table 4.4: Power regulations

Identifier	Requirement	Verification	Source
THA-REG-PWR-01	Each airplane engine and propeller shall be type certificated.	Inspection	CFR 23
THA-REG-PWR-02	The construction of each power plant installation shall account for sufficient clearance of moving parts to other airplane parts and their surroundings.	Inspection	CFR 23
THA-REG-PWR-03	The airplane shall provide safe flight and landing in case of the likely failure of any power plant system, component or accessory.	Analysis	CFR 23
THA-REG-PWR-04	Each fuel system shall be designed and arranged to provide independence between multiple fuel storage and supply systems.	Inspection	CFR 23
THA-REG-PWR-05	The air induction system for each power plant or auxiliary power unit and their accessories shall minimize the ingestion of foreign matter.	Analysis	CFR 23

Table 4.5: Design and construction regulations

Identifier	Requirement	Verification	Source
THA-REG-DEC-01	The landing gear shall be designed to provide stable support and control to the airplane during surface operation.	Analysis	CFR 23
THA-REG-DEC-02	The aircraft shall have a reliable means of stopping the airplane with sufficient kinetic energy absorption to account for landing over a 50 ft obstacle on a 2500 ft runway.	Analysis	CFR 23
THA-REG-DEC-03	With the cabin configured for takeoff or landing, the airplane shall facilitate rapid and safe evacuation of the airplane in conditions likely to occur following an emergency landing, excluding ditching.	Analysis	CFR 23
THA-REG-DEC-04	The aircraft shall have means of egress (openings, exits or emergency exits), that can be readily located and opened from the inside and outside. The means of opening must be simple and obvious and marked inside and outside the airplane.	Inspection	CFR 23
THA-REG-DEC-05	The applicant must account for all airplane design and operational parameters that affect structural loads, strength, durability, and aeroelasticity.	Inspection	CFR 23

4.3. Sub-System Requirements

In this section some sub-system requirements are listed. They describe the requirements the sub-systems have to adhere to in order to ensure a successful design. The requirements are given an unique identifier according to their respective sub-system. They can be seen in Table 4.6.

Table 4.6: Design and construction regulations

Identifier	**Requirement**
THA-SUB-CON-01	The control surfaces should provide moments to comply with all required manoeuvres.
THA-SUB-CON-02	The hydraulics actuator shall deflect the control surfaces during every operation.
THA-SUB-CON-03	The The vertical tail shall stabilize and be able to control the aircraft after one engine fails.
THA-SUB-CON-04	There shall be no single point of failure in the control surface actuation.
THA-SUB-APU-01	The Hardware and Software shall have a triple redundancy to work in case of error.
THA-SUB-APU-02	The de-icing system shall remove ice of the wing such that it is operable to fly under all weather conditions.
THA-SUB-APU-03	The environmental controller shall be able to provide a room temperature of 20°.
THA-SUB-APU-04	The batteries shall have a minimum state of charge equal to 20%.
THA-SUB-APU-05	The fuel pump shall be replaced at every engine overhaul.
THA-SUB-PWR-01	The propulsion shall have a power available of 180 kW.
THA-SUB-PWR-02	The reciprocating engines shall not produce more noise than 85 dB.
THA-SUB-STR-01	The structural integrity of the fuselage shall be able to withstand a load factor of 4.4.
THA-SUB-STR-02	The structural integrity of the wing shall withstand the aerodynamic load factor of 4.4.
THA-SUB-STR-03	The landing gear shall be able to withstand the loading it endures during all types of landings.
THA-SUB-STR-04	The fuel shall fit inside the wing box.
THA-SUB-AER-01	The wing shall be able to provide sufficient lift during all phases of the mission

5

Sustainability and Development Strategy

Sustainability is a crucial aspect in the aerospace industry and therefore in this project as well. Here, discussion on how sustainability is considered when designing the aircraft and how it is of influence on various subsystems and the aircraft as a whole is done.

Mass Sustainability

When designing an aircraft, it is essential to ensure that the mass budget is met and the aircraft does not become too heavy. A small increase in mass of a subsystem quickly leads to a large increase of the MTOW due to the famous snowball effect. In order to ensure this does not happen, at every step in the design phase, the weight of the respective component should be considered. It should be noted that a more compact design does not necessarily lead to a lighter structure and that not only the quality and performance of a subsystem should only be treated, but its weight should also be considered as well. A trade-off between the sustainable use of mass and performance should be done. As an example, the floor material is selected for low density and enough strength to sustain the load applicable to the said floor.

Space Sustainability

It is extremely important that the aircraft is designed in such a way that the internal space is used efficiently. This is necessary in order to reduce the wetted area and hence the drag. In order to achieve this optimal internal space, the inside-out approach will be used. This method uses the procedure for which, all internal parts of the cabin are placed in an efficient matter, after which the outer fuselage is designed. If the the internal configuration is made in an effective way, the internal space will be optimally used and there will be an optimal use of the space. In the case of this aircraft, the space needed to comfortably transport four passengers and one pilot is determined. Subsequently, a compact hull is designed. It should be noted that the cabin is non-pressurized, hence more creative cabin cross sections, such as a square, can be considered that are more effectively used for the available cabin area.

Aerodynamic Sustainability

The aircraft will be designed in such a way that the obtained drag is minimized, while maintaining comfort, reducing space and minimizing material use. This sustainable approach was previously explained in the Chapter 5. Since, the aircraft is designed for subsonic flight, no shock wave weakening is necessary. This means a round nose will be used as it is aerodynamically efficient. Secondly, a trade-off was also made between a retractable and fixed gear where the aerodynamic performance is weighed versus the mass, cost and reliability of both designs. The result of this trade-off showed that the increase in aerodynamic performance does not weigh the higher mass, cost and lower reliability

meaning a non-retractable gear design is used.

Operational Life Duration

The aircraft's lifespan should be long enough to ensure its profitability. Most small aircraft have a operational lifespan of ±40 years[1]), meaning that throughout the design process, thought should be given to the fact that the aircraft is designed to operate for around this period. Important effects such as fatigue was considered when selecting a material to ensure it will last the entire operational life, or could be replaced after a certain amount of cycles. Maximum stress levels could also be reduced in order to ensure that the lifespan of the part or aircraft is further extended. This is done through adjusting the mission profile by for example flying at a lower altitude. This however increases the drag meaning that once again, a thorough trade-off must be done in order to determine the most optimal design.

Environmental Sustainability

The environment is a key part of the requirements in the form of a noise requirements (**THA-CON-SUS-01**). The noise level of the airplane, measured and corrected as specified is not to exceed the level mentioned in the requirement. This can be achieved in several ways. First, the usage of smaller engines, which could limit the aircraft critical phases. Second, Flight at a higher altitude, which could necessitate the use of a pressurized cabin. The noise corresponding to the engine size and flight altitude will be calculated using available models for similar aircraft.

Safety Measures

When designing an aircraft, safety plays an extremely important role. As previously mentioned, no operator will want to fly a plane which is not safe or certified for flight. Hence, it is of extreme importance that a safe design is selected. Safety however comes at a price which is a higher weight. Any safety feature that may be implemented, from a live jacket to an extra engine for redundancy comes with a weight penalty. This weight penalty is once again increase through the snowball effect which is harmful to the performance of the plane. In order to tackle this problem, each safety measure must be weighed against its weight penalty and how necessary it is deemed. It must be noted however that at all times, the design should comply with all safety regulations for it to be certified for flight.

Noise Sustainability

The noise pollution is a key part of the requirements in the form of a noise requirement (**THA-CON-SUS-01**). The noise level of the airplane, measured and corrected as specified is not to exceed the level mentioned in the requirement. This can be achieved in several ways. To ensure passenger com

First, the usage of smaller engines, which could limit the aircraft critical phases. Second, Flight at a higher altitude, which could necessitate the use of a pressurized cabin. The noise corresponding to the engine size and flight altitude will be calculated using available models for similar aircraft.

[1] Airtug. (2018). In *What is the Life Span of a Small Plane?*. Retrieved from `https://airtug.com/blog/life-span-small-plane/` Accessed on November 21, 2018

Environmental Sustainability

All the above measures show that sustainability should be incorporated in order to ensure that an optimal aircraft design is delivered. Not only do all these measures reduce the operating and acquisition cost, drag, material use, fuel consumption; there is also a significant reduce in emission of polluting gasses. The above measures are thus not only a method to ensure technical sustainability, but also ensure the design is environmentally sustainable.

6

Risk Assessment

This chapter discusses the technical risks that are present when designing and operating the aircraft. These risks are explained, analyzed and steps are taken to lower the risk of events that are important for the success of the design in Section 6.1. The aforementioned risks are visualized in a risk map in Section 6.2 and their mitigation is elaborated on in Section 6.3.

6.1. Risks

Potential risks have been identified and split according to three respective categories; technical risks, design risks and cost & schedule risks. After the risks have been split among the mentioned categories, two scales are defined for an event: likelihood of occurrence (L) and severity of impact (I). The likelihood of a risk can be scaled as an event being improbable, very unlikely, unlikely, likely and very likely. On the other hand, impact can be scaled as being negligible, marginal, significant, critical and catastrophic. Each category is assigned a number from 1-5 according to its weight.

Table 6.1: Risk assessment

n°	Risk	Risk Description	L	I
		Technical Risks		
(A)	Primary engine failure	The failure of one of the engines would lead to the compromise of the mission. It has a catastrophic impact as it could endanger the life of passengers and the integrity of the aircraft. Engine failures are usually due to low and bad quality maintenance cycles or a bird strike. Both are very unlikely to occur as thorough maintenance checks can be done and bird strikes are not very common.	3	5
(B)	Failure of secondary propulsors	In the case of a failure of the secondary propulsors, the C_L will drop. The likelihood that all 6 propulsors fail is extremely small and even if this is the case, the C_L will still be high enough to land safely.	2	2
(C)	Battery failure	A failure of the battery will result in a loss of power for the secondary propulsors. This risk is mitigated by ensuring that in the case of a battery failure, the secondary propulsors can still be powered through power from the two primary engines.	3	2
(D)	Failure of retracting secondary propulsion	If the secondary propulsors cannot be retracted, extra drag will be created. This reduces the performance of the aircraft but since it can still perform it's mission, the impact is not very large.	2	2
(E)	Flat tire	The tire of an aircraft can blow during take-off which can result in aborting the take-off, as well as overheating can occur during landing, which could cause fire.	2	2
(F)	Windshield and window cracking	Cracks in window surfaces do not usually appear at once and take time to propagate. Hence the LOO is unlikely. This is a risk that has a marginal impact because it can easily be detected before significant damages or dangerous scenarios occur. Crack occurrence is a common risk in the aerospace industry	3	2
(G)	Cabin heating system failure	If thermal control or thermostats are damaged, the cabin heating system will malfunction or stop functioning altogether. The LOO is very unlikely as it rarely happens and will only affect the comfort of the passenger and pilot but not the functionally of the aircraft hence the impact is marginal.	2	2

Table 6.2: Risk assessment

n°	Risk	Risk Description	L	I
		Technical Risks		
(H)	Avionics failure	Due to instrument failures or dashboard malfunction, these will have a critical impact on the mission and the safety of the passengers. If in flight, this would result in the pilot having to fly VFR, assuming weather conditions are favorable. The likelihood of this happening is very unlikely as flight plans are made in advance and weather is always checked before taking off	2	4
(I)	Communications and radio failure	This would result in dangerous situations when contacting airport towers, authorities and airspace controllers. However, in recent years communication systems have proven very reliable and unlikely to fail. The impact would be critical, especially in take off and landing scenarios. This would require a diversion to the nearest airfield as the mission cannot be continued without a working communication system..	3	5
(J)	De-icing mechanism failure	In cold weather conditions and when flying through clouds, ice will aggregate on the control surface. In case of de-icing failure, lift will decrease and control surfaces may freeze. This is unlikely since in the design measures are taken to ensure de-icing and pre-flight checks are done to ensure proper functionality. The impact is critical and there have been reported flight crashing due to de-icing failures	3	4
(K)	Bad weather	Unpredictable deteriorating weather conditions in flight can be dangerous especially for small thin haul aircraft's. While there have been numerous reports of this occurring it is unlikely with the radar systems currently available. The impact is significant, not so much for flight performance but in case of comfort.	3	3
(L)	On board fire	An on board fire can be catastrophic if it is not extinguished in time and it gets out of hand. A fire could lead to a crash of the plane if the fire destroys critical systems and therefore has catastrophic consequences. The LOO of an on board fire is unlikely but this risk should still be mitigated and further reduced through for example the placement of a fire extinguisher on board.	2	5
(M)	Manufacturing error	As a result of a manufacturing error, it could be possible that the aircraft can no longer execute it's mission. Therefore, it is considering to have quite a large impact on the operation of the plane. However, the aircraft that is being designed is not extremely complex and will mostly consists of parts which are easily made. The LOO of this occurrence is thus relatively small.	2	4
(N)	Metal fatigue	As the aircraft will perform many operational cycles, fatigue may cause the metal on board to weaken as a result of the repeated loads. If this goes unnoticed and no action is taken, this may cause the part to fail. It is therefore important that this risk is avoided by for example performing a walk-around around the plane before each operational cycle and reporting any damages.	2	4
		Schedule & **Cost Risks**		
(O)	Converting units from SI to empirical	Confusing the conversion between SI to empirical units when presenting the final report. The likelihood of occurrence (LOO) is however unlikely since it is a simple conversion. The impact is significant since this would give false design parameters and iteration would need to be done with the correct units.	2	3
(P)	Utilizing a common script	Sharing a common script or excel file with the entire project group instead of having each design group make their own calculations is a risk. The LOO is likely since the project group is under time pressure and can be tempted to share calculating methods. The impact of this is significant, since while the other designs will give incorrect parameters, one design will still be correct and can be continued working on without hindering the schedule.	3	4
(Q)	Loss of a group member	When a group member is not available for the allocated project hours. A member not present has a very unlikely LOO. Group members are all committed to being present and have set personal contingencies to ensure their presence. The impact is critical to the schedule, since it would result in less manpower in the solving of the needed design parameters.	2	4
(R)	Powertrain design error	When designing a propulsion system that requires a complex integration or expensive components. An expensive propulsion system is unlikely, since basic propulsion concepts are available to the group. The impact would be significant to production cost but since there is no precise budget can be negotiated with the client.	4	3

Table 6.3: Risk assessment

n°	Risk	Risk Description	L	I
		Schedule & Cost Risk		
(S)	Material selection error	When delivering a design that would need expensive material to comply with the requirements. This could have a large LOO of consisting of materials that are complex in structure to achieve the payload limit. This could have a critical impact on cost since such material will be expensive. The client might then as for an iteration in terms of design to result in a lower cost.	4	4
(T)	Design certification	In case a design is chosen that might not comply with regulations such as for example emissions. This has very small LOO no matter the chosen design. The impact is marginal to cost, since there is no subsystem that could result in cost penalties.	2	2
		Design Risks		
(U)	Defining incorrect requirements	Omitting crucial requirements or creating un-realizable ones can be a catastrophic risk to the design process and the success of the mission. Requirements being one of the most important building blocks and starting position for the design, making a mistake is very unlikely as a lot of precaution was made when creating and selecting them.	2	5
(V)	Wrong trade-off weights	Applying the wrong weights to certain categories, either too low or too high, will strongly affect the design and the man-hours spent on certain design aspects. This is likely due to the fact that the allocation of weights is qualitative however as the trade-off is very detailed, the impact would be marginal.	5	2
(W)	Wrong trade-off categories	When defining the trade-off, the wrong categories could be selected for choosing and comparing certain aspects of the aircraft. This is unlikely due to the fact that at that point in the project, the group will have a good understanding of the mission and requirements. Help will also be found in the flow diagrams (work and functional) which give a good focus. As the trade-off is made in a spreadsheet, the document is flexible. If spotted early, mistakes will have a small impact on the design and its process as it can easily be corrected. On the long term this could prove problematic and involve a large number of wasted man-hours and delay in the schedule	2	4
(X)	Wing placement error	Making a mistake in the wing configuration (low, high, mid) will have strong influence on the design of the fuselage, the critical load paths, the available space/design of the cabin and other important structural aspects. A mistake in this choice would necessitate a redesign the aircraft from scratch. The likelihood of this is low as there are only 3 options and they all have different reasons to be chosen.	2	5
(Y)	Uncertainty in aero-propulsive interaction	The interaction between the propulsion group and the fuselage is an integral part of one of the concepts to be designed. The fact that the subject is relatively new for many of the group members means that mistakes can easily be made. The impact will be significant as this interaction influences many major design aspects such as wing planform, propulsion group, flight performance and more.	3	3
(Z)	Selecting unfeasible design options	It is possible that during the design selection process, some critical factors are overlooked such that an unfeasible design option is presented to the client. The impact on the operation is catastrophic as this means the project is no longer useful and the plane cannot be further developed. Considering the experience that the group has, having almost completed a BSc in Aerospace Engineering and the expert guidance that is given, this is very improbable.	1	5

6.2. Risk Map

After identifying all the risks in Section 6.1, these are plotted on a risk map shown on the next page. These risks are plotted according to the weights they obtained for both the likelihood of occurrence and the severity of the occurrence. The higher the risk, the more it shifts towards the red area. If an event is located in a red area, there is a very high risk associated with this occurrence. As the you move down and to the left in the risk map, the color becomes more green which is associated with a low risk. The risk map is displayed in Figure 6.1.

6.3. Risk Mitigation

This section explains how the aforementioned risks are mitigated. This can be done through two methods; by either lowering the severity of the consequence or reducing the LOO. This section explains how this is done to ensure that the risk associated with the events are lowered to an acceptable level.

Scheduling Risk

To mitigate the risk in scheduling, the big deliverable will be subdivided into smaller ones. Like this, a better overview of the progress will be visible as the modules are completed and aid can be given accordingly to where there are problems. To ensure that the schedule is not hindered by lack of knowledge in material, an online library will be compiled with all the material from previous study courses that could be needed. Additionally, contact professors will be allocated for each area and their schedule will be monitored in case such help is required.

Risk regarding Cost

The risk due to cost is not very concerning. The propulsion selection and integration could result in a budget overrun if not done carefully. Therefore, extra attention will be given to this aspect. Next to this, the material selection can also cause a budget overrun if too many expensive materials are selected. Nevertheless, the primary concern should remain getting a feasible design no matter the material or production.

Technical Risk

Technical risk mitigation can be effective through the use of a few different strategies. Regular maintenance cycles can help asses risks earlier and undergo corrective actions. This would apply to most components such as the engine, landing gear, window and windshields. Proper flight preparations will also lessen the impact of these risks. This can be done by walk-arounds, the use of a checklist along with pre-flight visual inspections by the pilot.

Structural Risk

This helps with detecting cracks, fatigue and minor exterior damages. Implementing operational safety factors will also allow for mitigation by allowing safety margins before critical scenarios occur. Lastly, extra attention will be given to safety in order to reduce the LOO. For example, a fire extinguisher may be place on board or fire and heat retarded material can be put around critical components in order to reduce the impact of an on board fire.

Design Risk

Design Risk mitigation will be done through the use of careful verification and validation methods. This will be applied to the tools developed and to the requirements themselves, as they are the most critical aspect of the design process. In order to mitigate certain design errors, 3 different concepts are developed. This adds a redundancy/fall back option if one of the design becomes clearly unfeasible. Finally, having two members analyzing the mistakes that could be done

in the design process in a later stage would be a strategic way to mitigate risks. This way, potential bottlenecks and risks can be assessed allowing the group to predict and anticipate if certain designs are worth continuing to work on. After the above mentioned actions, Figure 6.1 is reiterated resulting in a new risk map shown in Figure 6.2.

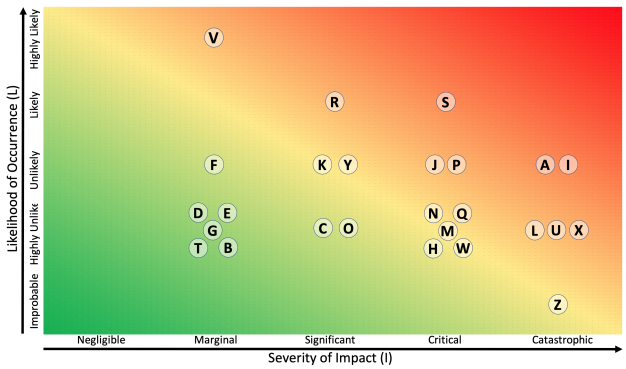

Figure 6.1: Pre-Mitigation Risk Map

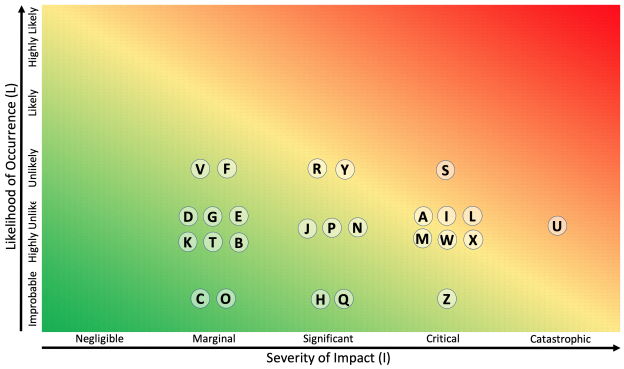

Figure 6.2: Post-Mitigation Risk Map

7

Market Analysis

The market analysis will help further define the missions and operations the air taxi will be undergoing, the typical client profiles it will transport and potential attractive routes. Section 7.1 will identify the market from different points of view. Lastly, Section 7.2 and Section 7.3 analyze the vehicles in the current market and predict the future market respectively.

7.1. Air Taxi Market Segmentation

In order to perform the market segmentation, typical key mission parameters were first taken into account. These consist of the preliminary values for the reference mission range of 135 nmi with an average ground speed of 180 kts. These requirements define the concept of "thin haul" in the case to be studied and the operations that will be supported by the air taxi. A typical client using the air taxi will travel within a range of 135 nmi in approximately an hour and a half.

7.1.1. Demographic Segmentation

The market segmentation was first approached through a demographic angle by identifying a specific customer profile with their respective needs. After thoroughly discussing with the team the disadvantages and malfunctions of modern air travel, the following issues were identified :

- Long waiting times at airports including queues at security, baggage drop off and passenger check in
- Limited choice of departure and arrival airports, involving extra travel time
- Rigid time tables and fluctuating ticket prices

These problems were used to define the needs of a population segment, namely the need for an easily accessible, on demand, cost-friendly and flexible air transport service. The customer would therefore prefer to fly instead of commuting by car or train, indicating the customer does not want to loose time in traffic jams or wants to be dependent on train timetables and delays. Moreover, the client will be looking for additional features an airline cannot offer, such as flexibility on a time and geographical basis. In order to narrow the focus further, the price range for an average ticket are between the price of renting a private jet and the price of taking a last minute business class ticket on a regional airline. According to the Belgium air taxi company "Fly Aeolus", who has been operating with Cirrus SR22 aircraft for the last 10 years in western Europe, the ticket price must remain as low as possible, even if that means reducing slightly

the comfort and user friendly aspect of the air taxi. This is due to the fact that flights are "thin-haul" and passengers are looking for cheap and efficient transportation from a point A to a point B. To support this observation, Fly Aeolus explained that when offering their clients the option to pay an extra 2 euro for a GreenSeat (a symbolic eco-friendly option to offset the carbon emissions during a trip), barely anyone opted to pay the small fee. This indicates that price is a major factor taken into account by clients and must not be underestimated.

This analysis defines our demographic segment which would first of all be mostly business related, as the gain of time, effort and money is a central theme. A typical client values the time they gain by using the air taxi over the money spent purchasing the service. This would therefore mainly apply to CEO's or individuals in managerial positions who need to travel thin-haul on a frequent basis. An important factor to consider is that these individuals are paid significantly by the hour and therefore purchasing an air taxi ticket could end up costing less than spending an hour in a traffic jam or waiting for a delayed flight. Finally, another smaller demographic segment could be made up of wealthy professionals such as artists, athletes or politicians who would fly for similar reasons or for leisure. This analysis is confirmed by a research lead by the American air taxi company "Imagine Air" who estimate that 70% of the customers are business travellers, and only 30% take an air taxi for leisure. Imagine Air used an uniform fleet of Air taxis and operated in eastern coastal states such as North Carolina and Pennsylvania. [1]

7.1.2. Geographic Segmentation

According to the mission, the aircraft will be sold to North American air taxi companies. North American statistical data maps were therefore used to combine different indicators and identify regions and cities that would be more beneficial to the development of an air taxi business model. The first significant map chosen as a reference is an isochrone map of the USA, displaying a time of up to five hours drive from the biggest American cities.[2] This time includes the possible traffic jams that will be encountered by commuters. According to the client segmentation and the reference mission requirements, geographical locations are identified. Clients will either be present in the city centres (represented in blue tones) in Figure 7.1 trying to reach the outer green and non colored limits a 463 km radius, or the other way around. To narrow down the geographical segmentation even more, literature and maps of population concentration, unemployment and economic growth are analyzed, identifying where higher chances of business opportunities lie. It is decided to focus on large companies and find statistics on company headquarter concentration per city. Finally, small regional airports will be used most of the time to pick up and drop off clients. This is due to the fact that they are more accessible, in higher numbers and require lower operational fees, therefore allowing cheaper flights, landing closer to the clients' origin and destination and involving fewer traffic jams and airport waiting lines.

[1] Imagine Air research - On-Demand Air Taxi Mass Market Adoption, accessed on 23-01-19, http://www.nianet.org/ODM/ODM%20Tuesday%20presentations%20Final/14%20Hamilton%20ODM%20Presentation%20ImagineAir.pdf

[2] The Washington Post. (n.d.). In *Leaving town at rush hour? Here's how far you're likely to get from America's largest cities.* Retrieved from https://www.washingtonpost.com/graphics/2017/national/escape-time/?noredirect=on&utm_term=.a05f212b30ab Accessed on November 21, 2018

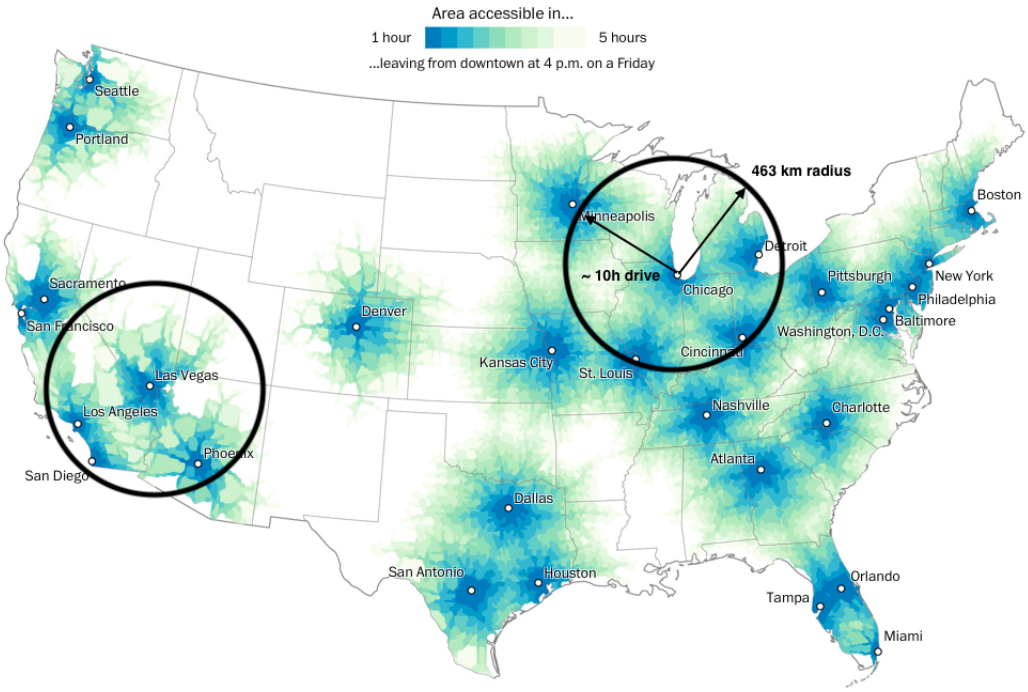

Figure 7.1: Isochrone map of USA commute times by car

Indirect competitors are identified to be regional airlines and charter operators who serve similar routes and destinations to the ones identified previously. These companies, however, offer different prices and services which are not always comparable to an air taxi mission. Direct competitors will be identified as other air taxi operators such as "imagine air," and "skyway air travel." Both these companies use Cirrus SR22's as the reference aircraft. The Cirrus has an average operating cost of 350 to 400 USD per flight from the statistics given by Fly Aeolus. This will be accounted for in the Chapter 17 to remain competitive. In Figure 7.2, a SWOT analysis is made of the air taxi market by analyzing the strength and weaknesses of the service provided, and the opportunities and threats it can encounter.

Figure 7.2: SWOT analysis of air taxi market

7.2. Scheduled Thin Haul Transport and Air Taxi Vehicle Market

It is assumed that a thin-haul aircraft operator or an air taxi operator select their aircraft based on two criteria, the performance of the aircraft and its associated cost which can be divided into operational costs and development costs. In order to analyze and compare the performance of current thin-haul aircraft, Table 7.1 shows a list of aircraft with relevant characteristics. They are a selection of a larger list of aircraft which were identified previously during the development of class I estimation tools. The values of the PA-46, Extra EA-400, the Beachcraft G36 and the Cessna 400 are taken from [5][6] [7][8] respectively.

Table 7.1: Table showing key characteristics of competitor aircraft Conv. = Conventional Aircraft Configuration

	PA-46-310P	**Cirrus SR22**[4]	**Cessna 206**[5]	**Extra EA-400**	**Extra EA-500**[6]	**Mooney M20**[7]	**Beechcraft G36**	**Cessna 400**	**Pipistrel Panthera**[8]	**Pipistrel Panthera**[8]	**Pipistrel Panthera**[8]	**Socata TBM 700**[9]
Pilot [-]	1	1	1	1	1	1	1	1	1	1	1	1
Range [nmi]	1550	1049	730	1100	1600	1100	716	1100	1000	659	216	1730
Purchase Cost [USD th.]	917	540	680	1000	1500	700	815	715	530	746	769	4000
First Flight [yyyy]	1979	2001	1962	1996	2002	1953	1945	2004	2013	2016	2020	1988

Upon analysis of the current air taxi market, the following factors need to be considered Table 7.1; First, the majority of the airplanes are outdated, having been developed in the past century. With the exception of one airplane, the Pipistrel Panthera, all airplanes were developed at least 15 years ago. While there have been some revisions, most of the technology and aircraft designs originate from the previous century. This presents an opportunity, as an aircraft developed in 2018 can incorporate new technologies which improve efficiency.

Upon analysis, a few things stand out in Table 7.1. To begin with, the majority of the airplanes were developed many years ago. With the exception of one airplane, the Pipistrel Panthera, all airplanes were developed at least 15 years ago. While there have been some revisions, most of the technology and aircraft designs originate from the previous century. This presents an opportunity, as an aircraft developed in 2018 can incorporate new technologies which improve efficiency.

Furthermore, it is notable that most airplanes are able to fly a range of at least 1000 nmi. As requirement **THA-REQ-DES-SIZ-01** states[3], the airplane shall be able to fly a minimum range of 250 nmi[1], significantly far less than the 1000 nmi average of the reference airplanes of thin-haul transport. As mentioned in Subsection 7.1.2, there is considerable demand for air travel up to 250 nmi. In the design process, it may therefore be considered to design for a larger range. However, in view of the significant demand for air travel up to 250 nmi, this will not become a requirement. Secondly, this is also another opportunity as airplanes designed to fly up to 1000 nmi will be heavier and more expensive. Designing an airplane for 250 nmi will thus produce a lighter, more efficient and cheaper airplane. Such an airplane could also be utilized for different purposes, such as training.

Looking at the configuration, it can be observed that all reference aircraft use the conventional configuration, but they employ different types of exits. In the table, the label "wing" indicates that the reference aircraft features an over-wing exit which requires the passengers and (the) pilot(s) to step onto the wing. The label "door" means the passengers and (the) pilot(s) enter through a dedicated door which is considered to be more comfortable.

Lastly, it should be noted that there is one competitor aircraft, the Pipistrel Panthera, that offers aviation gas, hybrid and electric versions. The hybrid engine was developed in 2016 and the electric version is expected to be developed by 2020. It must be noted, however, that for both these options, there is a smaller range and a limited payload in the

[4]Cirrus Aircraft. (2018). In *Explore the SR22.* Retrieved from `https://www.cirrusaircraft.com/aircraft/sr22/specifications` Accessed on November 21, 2018

[5]Cessna 206. (2018). In *Jane's by IHS Markit.* Retrieved from `https://janes.ihs.com/Janes/Display/jawa1233-jawa` Accessed on November 21, 2018

[6]EA-500. (2008). In *Extra Aircraft 500.* Retrieved from `https://web.archive.org/web/20080920230551/http://www.extraaircraft.com/media/500.pdf` Accessed on November 21, 2018

[7]Mooney. (2018). In *Mooney M20.* Retrieved from `https://www.mooney.com/aircraft` Accessed on November 21, 2018

[8]Pipistrel. (2018). In *Panthera.* Retrieved from `https://www.pipistrel-usa.com/panthera/` Accessed on November 21, 2018

[9]TBM Daher. (2016). In *TBM 900.* Retrieved from `http://www.tbm.aero/wp-content/uploads/2016/03/2016_TBM-900_SpecsPriceList.pdf` Accessed on November 21, 2018

case of electric propulsion.

7.3. Future Market Predictions

Predicting the future of the air taxi market with exact numbers is difficult at this stage of the development of this fairly new sector. Looking into trends, IATA predicts that the number of air passengers will increase drastically, from 4 billion a year to approximately the double by 2036 [3]. In the US only, they are expecting an annual growth of 2.3 %, leading up to hundred of millions of new passengers every year. This outlines the fact that the current infrastructure and the ways people travel will change. This prediction could suggest an increase of traffic jams around large airports, longer queues at the airports and therefore more time spent when commuting. This would push a certain amount of passengers towards the air taxi business models and increase the demand for this kind of service. With respect to electric and hybrid aircraft, these have already started to create their own emerging market and are expected to gain a lot of traction due to future regulation changes in the transport sector related to the ecological footprint of aircraft. They will also become cheaper alternatives when considering operating costs and the rising prices of fuel in the near future.

[3] IATA, accessed on 23-01-19, https://www.iata.org/pressroom/pr/Pages/2017-10-24-01.aspx

8

Summary of Trade-off

This chapter shortly summarizes the trade-off from the midterm report [3] and includes additional design choices that have been made since. Section 8.1 gives a brief summary of the previous trade-off made and Section 8.2 talk about the additions made to the design in the trade-off and the starting point in this report.

8.1. Synopsis of Previous Trade-off

As discussed in the midterm report [3], the hybrid, high wing, conventional tail design is chosen based on different criteria like, risk, manufacturing cost, operating cost, complexity of design, comfort, emissions, lifespan, noise, speed, range, payload capacity, creativity, ease of maintenance, accessibility, reliability and mass. This is done by using an 'Analytic Hierarchy Process', or AHP method. The first step consists of comparing each criterion with each other to objectively obtain relative weights for each criteria. This is followed by comparing every design option to every criterion in order to obtain the optional design for the mission's needs. This has been done in accordance with the client's desires. The most important criterion of the design are found to be operating cost, accessibility to different airports and designing complexity. The optimal three designs obtained before meeting the clients can be seen in Figure 8.1, Figure 8.2 and Figure 8.3. Initially, the fuel design was chosen, but after meeting the client and doing the trade-off again, with some changed parameters, this design was discarded and a new design was obtained, namely: a hybrid design with a conventional tail, fixed landing gear, 2 primary engines mounted close to the wing root and 2 secondary engines mounted at the wing tips to reduce the effect of vortexes. The power train was decided to be a series-parallel partial hybrid.

8.2. Additions to the Design

After the trade-off done in the mid-term report[3], a few changes were made, namely:

- the primary (main) engines which deliver the required thrust are mounted at the tip of the wing to decrease the noise the passengers experience and thus increasing passenger comfort.
- Four secondary engines (small propellers distributed along the wingspan) acting as high lift devices during take-off and landing have been added to increase the C_{Lmax}. This decreases the required wing surface which is constrained by take-off, and hence decreases operational empty weight. This means less fuel is needed for consumption and less batteries to be used. By decreasing the wing surface, the C_D is slightly decreased, which allows widening and elongating the cabin, increasing the comfort the passengers experience. The high lift devices are folded together and laid onto the wing during cruise to decrease the amount of parasitic drag.

The changes in the design between the midterm and this final phase of the project can be observed in Table 8.1.

Table 8.1: Most important changes in design

	Primary engines	Secondary engines	Powertrain motor controllers
Design at midterm	Close to root	2 (at wing tips)	6
Definite design	Wing tip	4 (distributed along leading edge)	4

As a result of placing the the main engines at the wingtips, the vertical tail plane has to become exceptionally large to ensure controllability during engine failure, a detailed explanation will be given in Section 14.5.

The properties of the final design concept can be observed in Table 8.2.

Table 8.2: Properties of the final design

Type:	Wing location:	Engine type:	Gear:	Powertrain:	Tail:	Cabin:	Pressurized:
Hybrid	High	Piston	Fixed	Parallel-series	Conventional	Rectangular	No

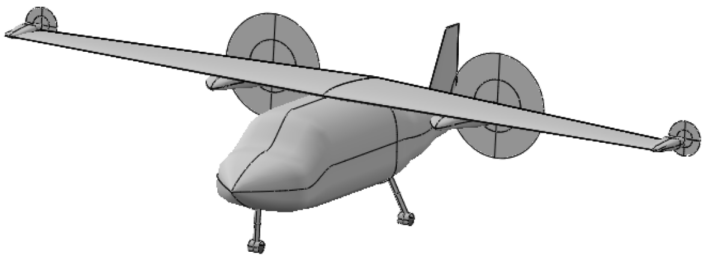

Figure 8.1: Hybrid design

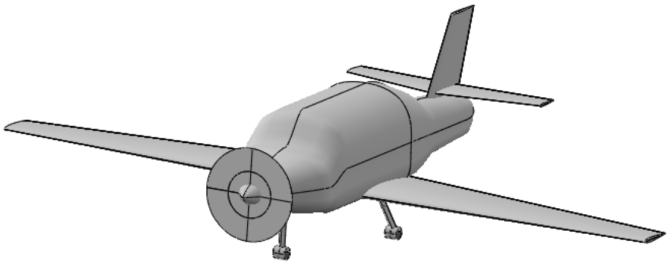

Figure 8.2: Fuel design

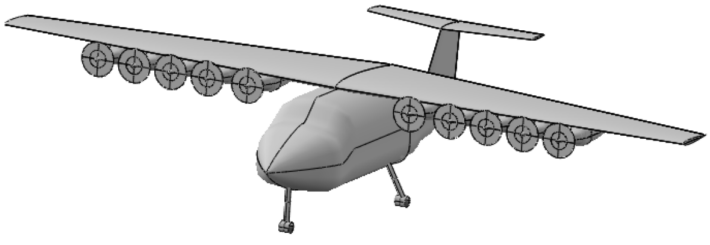

Figure 8.3: Electric design

9

Design Method

In this chapter the code used to generate the most important parameters of the aircraft is explained in Section 9.1. Then, a sensitivity study is performed in order to observe how changing certain inputs will affect the final outputs of the code in Section 9.2. An analysis on the selection of the design point is also discussed in Section 9.3. After that a summary of the most important outputs of the main code are given in **??**. Finally to give a clear and coherent overview of the code a N2 chart is given explaining the interactions and loops in the code.

9.1. Design Code

The final code, which was used for the generation of the aircraft layout, consists of two main scripts which were smoothly combined into one, outputting the driving design parameters needed in order to start with the subsystem design and cost estimations. The overall code can be seen in the N2 chart at the end of this chapter. The first part of the script, which is represented by the green segments, is provided by the team's supervisor and consists of a converging algorithm for generating a wing loading diagram and constructs the powertrain of the aircraft. The logic and science behind this code can be read in [9]. The second part of the code, the blue boxes, is written by the team and contains everything from wing planform to the vertical tail design.

In the first part of the code, the team had to decide on main parameter values such as aspect ratio, lift and drag coefficients, altitude, and fill in mission requirements and the like. The input with the largest impact on the calculations is the input where one must choose the powertrain configuration. The available powertrain options ranged from conventional to serial, parallel, turbo-electric and many more. The SPPH, Series Parallel Partial Hybrid power train [9] was chosen after a series of trade offs. The layout of the powertrain can be seen at Figure 10.1.

Other driving inputs for the code are the shaft power ratios (Φ), supplied power ratios (ϕ) and throttle setting (ζ) for each phase of the mission. The equations describing these inputs are represented by Equation 9.1, Equation 9.2 and Equation 9.3, where P_f is fuel power, P_{S1}, P_{S2} are power of system one and two respectively and P_{PE} represents the power of the piston engine.

$$\Phi = \frac{P_{bat}}{P_{bat} + P_f} \tag{9.1}$$

$$\phi = \frac{P_{S2}}{P_{S2} + P_{S1}} \tag{9.2}$$

$$\zeta = \frac{P_{PE}}{P_{PEmax}} \tag{9.3}$$

The crucial outputs of the code are the powertrain layout and wing loading diagram. Using this information a surface area can be found, as well as mass and power required for various mission stages. The resulting wing loading diagram can be seen when looking at Figure 9.1. Everything on the power train can be found in Chapter 10.

The second part of the code starts with wing planform design and goes all the way to the vertical tail design which is the last step in the analysis. Some important loops have to be mentioned which allowed the design to iterate and use less approximate reference aircraft values and more aircraft design theory and techniques. One loop is created at the drag calculation box. As stated above, drag coefficients were initial inputs taken from reference aircraft in the first part of the code. In the second part, the component method is used which gives a much more accurate value for the drag. Having the whole code in a loop and inputting the component method drag again in the first part resulted in a converged value of C_{D0} = 0.032. The same procedure is done for determining the maximum lift coefficient of the aircraft using the high lift device function. Furthermore, another loop which greatly influences the design is created from layout box in the N2 chart to the vertical tail design. Firstly, an initial layout was designed using reference aircraft and the input geometries are used for the potato diagram and the scissor plot. Using the scissor plot, the positions of the passengers, luggage and energy sources are iterated. The length of the aircraft is also adjusted according to the arm length between the main wing and horizontal stabilizer. Such changes are re-used as inputs in the drag function and the whole process is repeated until the changes between iterations are considered small enough. A difference of 0.05% was deemed reasonable and once that value is reached, the iteration stops.

For further clarifications, the N2 chart below explains the interactions between all the functions and the location of the loops where checks are performed to determine if new iterations are required or not.

Table 9.1 gives a short overview of the starting values of the design of the aircraft. Other design parameters shall be further elaborated on in their respective chapters.

Table 9.1: Summary of basic parameter values

Parameter	**Value**
MTOW [kg]	1440
OEW [kg]	990
Wingspan [m]	9.8
Aspect ratio [-]	10
Surface area [m^2]	9.5
Fuselage length [m]	8
CD$_0$ [-]	0.032
CL$_{max}$ [-]	2.1
MAC [m]	1.04
Ferry Range [km]	1360

9.2. Sensitivity Analysis

In this section a small sensitivity study is conducted in order to analyze how the main outputs, aircraft parameters and design points changed when certain driving input values were altered. A 10 percent decrease in the cruise speed and range is used as input along with a switch from a 4 to a 3 passenger configuration for the current aircraft configuration

(in [3] a more detailed sensitivity study was done on the optimal number of passengers). In addition, a design option with only 2 high lift motors is explored.

Running the design code several times yields the results shown in Table 9.2. It can be seen that the most significant changes appear when one alters the cruise speed, since it is one of the main constraining lines of the wing loading diagram as seen in Figure 9.1. The other major differences appear when switching from a 4 to 3 passenger configuration. The option with 2 high lift devices could not meet all the mission requirements, that is why it is left out as an option. A scenario with 6 high lift motors is not considered because the additional motors would not cover the flap area, thus making them inefficient. It is important to mention that all the inputs generate a completely new design from scratch, thus when changes in payload are made, this yields variations in the overall aircraft geometry, such as the wing area, power required for take-off and the like.

Table 9.2: Sensitivity analysis parameters

	MTOW	**Range (50% payload)**	$\mathbf{C}_{D_0}$	$\mathbf{dC}_{L_{max}}$
$\mathbf{V}_{Cruise}$ **(-10%)**	-13%	+36%	+ 2%	-1%
Range (Sizing range) (-10%)	-2%	+1.5%	+1%	2%
Payload (-25%)	-20%	-25%	+3.1%	-2%
$\mathbf{N}_{sec.eng}$ **= 2**	[-]	[-]	[-]	[-]

9.3. Design Point Selection

The first design choice consists of choosing what the aircraft should be sized for: maximum wing loading or maximum weight over power ratio. After many iteration the team decided to set the inputs for the best possible wing loading value. As stated in Section 9.2, changing the inputs creates a whole new aircraft, thus the wing loading diagram always changes. The obtained graph can be seen in Figure 9.1. The reasoning behind this choice is that designing for smallest engines resulted in an aircraft which is very similar to the conventional fuel reference aircraft, with same mass and wing area. This means that the point of having high lift propeller devices looses its advantageous effect. Much better results were achieved with the maximum wing loading point, the mass was reduced by almost 70 kg and the wing area reduced by 3 m^2, while keeping almost the same range and endurance.

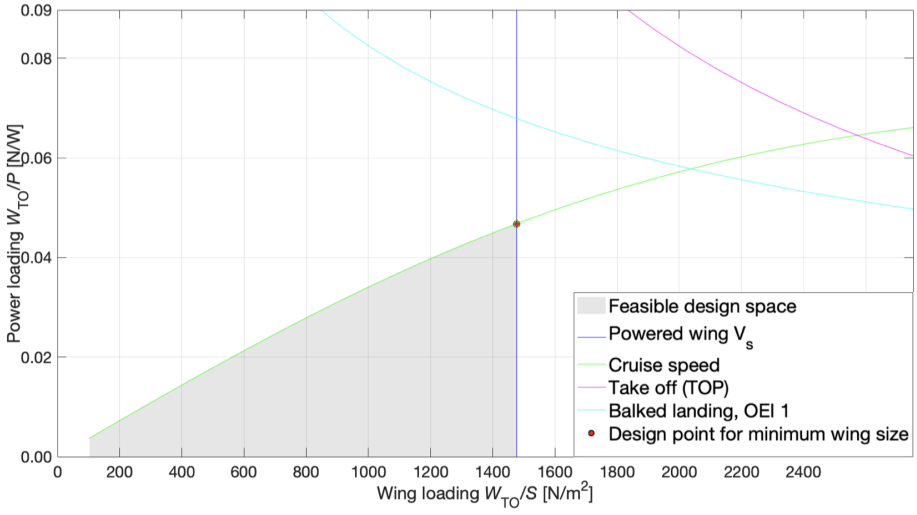

Figure 9.1: Wing loading - power loading diagram

A
CLs
CDs
e
R
E
Payload
h
Weight Fracctions
Shaft Power Ratios
Efficiencies
Initial Layout

WP/WS	P S	S mass_cruise	S	S		S					
	Class I Weight Estimation				M_fuel MTOW OEW	S					
		Wing Planform	Sweep_TE Sweep_LE t/c			Ct Cr Sweep_LE Sweep_TE b					
			Airfoil	CL_design							
	CD0			Drag Calculation	CD0 L/D	CD0					
R_max E_max					Mission Analysis						
	dCLmax					Aileron + HLDS sizing					
				L_nose L_fuselage L_tailcone			Make layout	payload_position batteries_position fuel_position	L_nose L_fuselage L_tailcone Lh		L_aircraft bf hf scrape_angle
							payload_position batteries_position fuel_position	Potato Diagram	CG_Range	CG_Range	CG_Range
				Sh_S			L_tailcone Lh XLEMAC Sh_S Zh	XLEMAC	S&C Analysis		
							scrape_angle			L.G. Design	
				S_v							Vertical Tail

10

Powertrain

The function of the powertrain is to displace the aircraft by converting stored energy into work. Besides this main function, the powertrain should also provide power to other systems of the aircraft. A detailed trade-off was made between a fully gas-powered, fully electric and multiple hybrid combinations in the Mid-Term report [3]. A serial-parallel hybrid configuration was chosen due to its ability to integrate aeropropulsive interaction devices, increasing possible wing loading of the aircraft. Detailed diagrams on this architecture can be found in Figure 11.1.

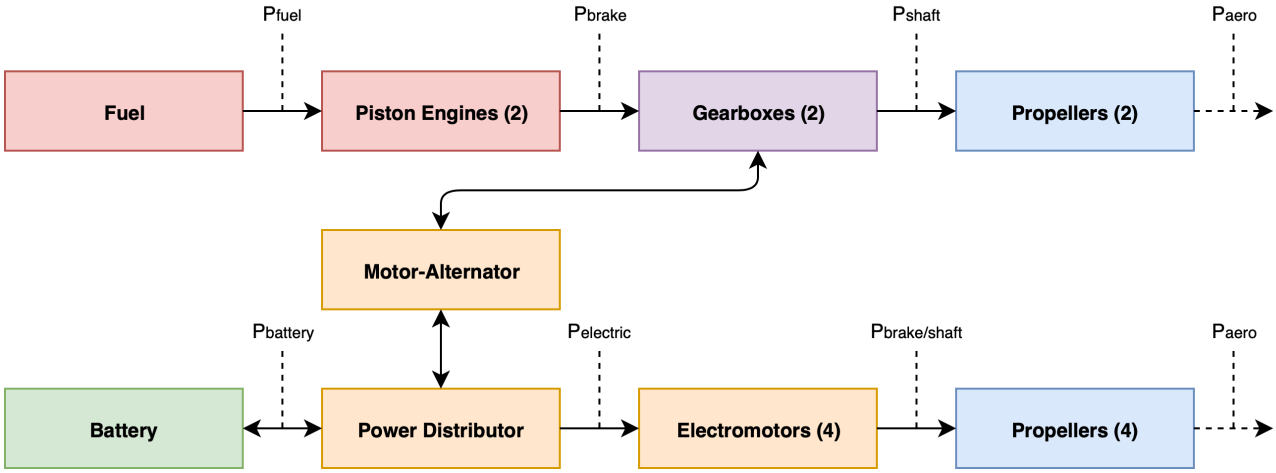

Figure 10.1: Powertrain configuration

10.1. Primary Propulsion Group

The counter rotating primary propulsion has a main function of providing thrust at the trailing edge near the wing-tips. This counteracts the tip vortices, which has the advantage of decreasing lift-induced drag and can be modelled as an effective increase of aspect ratio [10]. Besides this main function, the reciprocating engine delivers its power through a gearbox with an integrated motor-generator combination. This generator feeds its energy into the secondary propulsion system, by directly powering the electromotors and charging the main battery.

10.2. Secondary Propulsion Group

The main function of the secondary propulsion is to increase dynamic pressure over the wing, specifically, in the section where the high-lift devices are located. During takeoff and landing the motor-generator combinations in the gearboxes also contribute power to the main propellers.

10.3. Non-Propelling Group

As the power requirements of the systems on this circuit are rather low, and consequently light, they are not included in Table 10.1 and Table 10.2. Details on safety and redundancy can be found in Section 10.6.

10.4. Power Requirement

The power requirement is divided into a primary propulsion group and the secondary propulsion group. The primary group consists of two reciprocating engines, mounted at the tips of the aircraft on the trailing edge. The secondary group consists of two electromotors/alternators at the primary propulsor gearboxes and four electromotors mounted along the leading edge of the wing and close to the fuselage. The requirements are made with assumptions on specific power and specific energy of the devices. After a first iteration, devices in that specific power class are found and their specific power and energies are fed back into the calculation, further refining the power estimate. The chosen powertrain components are discussed in Section 10.5.

Table 10.1: Brake Power requirements at sea level

Brake level power [kW]	**Primary (Reciprocating)**	**Secondary (Electric)**		**Total**
	Tip-mounted pusher	**Gearbox mounted**	**Distributed**	
Takeoff	130	60	20	**210**
Cruise	210	-10	0	**200**
Landing	20	20	50	**90**
Design point	**210**	**60**	**50**	**320**

10.5. Powertrain Components

With the iterated brake power requirements from Table 10.1 the powertrain components are chosen and the battery and propellers are sized. The choices are shown in Table 10.2 with their associated weight and costs. Detailed information on the components meeting the requirements are discussed below.

The Lycoming O-360-series engines and Helix H50V propellers are chosen for the primary propulsion. These motors and propellers are certified by EASA[1] [2] for use in aircraft and therefore satisfying requirement **THA-REQ-REG-PWR-01**. The propeller is chosen to be four-bladed, as more blades tend to decrease noise at expense of slightly lowering efficiency. The sizing of the propeller blades is consecutively done according to $d = 0.5 \cdot \sqrt[4]{P}$[11]. This results in main propellers having a diameter of 1.65 m, whereas the secondary propeller diameters are suggested as 1.02 m by the motor manufacturer.

As for the gearbox-integrated motor-alternator, the flow of power through the motor and motor controller should be bi-directional. The EMRAX 188 meets the requirements for both regular and reversed power flow, as does the Unitek D3 controller. As this part of the system is embedded in a protected environment, the IP-standard of IP21 for the air

[1] https://www.easa.europa.eu/sites/default/files/dfu/EASA-TCDS-E.032_Lycoming_IO--360_series_engines-01-27092012.pdf

[2] https://www.easa.europa.eu/sites/default/files/dfu/EASA-TCDS-P.502_GEFA--Flug_GmbH_Helix_H50F_series_propellers-01-09032010.pdf

cooled motor is deemed sufficient.

Table 10.2: Powertrain components, prices and weights

Component	Name	Qty	Price [€]	Total Price [€]	W [kg]	W_t [kg]
Primary engines	Lycoming O-360 [3] [4] [5]	2	49,000	98,000	120	240
Primary propellers	Helix H50V [6]	2	1,500	3,000	5.7	11
Gearbox EM	EMRAX 188 [7]	2	2,500	5,000	7	14
Gearbox EM controller	Unitek D3-700-160 [8]	2	1,900	3,800	3.5	7
Secondary motors	T-motor U15 KV100 [9]	4	600	2,400	1.7	7
Secondary controllers	T-motor Flame 180A HV [10]	4	230	920	0.3	1
Secondary propellers	T-motor G40x13.1 [11]	4	200	800	0.2	1
Batteries	SolidEnergy LMP063767 [12]	1550 (20kWh)	10	15,500	0.029	45
Total				**129,420**		**326**

Table 10.3: Power available at aeropropulsive level

Aeropropulsive power [kW]	Primary (Reciprocating and Electric)	Secondary (Electric)	Total
	Tip-mounted pusher	Distributed	
Takeoff	150	20	***170***
Cruise	140	0	***140***
Landing	20	30	***50***

10.6. Safety Measures

10.6.1. Deicing

Deicing is done by means of cyclic resistive heating of all leading edges, tapping power from the low-power circuit of the aircraft for redundant operation. The method is certified on several general aviation aircraft and is able to deice a complete aircraft within one minute[13].

10.6.2. Electrical insulation and decoupling

To minimize interaction between the fuel system and the electrical systems, the batteries are located in the nose of the aircraft, whereas the fuel system is located in the wings.

All electrical wiring and components run below 100 VDC, minimizing risk of arcing. The electrical systems in and on the wing are also insulated to guarantee safe operation.

[3] Retrieved Jan 17, 2019 from http://www.airpowerinc.com/productcart/pc/TLEngineDetail.asp?catID=33&prodID=453144
[4] Retrieved Jan 17, 2019 from http://www.pilotfriend.com/aero_engines/engine_specs/Lycoming%200%20360.htm
[5] Retrieved Jan 17, 2019 from http://11hc.44rf.com/manuals/engine-prop/lycoming/aerosportspower-library/360_series_ops_manual/sec_3c1-sealevel-alt-performance-charts.pdf
[6] Retrieved Jan 17, 2019 from https://www.helix-propeller.de/fileadmin/user_upload/docs/data_sheets/H60V_1_75m_L-CS-3_en.pdf
[7] Retrieved Jan 17, 2019 from https://emrax.com/products/emrax-188/
[8] Retrieved Jan 17, 2019 from https://www.unitek-industrie-elektronik.de/news-article-7
[9] Retrieved Jan 17, 2019 from http://store-en.tmotor.com/goods.php?id=731
[10] Retrieved Jan 17, 2019 from http://store-en.tmotor.com/goods.php?id=733
[11] Retrieved Jan 17, 2019 from http://store-en.tmotor.com/goods.php?id=493
[12] Retrieved Jan 17, 2019 from http://assets.solidenergysystems.com/wp-content/uploads/2017/09/08171937/Hermes_Spec_Sheet1.pdf
[13] Retrieved Jan 22, 2019 from http://www.rddent.com/thermawingtrade.html

10.6.3. Thrust redundancy

Between the primary and secondary propulsion systems there is a level of redundancy. As the primary propulsion group is overpowered for both cruise and landing, as mentioned in Table 10.3 and Table 10.1, the aircraft will be able to land safely on the primary propulsion group if there is any failure in the secondary propulsion system. In case of a primary engine failure, please refer to Section 14.5.

10.6.4. Redundancy circuitry

The low-power systems of the vehicle run on a separate 28 VDC circuit. As the power-by-wire control is part of this, full redundancy is required. This is managed by having a DC-DC converter between the high/medium and low voltage circuits and having a separate battery in the low voltage circuit. If either of these power-providing systems fails, a redundancy circuit disables the faulty system to allow for full and undisturbed operation on the remaining power source.

10.7. Noise and environmental Characteristics

When selecting the engines, careful consideration is given to its noise characteristics. As discussed in Chapter 7, air taxi operators such as Fly Aeolus, and their passengers find the noise levels important but is not considered to be a decision changer. As a result, several methods to reduce noise will be discussed where for each method, the impact on noise levels is weighed against the impact it has on design and cost. First, noise insulation around the cabin is considered in order to reduce the noise in the cabin. Fibreglass batting is known to be an effective acoustic attenuator. This material is chosen as it is light, not electrically conductive and meets all regulatory flammability requirements [12]. A second method which is considered is the placement of the engine. Very early in the design stage, it was chosen to place this on the wingtips, as far from the cabin as possible. Even though this requires heavier wings, as they will bear more loads, the trade-off showed that this can be justified by the advantages. Once the engines were placed on the wings, the noise can be further reduced by sweeping the wings of the aircraft back. A same trade-off was done after which it was found that even though this would reduce the noise, it would mean that the wings would become even heavier. This weight increase led to the decision that sweeping the wings back would not be implemented in the design. Lastly, the engine selection process can also be used to ensure low noise emission. When selecting the engine, the dB's produced are also a factor used in the trade-off process. The data is in A-weighted decibels (dBA). At a distance of 15m the chosen engines produce a noise level of 69 dBA during cruise, and 85 dBA during take-off [13], which is the phase with the highest noise levels.

10.7.1. Fuel consumption

The fuel mass flow is 27 kg/hr per engine, for a total of 54 kg/hr, at a cruise thrust setting of 72% [14] per the cruise power requirement for the primary propulsion. This is 15 to 25% less than fuel burn of similarily sized aircraft [15] [16].

[14] https://www.lycoming.com/sites/default/files/O-HO-IO-HIO-AIO%20%26%20TIO-360%20Oper%20Manual%2060297-12.pdf
[15] https://www.flyingmag.com/what-most-fuel-efficient-airplane
[16] https://www.flyingmag.com/we-fly-diamond-da62

With a CO_2 emission of 3.17 kg per kg of AVGAS[17], the aircraft will produce 171 kg CO_2 per flight hour. Assuming the typical mission capacity of 4 passengers this comes down to 43 kg CO_2 per passenger per hour. With the typical mission speed of 92 m/s the effective emission is 128 g/pax/km of CO_2.

10.8. Retractable Propellers

The distributed propulsors shall only be used during take-off and landing since at these mission phases a high lift coefficient from the wing is required. This implies that during cruise the propellers are idle. To prevent unnecessary drag formation due to the large wetted area of the propellers exposed to the airflow a retraction system is implemented. The folding system resembles that of aircraft who have a similar problem with leading edge mounted high lift propellers.[14] Because the high lift propellers at the leading edge are mounted with an offset of 50% of the propeller diameter there is space behind the electromotor to store the propeller during cruise. In Figure 10.2 the propulsor configuration can be seen during deployment, while in Figure 10.3 the retracted propeller configuration can be seen.

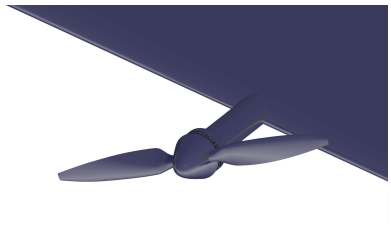

Figure 10.2: Deployed propeller configuration

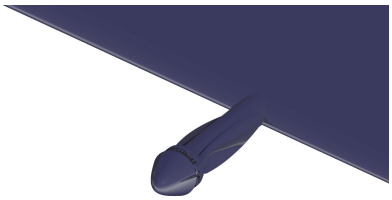

Figure 10.3: Retracted propeller configuration

[17] http://www.hjelmco.com/upl/files/2425.pdf

11

Aircraft Hardware & Software Architecture

The hardware (HW), software (SW), electrical, communication and data diagrams illustrate the interfaces between subsystems and their functions. The software functions are present in all subsystems of the vehicle, hence they are closely related to the hardware functions.

11.1. Hardware Architecture

Figure 11.1 lays out the hardware architecture of the vehicle. The subsystems are divided into powertrain, cabin, communication and control and stability. At the center, the main computer resides to monitor and direct the subsystems by being the main interface between them. To enhance flight behavior and controllability, the flight controller uses a real-time operating system. As the aircraft uses fly-by-wire, the control surfaces are also actuated electronically. The flight controller has triple redundancy, such that it is possible to determine which controller is malfunctioning when the results do not match.

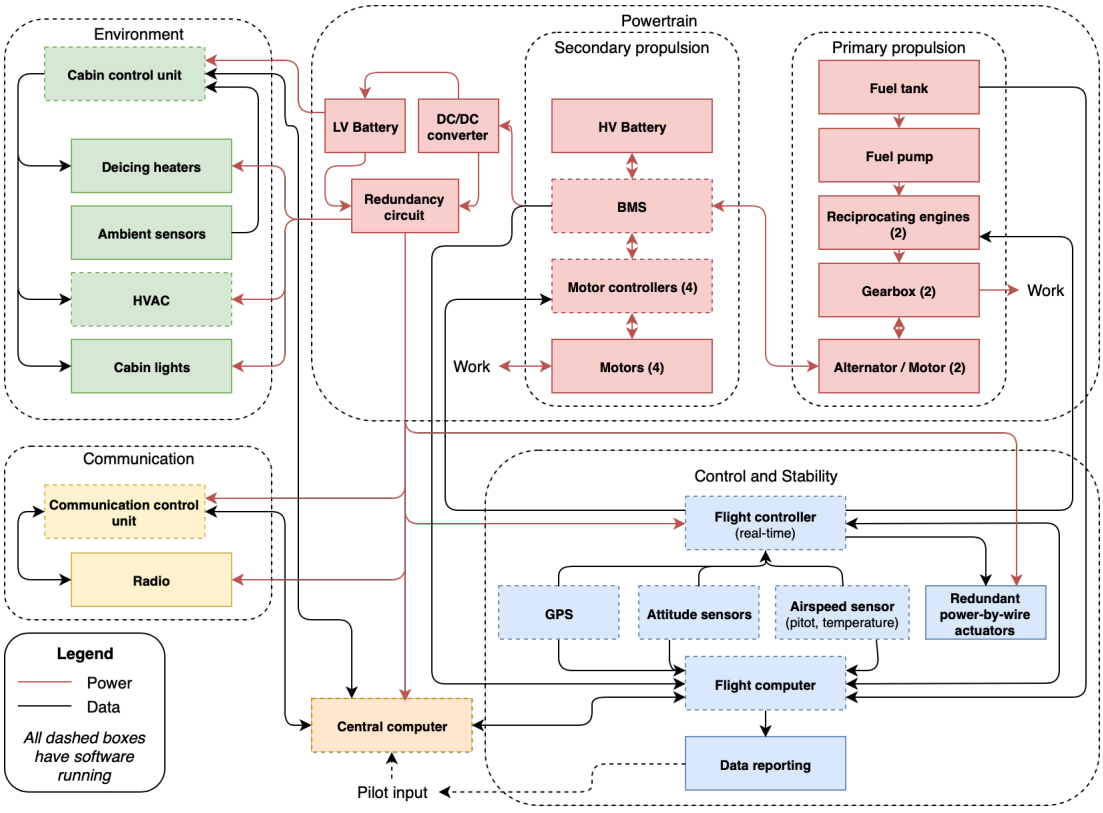

Figure 11.1: Hardware Block Diagram

11.2. Software Architecture

As for the software, Figure 11.2 shows the different software functions and their respective interfaces. All dashed lines are interfaces that are out of scope for the software development and general interactions with the environment. As mentioned, the central computer takes care of the main interfacing between subsystems and will be the point where actions, like start-up, shutdown sequences and checks are initiated.

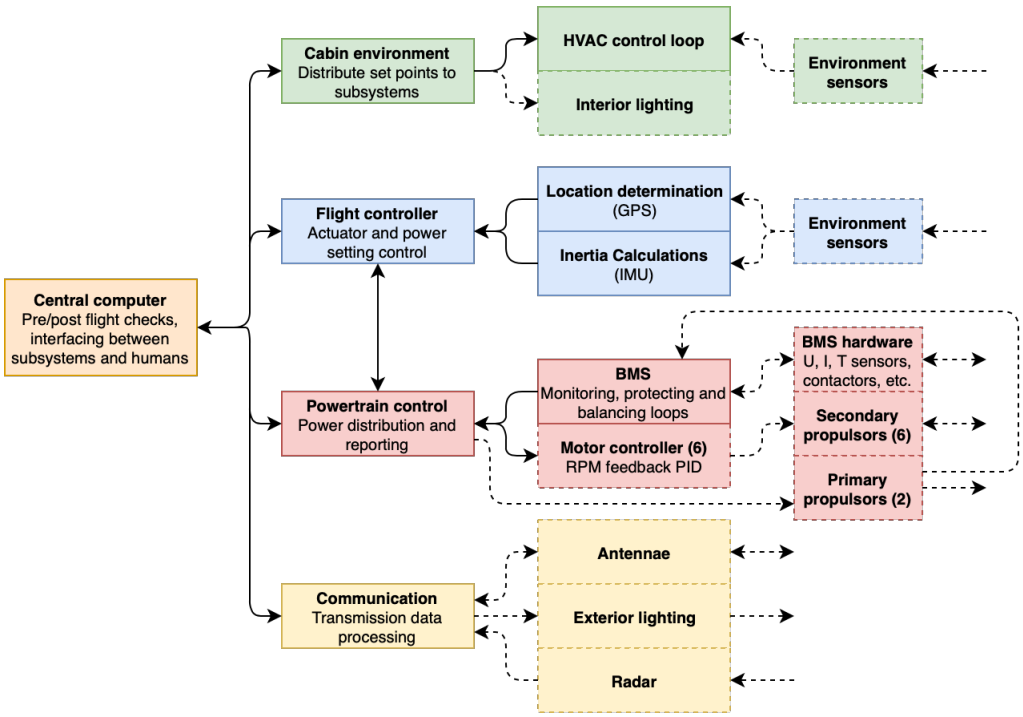

Figure 11.2: Software Block Diagram

11.3. Electrical Architecture

The electrical diagram, shown in Figure 11.3, is most useful for a more in-depth analysis of the powertrain, so that is where its focus lies. The electrical energy sources are split up in a high power (HP) circuit at 100VDC and a low power circuit at 28VDC. The HP circuit provides power to the distributed propulsion motors and the gearbox-mounted electromotors/alternators. The peak power capability lies around 100kW. Additionally, during cruise the batteries of this circuit are charged at 10kW by generating electricity from the main propulsors in the gearbox-mounted electromotors/alternators. As the distributed propulsion has a nominal voltage of 100VDC, this means the high-powered circuit will handle a current of 1kA at some moments. However, this is mainly caused by all systems drawing power in parallel, and therefore current flowing in the branches towards components is limited. From the first junction to the battery it is suggested to use insulated copper bus bars instead of wiring to be able to withstand the 500A peak current load. For further branches, the American Wire Gauge (AWG) ratings for copper are followed [1].

The low-power circuit energy source consists of the 28VDC battery, which is normally kept at charge by a DC/DC converter from the HP circuit. If either the HP circuit or converter fail or if the battery fails the circuit stays operational

[1] Retrieved at Jan 23, 2019 from `https://archive.org/details/copperwiretables31unituoft/page/n6`

by using a redundancy circuit to decouple the failing energy source. In addition to this, all essential components are doubly wired.

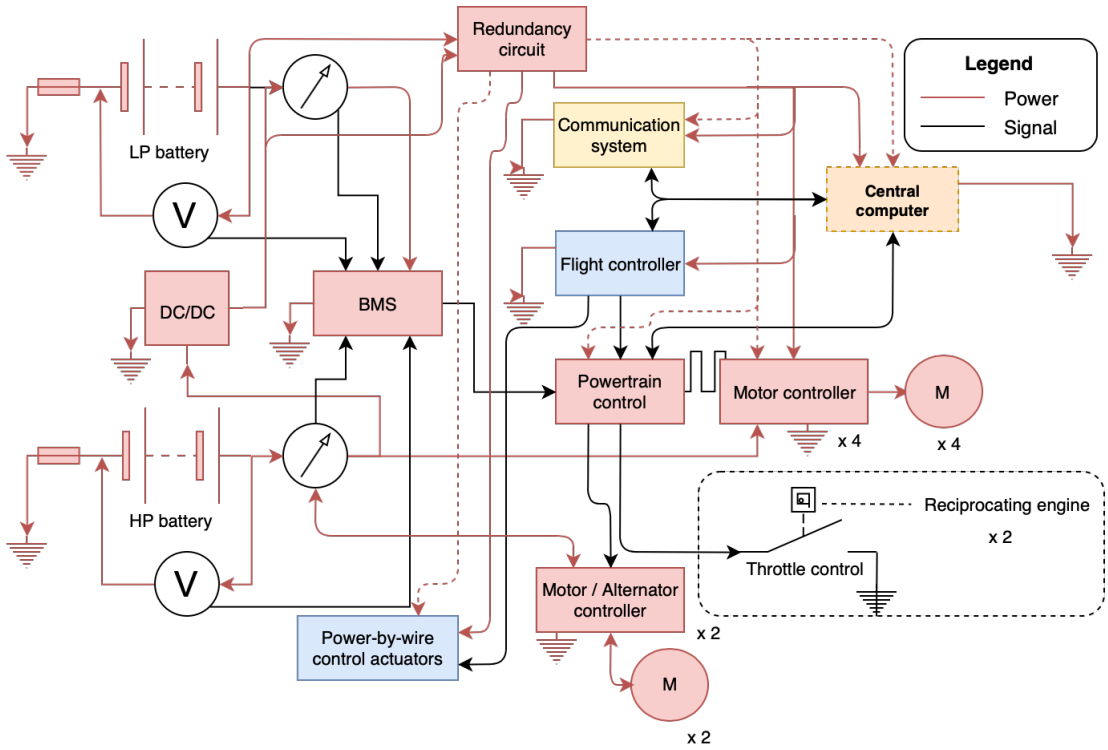

Figure 11.3: Electrical Block Diagram

11.4. Data Handling Diagram

The data handling diagram of the consists of a Proportional Integral Derivative (PID) controller which will control the roll, pitch and yaw. The gains of the controller will be determined later in the design process. A design at this stage would result in a controller which is sub-optimal flight behaviour.

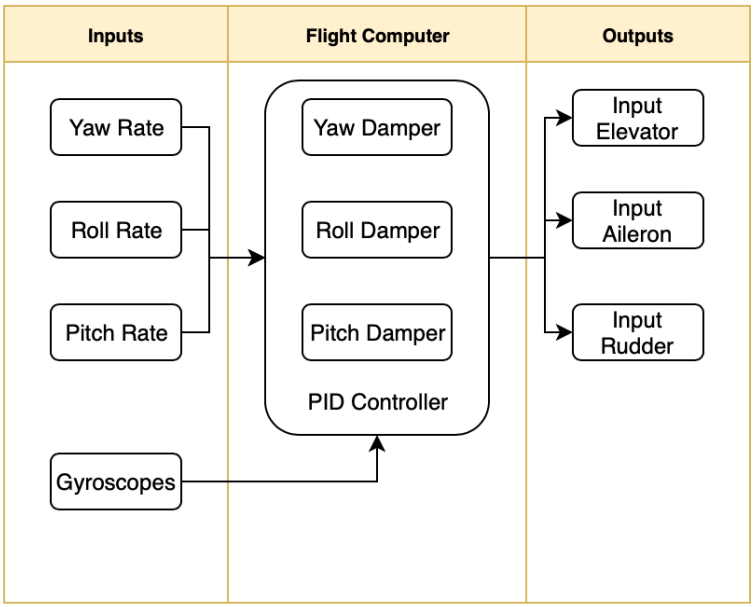

Figure 11.4: Data Handling Diagram of Flight Computer

11.5. Communication Flow Diagram

The communication flow diagram within the aircraft. As can be seen, either the autopilot or the pilot lie at the heart of the communication flow. They read their instruments and accordingly adjust the power, flight controls, communication system with ATC and the environmental control. It should also be noted that some flows can be both way, shown by an arrow on both ends, or it can only happen in one direct, shown by an arrow at one end of the line.

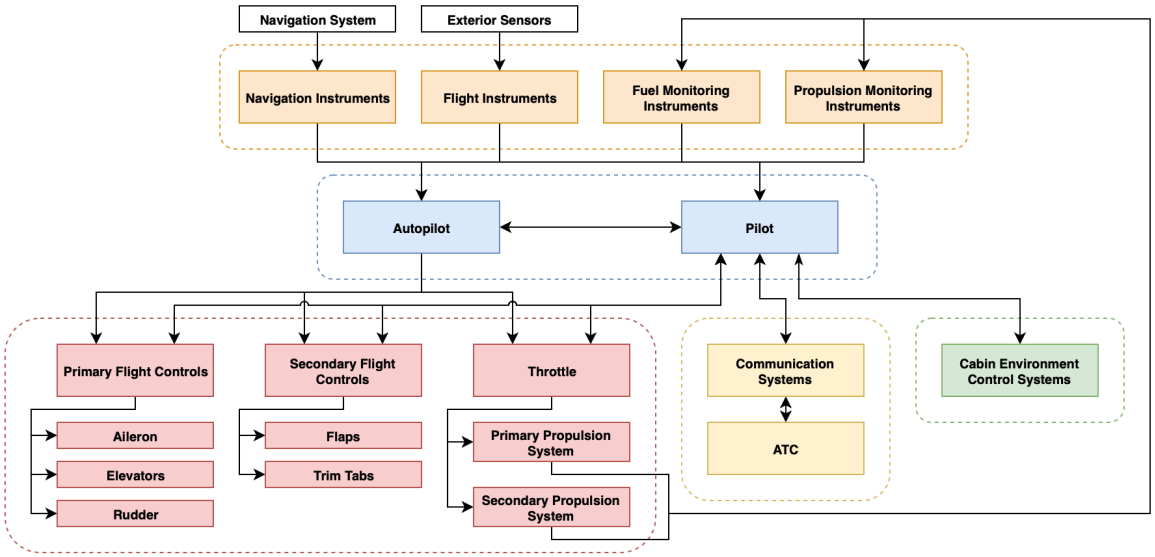

Figure 11.5: Communication Flow Diagram

12

Aerodynamic Analysis

This chapter treats the aerodynamics of the aircraft components in general and the aerodynamics of the main wing specifically. The aerodynamics of the aircraft components were modelled using XFLR5, a program that's able to analyze airfoils (using the integrated XFoil program), wings and plane-like structures. The purpose of this chapter is to analyze the aerodynamic performance of the Chauffeair, and to provide the means to obtain a load distribution for the wing for the structural calculations in Chapter 16.

12.1. Airfoil Selection

It has been decided that the main wing of the aircraft will have a constant airfoil profile along the span for simplicity. The airfoil profile is chosen based on reference aircraft with a similar wing performance. In Table 12.1, the airfoils that are compared to each other can be observed.[1]

Table 12.1: Reference aircraft and their airfoils

Reference aircraft	Mooney 301	Cessna 172/206	Beech 100 King Air
Airfoil	NACA64215	NACA2412	NACA23018

The airfoil characteristics are implemented into the aerodynamic analysis tool XFLR5, where the 2D aerodynamic behaviour of the airfoils are computed.[2] [3] Two curves are analyzed, namely the lift slope and the drag polar in Figure 12.1 and Figure 12.2 respectively. From the lift curve it can be noted that the NACA2412 outperforms the other airfoils while having similar stall angle. The performance of the airfoils, as seen in the drag polar, is very similar, however the performance of the NACA64215 is worse for higher lift coefficients, whilst the NACA23018 has the highest zero lift drag. Therefore, it is decided to use the NACA2412 as airfoil profile at the main wing.

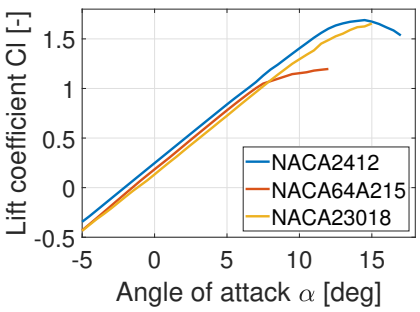

Figure 12.1: Lift alpha curve

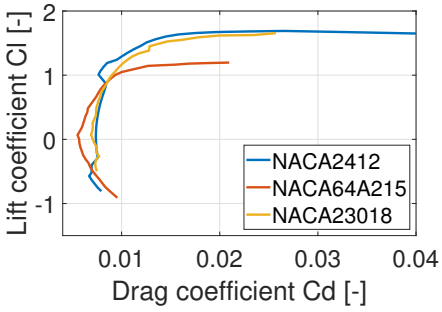

Figure 12.2: Drag polar

[1] Aerofiles, D. Lednicer, accessed on 15-01-19, `http://www.aerofiles.com/airfoils.html`
[2] XFLR5 v6.44, Aerodynamics Analysis for Airfoils and Wings, accessed on 14-01-19. `http://www.xflr5.com/xflr5.htm`
[3] Airfoil Tools, Tools for search purposes, compare and plot airfoils, Accessed on 14-01-19.`http://airfoiltools.com/index`

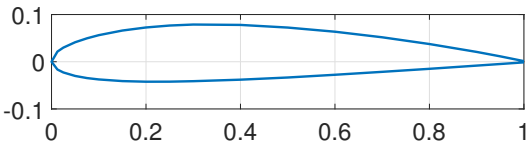

Figure 12.3: NACA 2412 airfoil of the wing

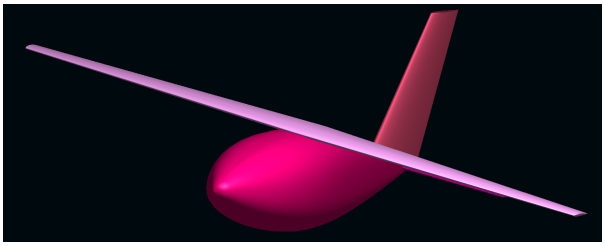

Figure 12.4: Model of the aircraft used inside XFLR5

Table 12.2: NACA 2412 airfoil characteristics

Maximum C_l/C_d	**Maximum** C_l	**Stall angle** (deg)	**Cruise** C_m	**Maximum** t/c
139	1.69	14.5	-0.054	0.12

The airfoil used for the vertical and horizontal stabilizer is chosen to be the symmetric NACA63015A, based on reference aircraft [15]. In Chapter 14 both stabilizers will be further elaborated on.

12.2. 3D Aerodynamics Model

The lift, profile drag and induced drag of the aircraft's lifting surfaces are modelled using XFLR5 which allows quick design and modification of geometry. XFLR5 offers four options for analysis: two vortex lattice methods, an older method which models lifting surfaces as a lifting line and a 3D panel method which can only be used for the wing. The method performed in this report uses a vortex lattice method based on ring vortices. It models the lifting surfaces as thin sheets of panels, each of which is subjected to a ring vortex, while the trailing vortices extend to infinity. The model created inside XFLR5 can be observed in Figure 12.4.

The contributions of the distributed propellers to the lift, profile drag and induced drag are estimated using the "aero-propulsive model" described and implemented by De Vries et al. [9], who in turn base their approach on Patterson and German [16]. It employs a number of simplifying assumptions which enable quick analysis, including:

- The wing is considered a flat rectangular plate. This means the effects of the airfoil and design parameters, such as sweep and taper in the actual wing design are not taken into account.
- The distributed propellers only affect the section of the wing right behind them and is assumed to be uniformly distributed along the location of the wingspan where they are deployed.
- Any effects due to the interaction between propellers are neglected.
- The diameter of the propellers is assumed to be much larger than the wing chord. This means the wing can be assumed to be fully immersed in the slipstream of the propellers.

The change in the lift along the section where the distributed propellers are deployed is calculated using Equation 12.1. It uses the angle of attack, α, the angle between the axis of propeller and the chord, i_p, a correction factor for the slipstream, β, and an axial induction factor at the quarter chord, $a_{c/4}$.

$$\Delta c_l = 2\pi[(\sin\alpha - a_{c/4}\beta\sin i_p)\sqrt{(a_{c/4})^2 + 2a_{c/4}\beta\cos(\alpha + i_p) + 1}] \tag{12.1}$$

The change in the drag along the section where the distributed propellers are deployed, given by Equation 12.2, is calculated as the sum of two parts: the change in viscous drag and the change in pressure drag.

$$\Delta c_d = \Delta c_{d0} + \Delta c_{di} \tag{12.2}$$

The change in the profile drag, calculated with Equation 12.3, is a result of the changed dynamic pressure.

$$\Delta c_{d0} = a_{c/4}^2 c_f \tag{12.3}$$

The change in the induced drag, given by Equation 12.4, is a result of the changed airflow around the section of the wing.

$$\Delta c_{di} \approx \frac{2C_{Lairframe}\Delta c_l}{\pi A} \tag{12.4}$$

By combining the results from Equation 12.1, Equation 12.2, Section 12.3 and Section 12.4, the lift curves and drag polars in Figure 12.5 and Figure 12.6 were created for the cruise phase of the aircraft.

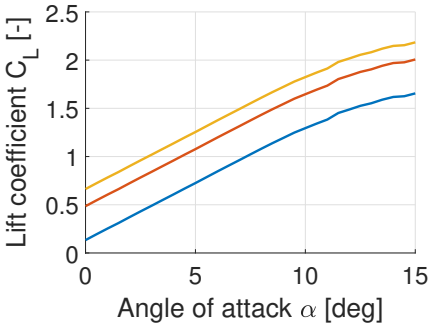

Figure 12.5: Lift curve of the aircraft: clean configuration (blue), distributed propellers (orange), HLDs (yellow).

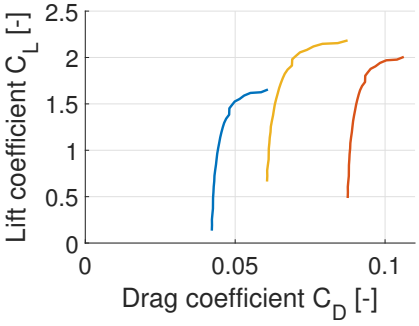

Figure 12.6: Drag polar of the aircraft: clean configuration (blue), distributed propellers (orange), HLDs (yellow).

It should be noted that, the analysis made above models the total lift of the wing during cruise with the distributed active propellers. However, in practice this situation shall rarely take place since during cruise, high lift is not required and thus the propellers shall be retracted as explained in Chapter 10.

According to Miranda and Brennan [17], the main benefit of using tip-mounted propellers behind the wing lies in a reduced required power due to improved propulsive efficiency. When air from the higher-pressure region below the wing moves toward the lower-pressure region above the wing, wingtip vortices begin to form. By placing the propellers in the flowfield behind the wingtip, energy can be recovered from these wingtip vortices. When the propellers rotate in the opposite direction of the wingtip vortices, the effective propeller blade pitch is increased. This leads to an increase of the propulsive efficiency which in turn reduces the required power. Using optimized propeller airfoils Nootebos has shown that propulsive efficiency can be increased by 11% [18]. For the tip-mounted pusher propellers in this aircraft,

similar performance benefits are possible with appropriate analysis and optimization.

12.3. Drag Estimation

Drag is generated by all components subjected to the outside airflow, such as the fuselage, canopy, landing gear, flaps and nacelles. The total aircraft drag coefficient can be predicted by combining the components drag contribution in coefficients using methods developed by Roskam [19]. It relies on various design parameters and factors based on geometry to produce its estimations. The results were combined with those obtained from analysis in XFLR5 and compiled in Table 12.3.

Table 12.3: Component drag coefficients of the aircraft

Component	Fuselage	Wing	Empennage	Landing Gear	Flaps	Total
Drag Coefficient	0.0124	0.0053	0.0018	0.0021	0.0136	0.0352

12.4. High Lift Devices

The $C_{L,max}$ that is obtained from the airfoil might not be enough to meet take-off and landing requirements. To reduce the take-off and landing distance, high lift devices (HLDs) are installed onto the aircraft. For this aircraft only trailing edge (TE) HLDs are considered, since the distributed propulsers are deployed at the leading edge. The calculations for the HLDs are almost entirely based upon the method of Torenbeek [20]. The method of calculating HLDs is an iterative process. Firstly, one assumes a certain value over the span where the HLDs act on (S_{wf}/S). Under this assumption, the $\Delta C_{L,max}$ can be calculated using Equation 12.1. A final check is performed on the new achieved $C_{L,max}$ to make sure it's sufficient for the take-off and landing requirements. There is a reverse way of calculating this, by assuming a value for $\Delta C_{L,max}$ and then to check whether the HLDs fit on the wing. However, the first approach was used in this case. The trailing edge flaps are installed with a 0.3 flap-to-chord ratio and a 0.55 flap-to-span ratio.

$$\Delta C_{L,max} = 0.9 \delta C_{l,max} \frac{S_{wf}}{S} cos(\Lambda_{hinge-line}) \tag{12.5}$$

In Equation 12.5, $\delta C_{l,max}$ depends on the type of HLDs used. Plain flaps are chosen, since the difference in $C_{L,max}$ required is not too high and the complexity of these flaps is much lower than chord extending flaps, e.g. Fowler flaps. Finally, the wing planform including the dimensions of the flaps and the ailerons are shown in the Figure 12.7. It is furthermore intended to include the ailerons dimensions in this figure to get the full impression of the wing planform.

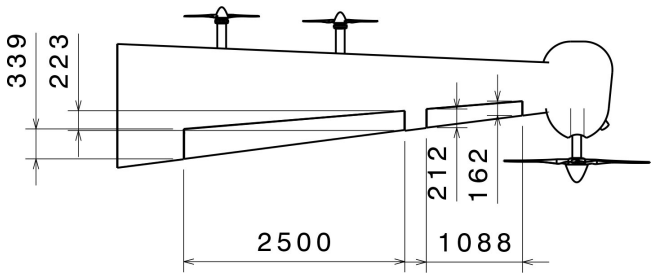

Figure 12.7: Wing planform including dimensions, all dimensions are indicated in [mm]

13

Performance Analysis

This chapter is concerned with the performance of the aircraft. First, the payload range diagram is shown in Section 13.1. Secondly, Section 13.4 gives the method for analysis regarding take-off and landing. The same applies to Section 13.5, but then regarding climb and descent. Section 13.6 Discusses the turning performance of the aircraft. Then Section 13.7 gives an overview of the reference and sizing mission performance. Lastly, Section 13.8 and Section 9.2 show the summary of the general performance of the aircraft and a sensitivity analysis of certain performance parameters.

13.1. Payload Range Diagram

The first step in analysis of the aircraft is to construct the payload range diagram. It shows the trade-off between payload and fuel for achieving longer ranges. In Figure 13.1 one can see the range the aircraft can achieve for different weight operations. When the range for MTOW is reached, the payload weight reduces and the fuel weight is increases until the fuel tanks are at maximum capacity. Finally, the payload is reduced until it reaches zero. The maximum range of the aircraft can fly is defined as the ferry range.

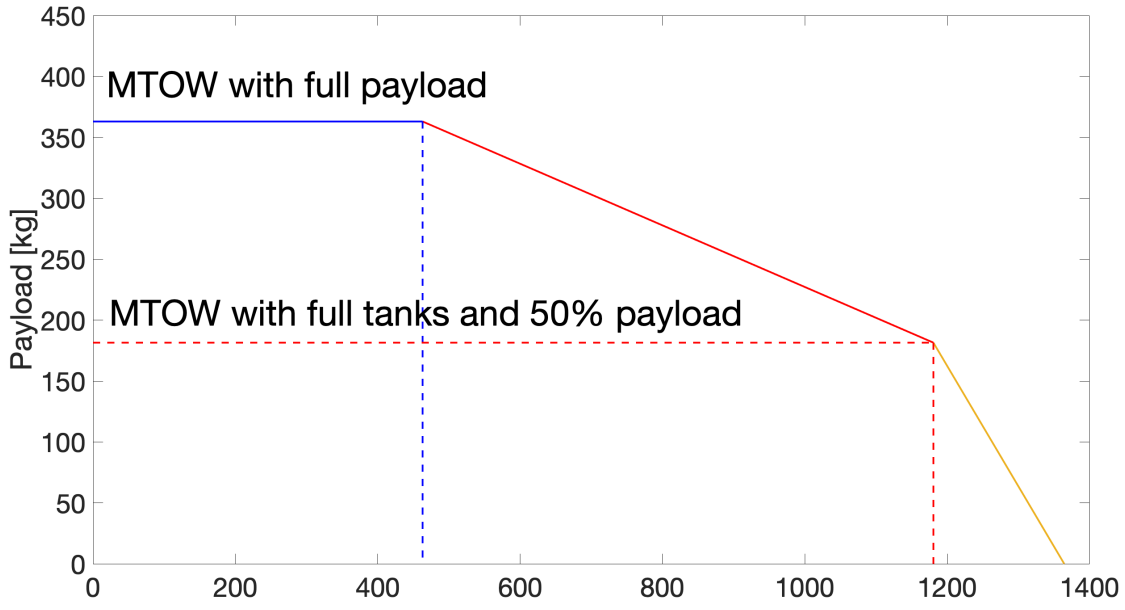

Figure 13.1: Payload range diagram

13.2. Flight Envelope

Next, there is the flight envelope. It is used to check whether the aircraft can sustain critical loads throughout the flight. Two graphs were created and thereafter were super imposed on one another. One which considers the basic aircraft maneuvering loads and the other for the corresponding gust loads. The ultimate load factor obtained from the graph is $n = 4.4$ [1]. The following conditions were considered, V-S which is the stall speed, V-A which is the maneuvering speed, V-C which is the design cruise speeds and V-D corresponding to the design dive speed. Then the gust loading envelope was created and superimposed over the maneuvering load diagram. The gusts speed values are taken for altitude of 2400 m [21]. The resulting diagram can be seen at Figure 13.2. It can be seen that the U_b, which is the gust load of altitudes between sea level and 6000 m [21] is limiting the envelope and the possible survive region is surrounded by its dashed lines.

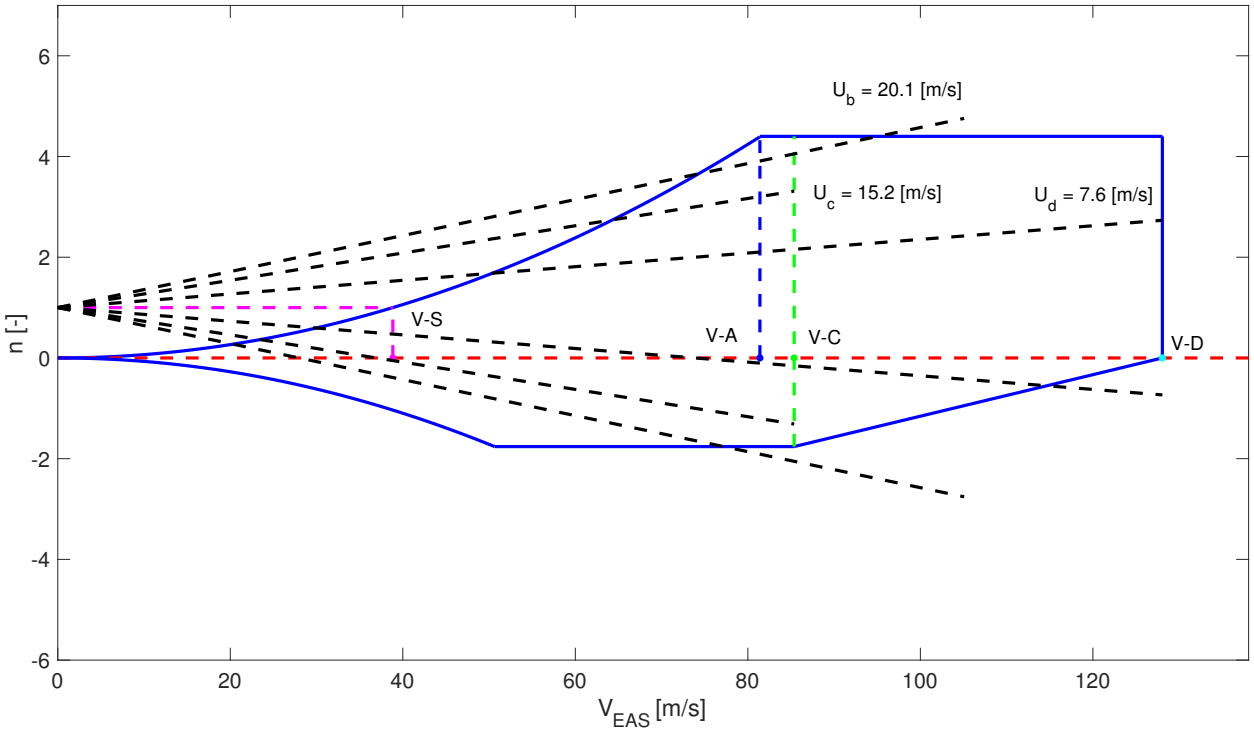

Figure 13.2: Flight envelope

13.3. Velocities

The velocities that are the most interesting for this aircraft are the minimum speed (stall speed) and the maximum speed. The stall speed is all dependent on the $C_{L,max}$ of the aircraft and thus mainly on the flap setting. The stall speed thus differ from clean, take-off and landing configuration. The equation for the stall speed is shown in Equation 13.1. The other speed chosen is logically the maximum speed. Unlike for a jet aircraft, a propeller aircraft does not have a standard equation for maximum speed. The speed must be found from the power required (PR) and the power available (PA) equations. The intersection where this occurs is the maximum airspeed, this can be seen in the crossing

[1] 14 CFR 23.337 - Limit maneuvering load factors., accessed on 21-01-19, https://www.law.cornell.edu/cfr/text/14/23.337

point on the right hand side of the Figure 13.3. One major assumption that is made throughout this whole chapter is that the power available is constant with airspeed.

$$V_{stall} = \sqrt{\frac{W}{S}\frac{2}{\rho}\frac{1}{C_{L,max}}} \tag{13.1}$$

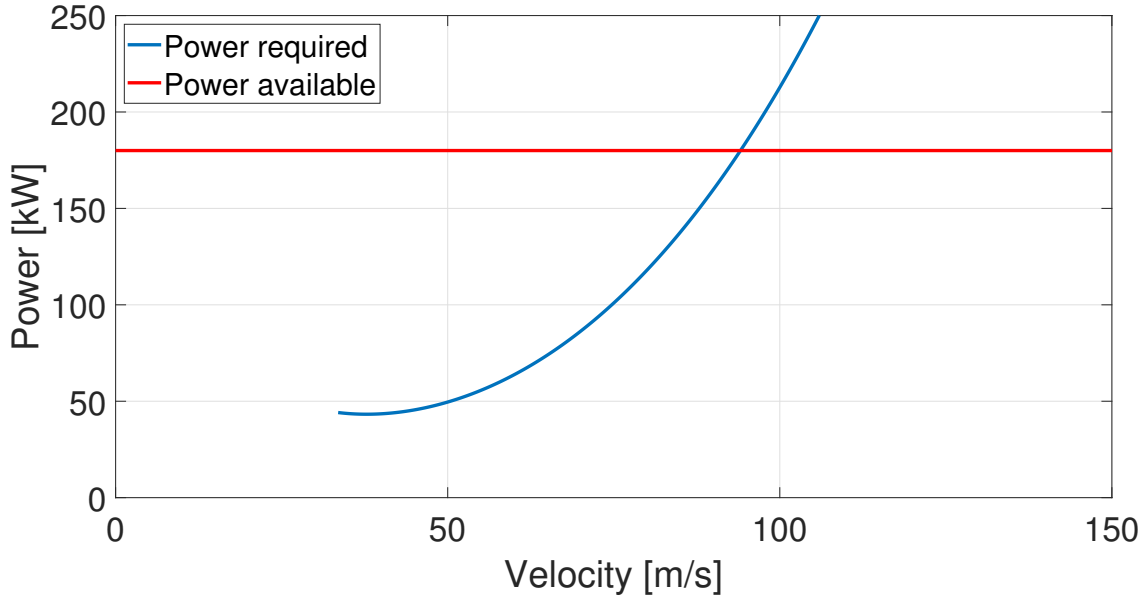

Figure 13.3: Power available and Power required plot

13.4. Take-off and landing

Both the take-off and landing are based upon the methods [21] and [22]. If anything is not clear about the method or want to get a better understanding, please refer to either of those books.

Take-off

With take-off, it is defined as the start on the runway until the 50 ft (15.2 m) obstacle. This generally consists of three phases. The ground phase, the transition phase and the climb phase as can be seen in Equation 13.2[21].

$$X_{take-off} = X_{ground} + X_{trans} + X_{climb} \tag{13.2}$$

The ground phase is based on the acceleration until the lift-off velocity (V_{lof}) is reached. The lift-off velocity is considered to be $1.05 \cdot V_{stall}$. Where V_{stall} is the minimum velocity it can fly at. Equation 13.3 shows the equation for the average acceleration of the aircraft[21]. The values for average thrust barT, average drag barD and average ground drag $barD_g$ are taken at average velocity, which is calculated as $V_{lof}/\sqrt{2}$ For the average ground drag, a 0.02 ground friction coefficient is used for a grass runway and for a asphalt runway [21].

$$\bar{a} = g/W(\bar{T} - \bar{D} - \bar{D_g}) \tag{13.3}$$

$$X_{ground} = \frac{{V_{lof}}^2}{2 \cdot \bar{a}} \tag{13.4}$$

The next phase is the transition phase which uses the very basic relation shown in Equation 13.5. The last phase is the climb phase. This is a simplified equation as this design is still conceptual[22]. The equation for the climb phase can be seen in Equation 13.6, where γ_{climb} was calculated using Equation 13.7 with a screen height of 50 ft.

$$X_{trans} = \frac{V_{lof}^2}{0.15g} sin(\gamma_{climb}) \quad (13.5) \qquad X_{climb} = \frac{h_{scr} - h_{take-off}}{\tan(\gamma_{climb})} \quad (13.6) \qquad \gamma_{climb} = \arcsin(\frac{\bar{T} - \bar{D}}{W}) \quad (13.7)$$

Landing

Now landing is the exact opposite of taking off. The landing distance however is based on the same length as take-off. It is defines as from the 15.2 m obstacle until the aircraft is at a standstill. The landing phase also consists of three phases. These phases are the same as for take-off but in the exact opposite order. So first comes the airborne phase, then the transition phase and finally the ground phase. First,the airborne phase. This phase is the same as Equation 13.6, except the angle (γ) is different. Secondly, the transition phase. This phase is very simplified and is calculated by using Equation 13.8. The approach speed (V_{ap}) is taken to be $1.3V_{stall}$.

$$X_{trans} = t_{trans} \cdot V_{ap} \quad (13.8)$$

Lastly, is the ground phase. This phase also includes the breaking, that uses a formula that is a bit similar to that of Equation 13.3. This formula is used for the ground phase. The speed used for the thrust and drag is $V_{ap}/\sqrt{2}$.

$$X_{brake} = \frac{W^2}{2gS} \frac{2}{\rho} \frac{1.3^2}{C_{L,max}} \frac{1}{\bar{T} + \bar{D} + \bar{D}_g} \quad (13.9)$$

By summing up the airborne phase, the transition phase and the braking phase, the total landing distance of the aircraft can be achieved and will be shown together with the take-off distance in Section 13.8.

13.5. Climb & Descent

For climbing and descending there are a few things to consider. Mainly the maximum rate of climb, the maximum climb angle, the minimum rate of descent and the minimum glide angle. The Maximum rate of climb is calculated using the maximum difference between the power available and the power required, also called the excess power. Since, power available is taken to be constant with airspeed, this occurs at the minimum of power required. This can be seen in the lowest point of Figure 13.3 [21]. Finally, using Equation 13.10 the rate of climb (ROC) can be computed. Here, PR_{min} occurs for the lift coefficient stated in Equation 13.11.

$$ROC_{max} = \frac{PA - PR_{min}}{W} \quad (13.10) \qquad C_L = \sqrt{3 \cdot C_{D0} \cdot \pi \cdot A \cdot e} \quad (13.11)$$

The maximum climb angle for light propeller aircraft is usually at such low speeds that it is below the stall speed [22]. Now, logically the aircraft cannot fly at that speed. Thus the maximum climb angle was found analytically by dividing Equation 13.10 by the velocity, in order to get the climb angle (Equation 13.12. This was done for different speeds and eventually a maximum climb angle was found.

$$sin(\gamma_{max}) = \frac{PA - PR_{min}}{W \cdot V} \tag{13.12}$$

The minimum rate of descent is very important if the engine malfunctions or hazardous to use. For this calculation, it is thus assumed that the thrust is zero. Equation 13.10 is then modified since PA is also zero. This results in Equation 13.13.

$$ROD_{min} = \frac{-\sqrt{W \cdot 2}}{\sqrt{\rho} \cdot C_L^{3/2}/C_D} \tag{13.13}$$

$$C_L = \sqrt{3 \cdot C_{D0} \cdot \pi \cdot A \cdot e} \tag{13.14}$$

To minimize the ROD, maximizing of $C_L^{3/2}/C_D$ is necessary. This happens when an optimum lift coefficient, which can be found in Equation 13.14. To finalize this section the minimum glide angle will be analyzed. For this calculation, no thrust is assumed again. This is the minimum angle to glide, also assuming zero thrust, to cover the most horizontal distance. The relation is given in Equation 13.15. Inputting the C_L, which maximizes C_L/C_D, given in Equation 13.16.

$$\gamma_{desc,min} = \arcsin(\frac{-1}{C_L/C_D}) \tag{13.15}$$

$$C_L = \sqrt{C_{D0} \cdot \pi \cdot A \cdot e} \tag{13.16}$$

13.6. Turning

Taking-off and landing are all very important, but in the end the aircraft will not only fly in a straight line. The aircraft will eventually need to make some turns. The four standard turns were analyzed for the aircraft; the quickest turn, the minimum turn radius, the maximum load factor during turning and the maximum bank angle. It is assumed that the turns will be performed in a steady, coordinated and horizontal flight. This means that the linear and angular accelerations, the side slip angle and the flight angle are all zero. Also, the height at which the aircraft flies does not change. This leads to the equations of motion shown in Equation 13.17 to 13.19.

$$T = D \tag{13.17}$$

$$L \cdot cos(\Theta) = W \tag{13.18}$$

$$\frac{WV^2}{gR} = L \cdot sin(\Theta) \tag{13.19}$$

Then for the standard turn rates. By dividing the cruise speed by the angular velocity the turn radius can be found [21]. Then using Equation 13.20 the bank angle corresponding to the rate 1 turn can be computed with the corresponding load factor(Equation 13.21),

$$R = \frac{V^2}{g \cdot tan(\Theta)} \tag{13.20}$$

$$n = \frac{1}{cos(\Theta)} \tag{13.21}$$

The next three parameters are all done the same way. By calculating the power required and the lift for all kinds of different speeds. With the acquired lift, the load factor and the bank angle can be obtained in that order. Plugging the speed and the corresponding bank angle in Equation 13.20, the radius can be obtained. Lastly, the turn time can be calculated with Equation 13.22.

$$T_\pi = \frac{\pi R}{V} \tag{13.22}$$

The calculations carried out for all the speeds and with the corresponding C_D and C_L values, the minimum turn radius, the quickest turn and the maximum load factor can be calculated. The speeds at which these conditions occur in

subsequent order are: $V_{R,min} < V_{T,min} < V_{n,max}$.

13.7. Reference & Sizing Mission Analysis

This section will go through the reference mission and sizing mission of this aircraft. The reference mission will be performed with 50% payload (Table 13.1) [1]. The sizing mission on the other hand will performed on 100 % payload (Table 13.2), essentially at MTOW. The values of fuel, for the take-off phase and the landing phase are very preliminary. Also, the fuel flow during climbing and descending has been taken as constant. A reminder is that the power available is still constant with airspeed. After studying Table 13.1, it is seen that not much fuel has been used after fulfilling the entire mission. One other observation is that the requirement of total flight of the three 'flight' segments should be ≤ 45 minutes, is just reached. The total time of the climb1, cruise and descent1 phase is 44.6 minutes. This together with the range of 135 nmi (250 km) has to be reached during these three phases. This also has been reached as the range (including range credit) is 250 km.

Table 13.1: The distance, time, weights of the Reference mission per mission phase

Phase	Time per phase [min]	Distance per phase [km]	Weight begin [kg]	Fuel Used [kg]	Weight end [kg]
Take-off	0.25	0.40	1253	0.35	1253
Climb1	4	12	1252	3.8	1249
Cruise	35	211	1249	16.2	1233
Descent1	5.6	27	1233	5.3	1227
Climb2	1.6	4.3	1227	1.6	1226
Loiter	47.3	N.A	1226	11	1215
Descent2	2.8	10	1219	2.6	1212
Landing	0.5	0.56	1212	0.4	1212
Total	97.0	265.3	N.A	41	N.A

Next to the reference mission, there was also the sizing mission. This mission had no time requirement, but only a range requirement of 250 nmi (463 km) over the same segments as for the reference mission. Then looking at Table 13.2, it can be noticed that the aircraft complies with that range requirement as the total distance over these segments is 460 km (251 nmi). Also, for this mission almost all the fuel is used. This indicates that the fuel that aircraft carries is not some dead weight.

Table 13.2: The distance, time, weights of the sizing mission per section

Phase	Time per phase [min]	Distance per phase [km]	Weight begin [kg]	Fuel Used [kg]	Weight end [kg]
Take-off	0.4	0.5	1434	1	1434
Climb1	6.6	20	1434	6	1427
Cruise	75	411	1427	41	1386
Descent1	8.2	34	1386	7	1378
Climb2	2.5	6.3	1378	2.5	1377
Loiter	47	N.A.	1377	16	1362
Descent2	3.8	12	1362	3.8	1358
Landing	0.5	0.6	1358	0.5	1357
Total	144	484	N.A	78	N.A

13.8. Performance Summary

Using the information provided in Section 13.4 to 13.6, the Table 13.3, 13.4 and 13.5 were generated. All the values are taken at MTOW. The take-off and landing distance were taken at sea level. The only elements that were not discussed before were the service and absolute ceiling. The service ceiling is the point where the ROC_{max} reaches a value of 0.5 m/s, while the absolute ceiling is where the aircraft cannot climb at all. These values can also be seen in Table 13.3.

Table 13.3: Climbing, cruise, take-off and landing performance

Parameter	MTOW Sea Level	MTOW Cruise Altitude
ROC_{max} [m/s]	9.2	3.4
γ_{max} [°]	15.4	13.0
ROD_{min} [m/s]	-3.5	-4.0
$\gamma_{glide,min}$ [°]	-7.0	-7.0
V_{max} [m/s]	94	101
V_{min} [m/s]	33.5	37.7
Service ceiling [m]	3662	
Absolute ceiling [m]	3883	
Take-off distance [m]	500	
Landing distance [m]	630	

Looking at Table 13.4 a few observations can be made. For example the smallest turn radius and turn time increase with altitude, and the maximum load factor and bank angle decrease with an increase in altitude. This is logical, since the thrust decreases with altitude[21]. Also, the velocity where the minimum or maximum occurs, will increase for the same reason. The last thing that was noted is that the the corresponding velocities are in the order that was mentioned in Section 13.6.

Table 13.4: Special turning performance

Parameter	MTOW at sealevel	Corresponding velocity [m/s]	MTOW at cruise altitude	Corresponding Velocity [m/s]
Minimum turn Radius [m]	178	64	230	69
Minimum time to turn 180° [s]	8.5	73	10	76
Maximum Load factor	3.1	85	2.8	87
Maximum bank angle	72	85	68	87

The last table that will be discussed will be Table 13.5. This table shows the standard turning performance. Three standard turn rates were devised as inputs and with the equations in Section 13.6. The velocity for the equations was taken to be cruise speed.

Table 13.5: Standard turn rate performance

Turn rate	Turn Radius [km]	bankangle [°]
Rate 1/2	3.5	13.8
Rate 1	1.7	26.3
Rate 2	0.88	44

13.9. Performance Verification & Validation

The values in this chapter were all verified by different kinds of methods. The code developing these calculations was read through and verified by various engineers. Also, the values found were compared to reference aircraft and were deemed logical. The same yields to the plotting of certain figures. For example looking at Figure 13.3 and some pictures in literature [21] [22], a comparison was made and the pictures were quite similar.

Validation however, is a lot harder to perform at this stage of the design. Most of the validation will happen during an actual flight test. Until actual testing can be performed the values in this chapter are just theoretical.

14

Control & Stability

This chapter explains the control surface designs and their effectiveness. Firstly the control surface actuation is discussed, then in Section 14.2 the aileron design procedure is explained. Further, in Section 14.3 the design of the tail is considered including the procedure of making the potato and scissor plots. Then the vertical tail sizing is explained in Section 14.5. Finally, in Section 14.6 the dynamic stability is analysed.

14.1. Control Surface Actuation

There are multiple methods of actuating the control surfaces of an aircraft, the most notable difference is between manual mechanical operation and (semi-)computerized operation (fly-by-wire). Both should not have any single point of failure (SPOF) in either hardware or software.

Whereas conventional mechanical operation of the control surfaces is still the standard in smaller aircraft, fly-by-wire offers advantages over it for system mass, redundancy and ease-of-operation. Furthermore, while at this point a pilotless aircraft is not investigated further due to regulatory limitations, a fully redundant fly-by-wire system makes the aircraft ready for such an implementation in the future. A downside of fly-by-wire is the required investment in software, due to added complexity in fault detection and mitigation, as well as certification of the system.

14.1.1. Flight Control Redundancy

The first step in making the control system compliant with regulations is to eliminate SPOFs. This entails all critical hardware like sensors, power lines, data lines, actuators and computers as well as in software. By combining multiple sensors, predicting their expected values and filtering their inputs accordingly, the flight computer determines its location, attitude and path with accuracy and redundancy [23].

14.1.2. Power-by-wire Redundancy

As the aircraft has a redundant low power source, as described in Section 10.6, a power-by-wire implementation makes sense. Power lines of the 28VDC system already run through the aircraft to numerous components, making it possible to combine their function with the actuation of control surfaces. It is suggested to have a redundant power and data path to each critical component, so at least two paths between the power source and component and flight controller and component should be available.

14.1.3. Actuator Redundancy

Using two undersized actuators per control surface and utilizing a clutch to decouple a failing actuator makes it possible to have a weight efficient solution at the cost of operating with limited deflection capabilities. Actuators with magnetic clutches are readily available and have been demonstrated in fly-by-wire systems on smaller aircraft [24].

14.2. Aileron Design

Ailerons are essential to the roll ability of the aircraft; other options are flaperons and elevons, but as mentioned in [3], these have been discarded. To design a proper aileron, one first has to know the requirements. The aircraft roll requirement is established by FAA regulations and for performance level: low speed (small, light aircraft); the roll rate of such an aircraft has to equal 60 degrees in 1.3 seconds at 1.2 times the stall speed. [1] Firstly, the aileron control derivative is calculated in Equation 14.1:

$$C_{l_{\delta a}} = \frac{2 \cdot c_{l_\alpha} \cdot \tau}{S_{ref} \cdot b} \cdot \int_{b_1}^{b_2} c(y) \cdot y dy \tag{14.1}$$

In which c_{l_α} equals the airfoil lift curve slope, τ the aileron effectiveness (which is a function of the ratio of the aileron chord to the wing chord), S_{ref} the wing surface, b the wingspan, b_1 the distance to the starting point of the aileron (measured from the root) and b_2 the end point of the aileron. The end point of the aileron is chosen to be at the wingtip, with an adjustable margin between the wingtip and the end point of the aileron. The aileron effectiveness, τ is taken to be 0.5, which corresponds to an aileron chord over wing chord ratio of 27%, which is realistic compared to reference aircraft [15]. Furthermore, y equals the distance measured from the root chord and $c(y)$ is the chord length as a function of y. Subsequently, the roll damping coefficient is calculated in Equation 14.2:

$$C_{l_p} = \frac{4 \cdot (c_{l_\alpha} + c_{d_0})}{S_{ref} \cdot b} \cdot \int_0^{b/2} y^2 \cdot c(y) dy \tag{14.2}$$

$$P = -\frac{C_{l\delta a}}{C_{l_p}} \cdot \delta a \cdot \frac{2 \cdot V}{b} \tag{14.3}$$

In which δa equals the maximum aileron deflection (in radians), which is set to be 25 degrees, if the aileron deflects more than that, flow separation starts to occur [15]. V equals $1.2 \cdot V_{stall}$ and P the roll rate. Knowing these values, the starting position of the aileron , b_1 and the aileron length can be calculated analytically, provided that the high lift devices and the aileron do not overlap. This gives an aileron length of 1.09 m.

14.3. Horizontal Tail

The stability and controllability curves of an aircraft are generated to design the horizontal tail and to position the wing along the fuselage. The design process is borrowed from the book "Synthesis of subsonic Airplane Design"[20]. The important parameters that are needed for this task are the CG excursion, cabin interior as well as tail cone length and type of tail.

[1] Legal information institute In *14 CFR 23.157 - Rate of roll.* Retrieved from `https://www.law.cornell.edu/cfr/text/14/23.157`, accessed on 13th of December.

14.3.1. Potato plot- X_{cg} Range

The potato diagram adjusts the center of gravity (CG) position along the fuselage of the operational empty weight (OEW) after adding the weight of passengers, cargo, battery and fuel. It provides a range of values along the MAC which would be the possible extreme front and aft CG positions.

14.3.2. Stability and Controllability

The aircraft must be defined such that it is stable enough to react to a disturbance by generating opposite pitching moment for going back to equilibrium. It also needs to be able to control the flight, so an effective balance between stability and controllability of the aircraft needs to designed. This is possible by creating the scissor plot.

The scissor plots are developed by plotting the stability and controllability curve over the leading edge position of MAC (X_{LEMAC}) over the fuselage length (X_{FUS}). The longitudinal stability is derived from the neutral point equation and is rewritten as Equation 14.4. The stability gradient accounts for down wash developed on the tail due to the wing. Similarly, the controllability gradient is achieved from the trim equation (Equation 14.5). The tail volume fraction for both equations are plotted against the CG position over the MAC in the figure Figure 14.4.

$$\frac{S_h}{S} = \frac{\bar{x}_{cg} - \bar{x}_{ac} + 0.05}{\frac{C_{L\alpha_h}}{C_{L\alpha_{A-h}}}\left(1 - \frac{d\varepsilon}{d\alpha}\right)\frac{l_h}{\bar{c}}\left(\frac{V_h}{V}\right)^2} \tag{14.4}$$

$$\frac{S_h}{S} = \frac{\bar{x}_{cg} - \bar{x}_{ac} + \frac{C_{mac}}{C_{L_{A-h}}}}{\frac{C_{L\alpha_h}}{C_{L\alpha_{A-h}}}\frac{l_h}{\bar{c}}\left(\frac{V_h}{V}\right)^2} \tag{14.5}$$

14.3.3. Tail Cone and Horizontal Tail Sizing

The next step taken for stability analysis is designing the tail of the aircraft. For this task, first the C.G. range was checked from the potato diagram (Figure 14.3) showing all possible CG locations. The OEW CG is assumed to be roughly around 37% of the MAC. Then the estimated CG range is plotted for varying leading edge position.

Furthermore, the preliminary sizing of parameters are defined from the class I estimate and the chosen airfoil: NACA 63-015A from reference aircraft [15]. With the inputs, stability and controllability curves are obtained. A stability margin of 5% is taken for the stability curve.

Now the two plots, are superimposed and analyzed whether the leading edge position is reasonable and that the horizontal tail area is not more than one quarter of the main wing area. Iterations are carried out by changing the arm between the two aerodynamic centers and shifting the vertical distance between the two wings. Small changes in the cabin and shifting the position of batteries or fuel are also explored if they are beneficial to the design a lighter aircraft. In addition, the team explored two configurations for the horizontal stabilizer: conventional and t-tail, as can be seen when looking at Figure 14.2 and Figure 14.1. A trade-off is done by comparing the tail weights by using statistical data [25], as well as comparing the horizontal tail surface. From the quantitative analysis, it turns out that the t-tail is heavier by roughly 2% while keeping almost the same surface area ratio as the conventional one. This is due to the fact that t-tail requires a stronger vertical stabilizer in order to carry the weight of the horizontal control surface. Secondly, the surface area ratios remain almost equal, thus no significant benefit is achieved. In addition, t-tail loses in the complexity criterion which has significant weight in the trade-off done in [3]. Finally, the t-tail is more

vulnerable for deep stall compared to the standard design option. Thus, final decision is made to use conventional tail located at the centroid of the fuselage.

The superimposed graph can be seen when looking at Figure 14.4. It yields a leading edge position at roughly 36% and surface area ratio of 0.244.

Figure 14.1: T-tail design

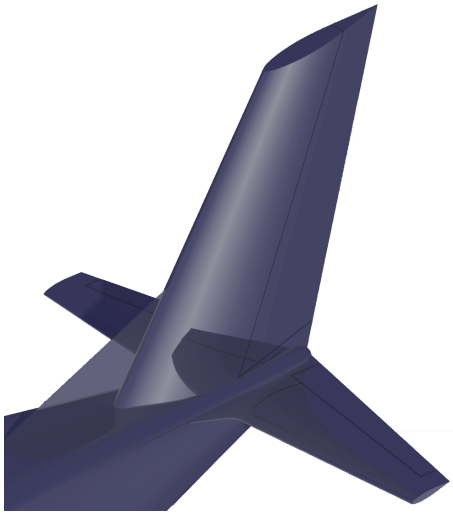

Figure 14.2: Conventional tail

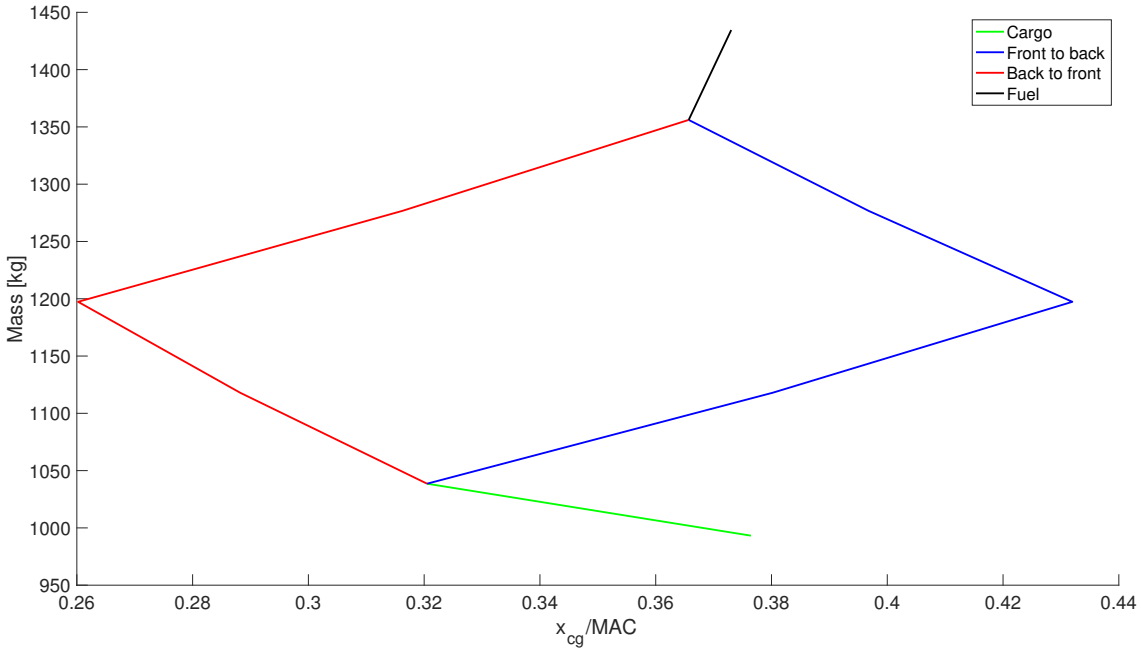

Figure 14.3: Potato diagram

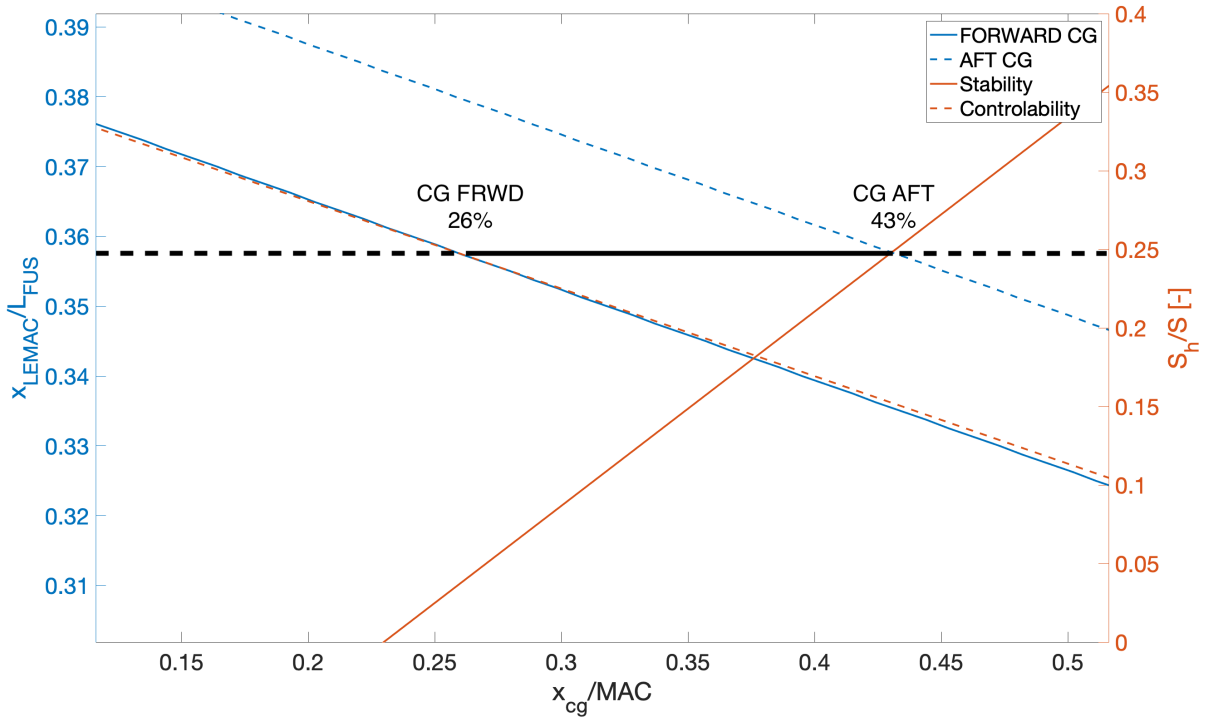

Figure 14.4: Scissor plot

14.4. Landing Gear Position

After having a fixed aircraft length and most importantly the CG excursion, the team could continue with the landing gear design. Firstly, a tire and suspensions system is chosen based on reference aircraft. The tire model should sustain the landing loads as well as being able to land on runaways which are not in perfect condition. The chosen dimensions are: 15x6.00-6 inch [1]. An oleo strut is chosen as a shock absorber for the aircraft. Next the longitudinal position of the landing gear is considered. The placement mainly depends on the most aft CG longitudinal and vertical position. The longitudinal position is known from the potato plot (Figure 14.3) and the vertical position estimation is done based on the weight fractions of different subsystems in relation to their position from the middle of the aircraft [25]. The gear is chosen to be positioned with a 16 degrees angle from the CG. Then a check is made for the angle between the landing gear and the tip of the tail cone, the so called scrape angle, to be less than 15 degrees. Adjusting the strut length until this condition is met resulted in the final design of the main landing gear. Regarding the lateral position, the track width of the main landing gear must be sufficiently wide to guarantee that the aircraft does not tip over during a sharp turn. For this a turn over angle 55 degrees is considered as suggested by Roskam [26]. Additionally, the landing gear provides 17 degrees clearance for the propellers not to hit the ground. On the other hand, the arm between the nose gear and the most aft CG is designed in such a way, that the nose gear could carry 7% of the total load [26]. The rest of the load is is carried by the main landing gear. The final dimensions can be seen at Figure 14.5.

[1] SkyGeek Aircraft Tires, accessed on 21-01-19, `https://www.skygeek.com/cirrus-tires.html`

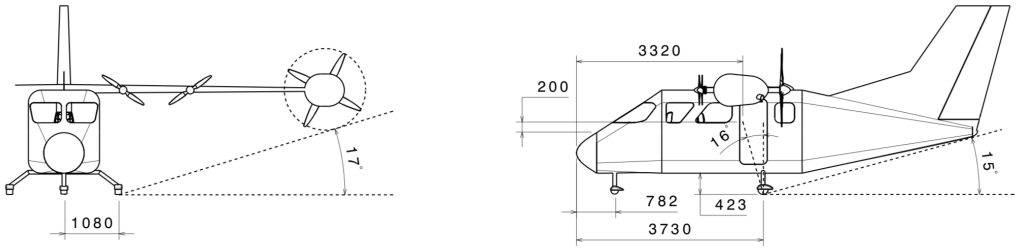

Figure 14.5: Dimensional 2D drawing of the side view

14.5. Vertical Tail Sizing

The vertical tail of an aircraft is essential to ensure directional stability. If the aircraft yaws into a certain direction, the free stream will flow at the vertical tail with an angle. This induces force on the vertical tail plane.

If the vertical tail is placed behind the CG, it forces the airplane back to its stable direction and $C_{N\beta}$, or the weathercock stability, (the change in the yawing moment due to a change in side slip) will be positive. Because the horizontal wing has no quarter chord sweep, the contribution to $C_{N\beta}$ of the wing and horizontal stabilizer, are very small and thus neglected [27].

To size this vertical tail, several requirements are to be taken into account, namely:

- According to the control requirement: The aircraft should still be able to be controllable if one of the two main engines fails [2]. If only one of the two main engines is functional, a yawing moment is caused. The rudder should be able to counteract this moment. This moment is highest during take off, when the operative engine has its greatest force.
- According to stability requirement: As mentioned above, the vertical tail should be able to return the aircraft to directional stability. According to Roskam II[28], the $C_{N\beta}$ should be at least 0.001 $\frac{1}{deg}$, or 0.0571 $\frac{1}{rad}$.

Both of these requirements will give a vertical tail plane area. The larger of the two surfaces is chosen.

Because the aircraft is designed to have the two main engines at the wing tips (to increase the passenger comfort by decreasing the noise the passengers experience and for use of tip vortices) the yawing moment is relatively large. One can foresee that that the control requirement is going to be determining, nevertheless both calculations will be shown.

The moments that act on the aircraft when one engine fails are shown in Equation 14.6 and Equation 14.7.

$$N_E = \frac{T_{TO}}{n_E} \cdot y_E \tag{14.6}$$

$$N_D = 0.75 \cdot N_E \tag{14.7}$$

$$N_V = N_E + N_D \tag{14.8}$$

With N_E being the moment caused by the thrust of the operative engine, T_{TO} being the total engine thrust (which is

[2] Legal information institute In *14 CFR 23.2135 - Part 23—airworthiness standards: Normal category airplanes* Retrieved from `https://www.ecfr.gov/cgi-bin/text-idx?SID=1882f767fcbf77385be9d4d383329693&mc=true&node=pt14.1.23&rgn=div5`,m accessed on 18th of January 2019.

highest at takeoff), n_E the numbers of main engines, y_E, the distance from the engine to the plane of symmetry, N_D being the the moment caused by the drag of the inoperative engine. It is assumed that the moment caused by engine failure is to be compensated solely by rudder deflection and without side slip angle [29]. The moment caused by the rudder deflection is calculated by Equation 14.9.

$$N_V = \frac{1}{2} \cdot \rho \cdot V_{MC}^2 \cdot \delta_F \cdot \left(\frac{c_{L,\delta}}{(c_{L,\delta})_{theory}}\right) \cdot (c_{L,\delta})_{theory} \cdot K' \cdot K_\Lambda \cdot S_V \cdot l_V \tag{14.9}$$

In which ρ equals the air density at takeoff height, which equals 1.225, V_{MC} the minimum control speed, which equals $1.2 \cdot V_{stall}$, δ_F the maximum rudder deflection, which equals 25 degrees, after which flow separation starts to play a significant role, $\left(\frac{c_{L,\delta}}{(c_{L,\delta})_{theory}}\right)$, $(c_{L,\delta})_{theory}$ and K' being functions extracted from DATCOM 1978, which are functions of $\frac{c_f}{c}$, which is assumed to be 35% from reference aircraft [30], and t/c, which equals 15%, as the airfoil chosen for the vertical tail is the NACA 63-015A taken from reference aircraft [15]. Furthermore, K_Λ (from DATCOM 1978) is a function of the quarter chord sweep, which is taken to be 35 degrees from reference [15]. Furthermore, S_V is the vertical tail surface and l_V the distance between the CG of the aircraft and the center of the vertical tail plane. When combining Equation 14.8 and equation Equation 14.9, S_V can be calculated by Equation 14.10.

$$S_V = \frac{N_E + N_D}{\frac{1}{2} \cdot \rho \cdot V_{MC}^2 \cdot \delta_F \cdot \left(\frac{c_{L,\delta}}{(c_{L,\delta})_{theory}}\right) \cdot (c_{L,\delta})_{theory} \cdot K' \cdot K_\Lambda \cdot l_V} \tag{14.10}$$

For the stability requirement, the Equation 14.11 is calculated.

$$S_V = \frac{C_{N,\beta} - C_{N,\beta,F}}{-C_{Y,\beta,V}} \cdot \frac{b_w}{l_V} \cdot S_W \tag{14.11}$$

With $C_{N,\beta}$ being 0.0571 $\frac{1}{rad}$ as mentioned above. $C_{N,\beta,F}$ can be estimated using Equation 14.12 from DATCOM 1978:

$$C_{N,\beta,F} = \frac{-360}{2 \cdot \pi} \cdot k_N \cdot k_{R,l} \cdot \frac{l_f^2 \cdot d_F}{S_W \cdot b} \tag{14.12}$$

With l_F being the fuselage length, d_F being the approximated fuselage diameter (height of fuselage + width of fuselage divided by two), S_W the wing surface area, b the wingspan and k_N being defined in Equation 14.13.

$$k_N = 0.01 \cdot \left[0.27 \cdot \frac{x_m}{l_F} - 0.168 \cdot ln\left(\frac{l_F}{d_F}\right) + 0.416\right] - 0.0005 \tag{14.13}$$

in which x_m is the length from the nose to the CG and $k_{R,l}$ being defined inEquation 14.14.

$$k_{R,l} = 0.46 \cdot log\left(\frac{Re}{10^6}\right) + 1 \tag{14.14}$$

$C_{Y,\beta,V}$ being defined as $-(C_{L\alpha})_V$ which is shown in Equation 14.15

$$(C_{L\alpha})_V = \frac{2 \cdot \pi \cdot A_v}{2 + \sqrt{\frac{A^2 \cdot \beta^2}{\kappa^2} \cdot \left(1 + \frac{tan(\theta_{50})^2}{\beta^2}\right) + 4}} \tag{14.15}$$

In which θ_{50} is the sweep at half the chord length, A_v the aspect ratio of the vertical tail from reference aircraft, which equals 1.5 [15] [11] and β being defined as in Equation 14.16 and κ in Equation 14.17.

$$\beta = \sqrt{1 - M^2} \tag{14.16}$$

$$\kappa = \frac{c_{L,\alpha}}{2 \cdot \pi / \beta} \tag{14.17}$$

This gives the following parameters:

Table 14.1: Rudder parameters

S_v	c_{root}	c_{MAC}	c_{tip}	b_v	Λ_{LE}	Taper ratio
4.18 m^2	2.15 m	1.67 m	1.07 m	2.51 m	35°	0.5

A 2-dimensional view including dimensions is given in Figure 14.6.

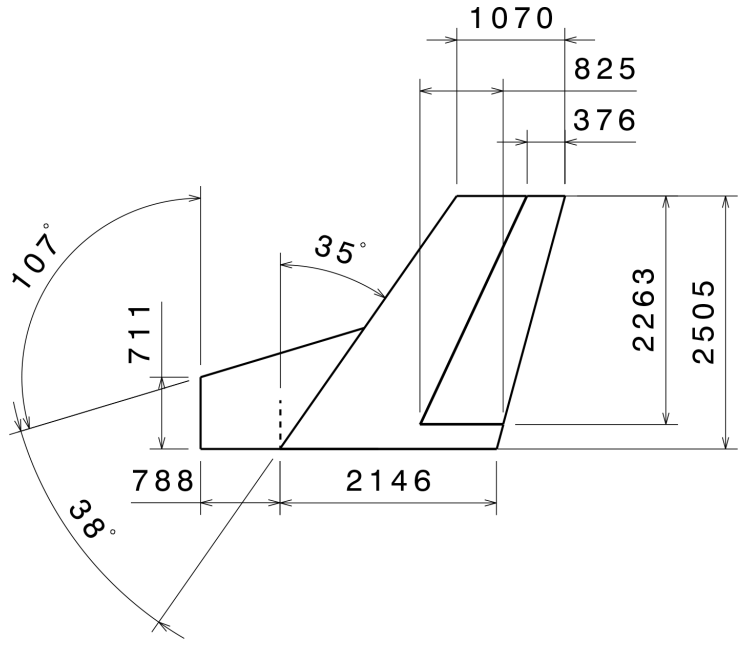

Figure 14.6: Dimensional 2D drawing of the vertical tail

It is assumed that the aircraft will be able to recover from spin if $\frac{2}{3}$ of the vertical tail plane is out of the wake of the horizontal tail (which is assumed to be induced at 60 degrees [15]) [30]. Because the vertical tail plane is on the relatively large, this requirement is met by inspection.

The rudder is taken to be 35% of the chord along the vertical wingspan as mentioned above. The rudder span, however is taken to equal the vertical wing span, according to reference aircraft [15].

As can be observed in 14.1, the vertical tail has a sweep. This is due to multiple reasons, namely:

- The arm between the lateral force and the CG is increased.
- A larger part of the vertical tail plane is outside the wake of the horizontal stabilizer.
- Vertical tail sweep causes the critical side slip angle β_{crit} to be increased, at expense of the lateral force created

on the vertical tail plane, and thus C_{Nmax}. This means that the vertical tail stays effective at a longer range of side slip, but its stability is decreased.

A dorsal fin is added to avoid the loss of the lateral force component, by which the turning stability, C_{Nmax} is increased [31].

14.6. Dynamic Stability

As a final step in the stability analysis of the aircraft, a rough dynamic stability study is done. Before starting any calculations some of the most important assumptions are stated in order to clarify the model used. The main ones are [27]:

- Steady, horizontal, symmetric flight is used for calculating the aerodynamic coefficients
- The aircraft is a rigid structure
- The thrust vector is in the x-z plane
- The moment of inertia is zero around 2 axes depending on the motion

The reference system used for this analysis can be seen when looking at Figure 14.7

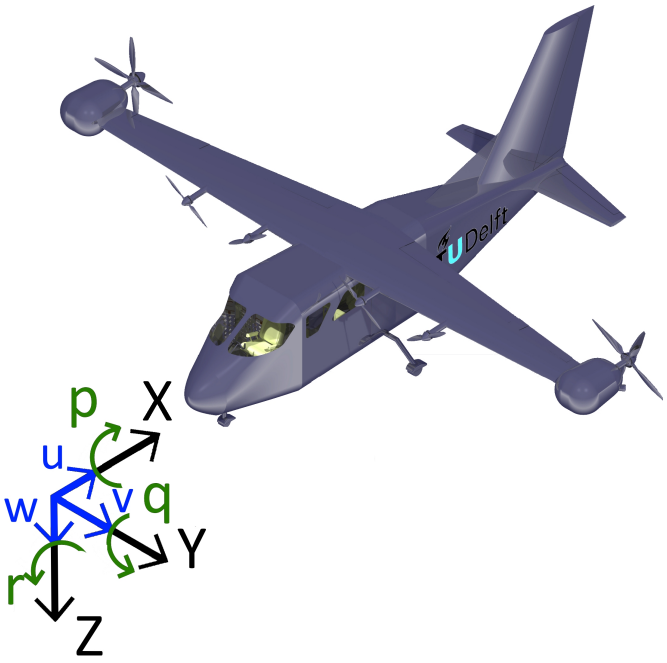

Figure 14.7: Axis system used for dynamic analysis

Assuming these conditions, the team decided on using Digital Datcom as the program for determining the control derivatives of the aircraft [1]. A simple input file is created including basic geometry properties such as surface areas and position of control surfaces, fuselage geometry, CG excursion and the like. The output of the Digital Datcom program represents all asymmetric derivatives needed for solving matrix 14.19 regarding the three asymmetric motions: aperiodic roll, dutch roll and spiral. On the other hand, an analytical approach is taken for determining the missing control derivatives for the analysis of symmetric motions, such as short period and phugoid. The formulas are taken from "Flight Dynamics"[27].

[1] Digital Datcom (USAF), accessed on 15-01-19, `http://www.pdas.com/datcomDescription.html`

Beginning with the symmetric Matrix 14.18 and asymmetric Matrix 14.19 one can start simplifying the two matrices to simple equations which result in the wanted eigenvalues.

$$\begin{bmatrix} C_{X_u}-2\mu_c D_c & C_{X_\alpha} & C_{Z_0} & 0 \\ C_{Z_u} & C_{Z_\alpha}+(C_{Z_{\dot\alpha}}-2\mu_{h_c})D_c & -C_{X_0} & C_{Z_q}+2\mu_c \\ 0 & 0 & -D_c & 1 \\ C_{m_u} & C_{m_\alpha}+C_{m_{\dot\alpha}} & 0 & C_{m_q}-2\mu_c K_Y^2 D_c \end{bmatrix} \begin{bmatrix} \hat{u} \\ \alpha \\ \theta \\ \frac{q\bar{c}}{V} \end{bmatrix} = \begin{bmatrix} -C_{X_{\delta_e}} & -C_{X_{\delta_t}} \\ -C_{Z_{\delta_e}} & -C_{Z_{\delta_t}} \\ 0 & 0 \\ -C_{m_{\delta_e}} & -C_{m_{\delta_t}} \end{bmatrix} \begin{bmatrix} \delta_e \\ \delta_t \end{bmatrix} \tag{14.18}$$

$$\begin{bmatrix} C_{Y_\beta}+\left(C_{Y_{\dot\beta}}-2\mu_b\right)D_b & C_L & C_{Y_p} & C_{Y_r}-4\mu_b \\ 0 & \frac{-D_b}{2} & 1 & 0 \\ C_{l_\beta} & 0 & C_{l_p}-4\mu_b K_{XX}^2 D_b & C_{l_r}+4\mu_b K_{XZ} D_b \\ C_{n_\beta}+C_{n_{\dot\beta}}D_b & 0 & C_{n_p}+4\mu_b K_{XZ} D_b & C_{n_r}+4\mu_b K_{ZZ}^2 D_b \end{bmatrix} \cdot \begin{bmatrix} \beta \\ \varphi \\ \frac{pb}{2V} \\ \frac{rb}{2V} \end{bmatrix} = \begin{bmatrix} -C_{Y_{\delta_a}} \\ 0 \\ -C_{l_{\delta_a}} \\ -C_{n_{\delta_a}} \end{bmatrix} \cdot \delta_a + \begin{bmatrix} -C_{Y_{\delta_r}} \\ 0 \\ -C_{l_{\delta_r}} \\ -C_{n_{\delta_r}} \end{bmatrix} \cdot \delta_r \tag{14.19}$$

Following the method described in "Flight Dynamics" [27], which is applying various assumptions in order to simplify the matrices, one can obtain the following set of equations regarding each eigenmotion.

Short Period

$$\begin{bmatrix} C_{Z_\alpha}+(C_{Z_{\dot\alpha}}-2\mu_c)\lambda_c & C_{Z_q}+2\mu_c \\ C_{m_\alpha}+C_{m_{\dot\alpha}}\lambda_c & C_{m_q}-2\mu_c K_Y^2 \lambda_c \end{bmatrix} \cdot \begin{bmatrix} \alpha \\ \frac{q\bar{c}}{V} \end{bmatrix} = 0 \tag{14.20}$$

Phugoid

$$\begin{bmatrix} C_{X_u}-2\mu_c\lambda_c & C_{Z_0} & 0 \\ C_{Z_u} & 0 & 2\mu_c \\ 0 & -\lambda_c & 1 \end{bmatrix} \cdot \begin{bmatrix} \hat{u} \\ \theta \\ \frac{q\bar{c}}{V} \end{bmatrix} = 0 \tag{14.21}$$

Aperiodic roll

$$C_{l_p}-4\mu_b K_{xx}^2 \lambda = 0 \tag{14.22}$$

Dutch roll

$$\begin{bmatrix} C_{Y_b}-2\lambda\mu_b & -4\mu_b \\ C_{nb} & C_{nr}-4K_Z^2\mu_b\lambda \end{bmatrix} \cdot \begin{bmatrix} \beta \\ \frac{rb}{2V} \end{bmatrix} = \begin{bmatrix} 0 \\ 0 \end{bmatrix} \tag{14.23}$$

Spiral

$$\lambda_{b_4} = \frac{2C_L(C_{l_\beta}C_{n_r}-C_{n_\beta}C_{l_r})}{C_{l_p}(C_{Y_\beta}C_{n_r}+4\mu_b C_{n_\beta}-C_{n_p}(C_{Y_\beta}C_{l_r}+4\mu_b C_{l_\beta}} \tag{14.24}$$

The results from solving the matrices and the handling qualities [32] can be seen in Table 14.2 and the plotted eigenvalues can be seen in Figure 14.8. The results yield that the aircraft is dynamically stable in all motions.

Table 14.2: Dynamic Stability Results Summary

	Eigenvalue [-]	**Damping Ratio [-]**	$T_{1/2}$ **[s]**	**P [s]**	**Handling Quality**
Short Period	-2.23 + 1.51i	0.82	0.0035	0.04	Level 1
Phugoid	-0.0001 + 0.14i	0.001	52	0.47	Level 2
Aperiodic Roll	-3.32	[-]	0.02	[-]	Level 1
Dutch Roll	-0.78 + 2.98i	0.26	0.10	0.03	Level 1
Spiral	-0.063	[-]	1.12	[-]	Level 1

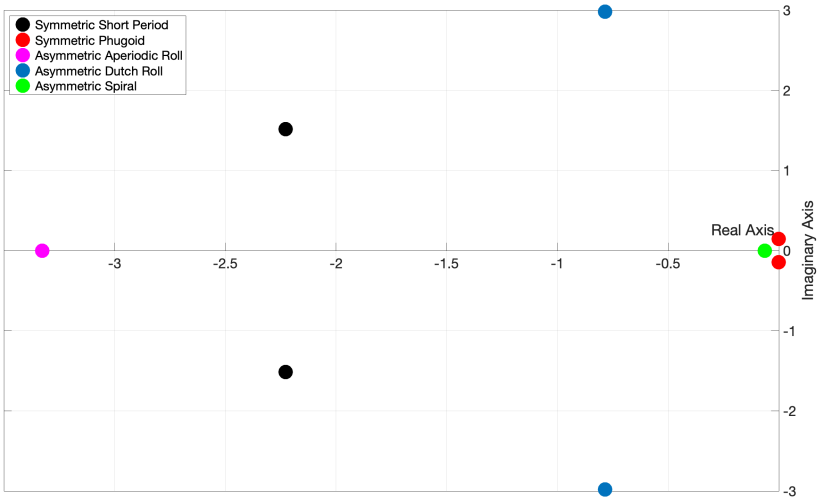

Figure 14.8: Eigenvalues plot

Results and Verification

The results also seem too unrealistic for many of the motions, such as the short period and spiral for example. Some of the reasons why such improbable results appear might be because the input for the Digital Datcom is not detailed enough. In addition, the program itself is only used for very rough approximations. Then, mixing the software approach with analytic formulas also introduces discrepancies in the model, on top of all the simplifications that are made in order to get to the simple matrices stated above. The moment of inertia is also just a rough approximation from the CAD model of the aircraft, which also introduces errors. As a conclusion, this analysis is done only for an initial look to see whether the aircraft is dynamically stable and to have a general idea of its handling qualities. Since CFD analysis and actual flight tests need to be done in order to verify the model, the accuracy of the current results should be used only for a very rough check whether the wing and tail design can provide some dynamic stability.

15

Aircraft Geometry

This chapter is dedicated to visualize the design of the aircraft and show the weight breakdown. The design has been modelled in the 3D modeling software CATIA V5 [33]. Firstly, in Section 15.1 the interior design is explained and visualized. Secondly, in Section 15.2 3D renders are displayed after which in Section 15.3 2D drawings are displayed giving relevant dimensions. Finally, in Section 15.5 the weight and balance of the aircraft is discussed.

15.1. Internal layout

The cabin and cockpit are designed using an inside out approach. This means it is sized based on the internal space required by passengers and cargo and that the cabin is designed around this required space. In Figure 15.1 an isometric view of the cabin is shown, while in Figure 15.2 a 2D drawing of the interior design is depicted including dimensions. In these figures, it is visible that the seats are facing each other and that the pilot can access his seat through the aisle between the two rear-facing seats. The market analysis showed that for the target audience, seats facing each other are preferred. A luggage storage compartment is also present in the cabin, which is also accessible in-flight. Heating ventilation and air-conditioning (HVAC) (from Figure 11.1) is used to maintain the temperatures of the cabin to 20°for a comfortable travel experience.

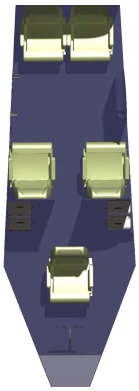

Figure 15.1: Render of the interior design of the aircraft

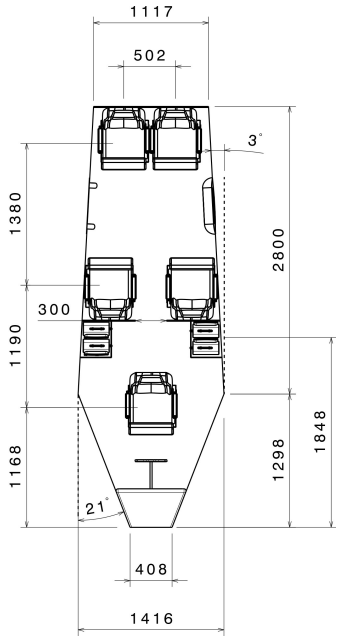

Figure 15.2: Internal layout of the aircraft including dimensions

15.2. Three-Dimensional Aircraft

Now that the geometry of the aircraft has been designed a detailed computer aided design can be made. As stated in the chapter introduction above CATIA V5 from Dassault Systemes has been used as this design software is considered an aerospace standard [33]. In Figure 15.3 the isometric view can be observed. Then in Figure 15.4, Figure 15.5 and Figure 15.6 the top-, side- and front view are shown.

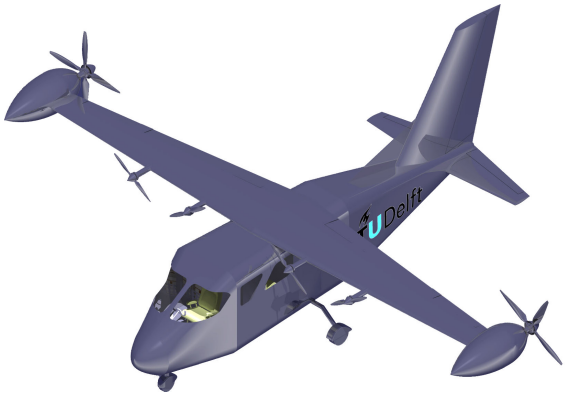

Figure 15.3: Isometric view of the aircraft

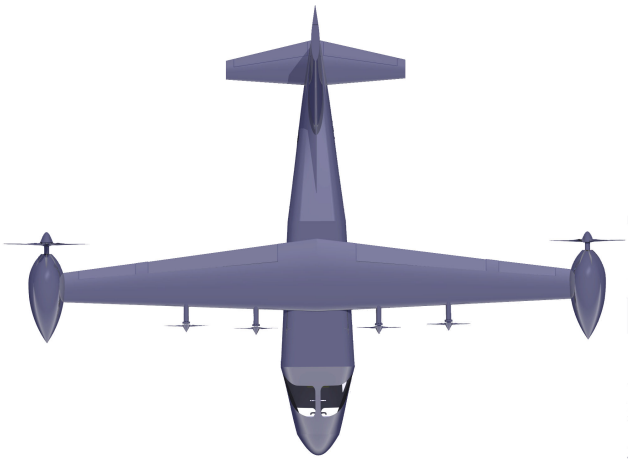

Figure 15.4: Top view of the aircraft

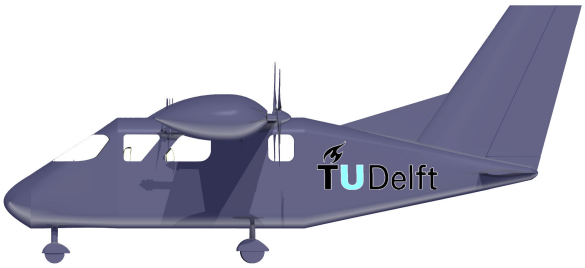

Figure 15.5: Side view of the aircraft

Figure 15.6: Front view of the aircraft

15.3. 2D Drawings

In order to clearly indicate the dimensions of the aircraft, a 2D engineering drawing has been made. To ensure readability the 2D drawings are presented on a sheet of A3 paper. All dimensional values are indicated in mm and all angle dimensions are indicated in degrees.

Top view
Scale: 1:60

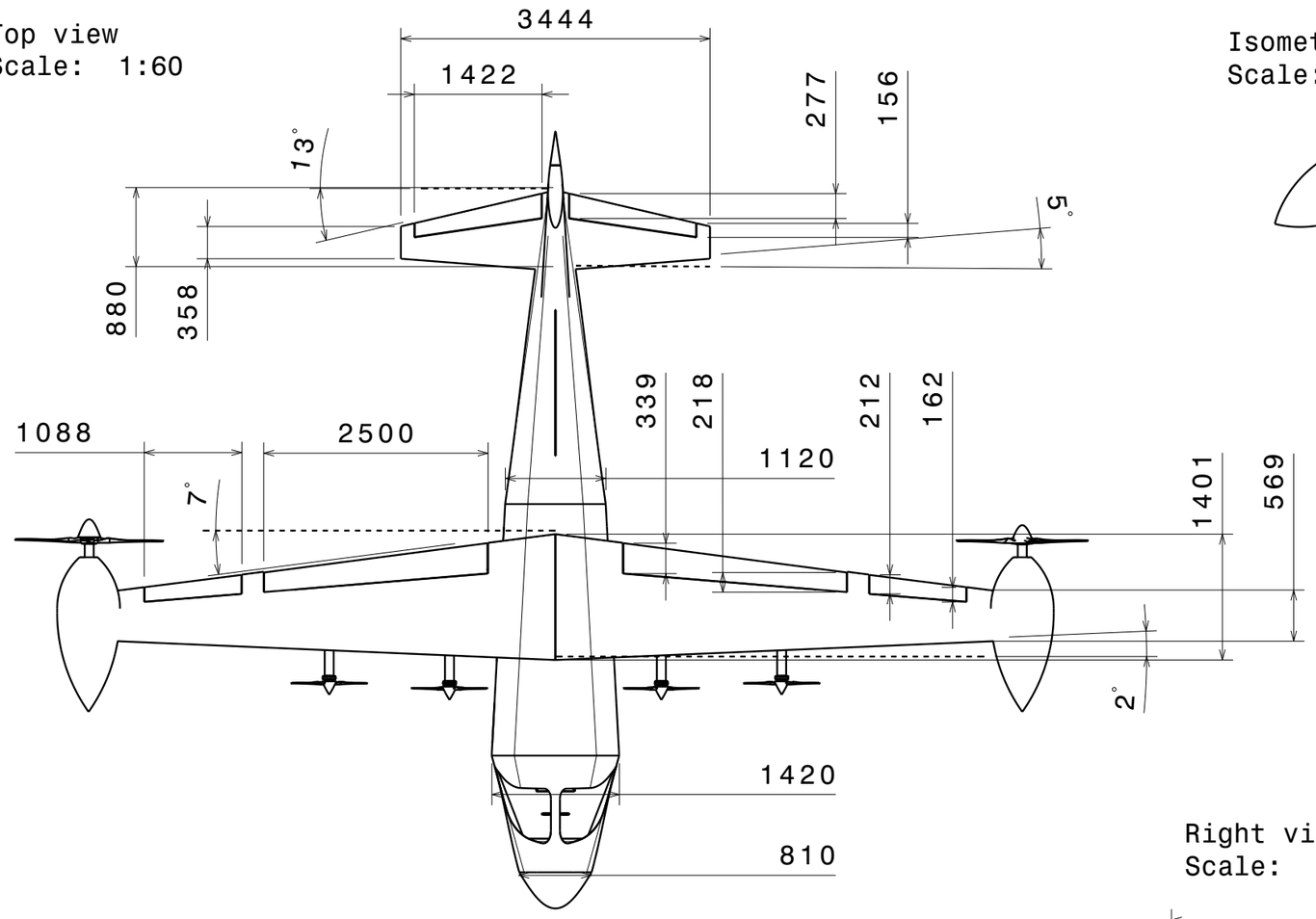

Isometric view
Scale: 1:60

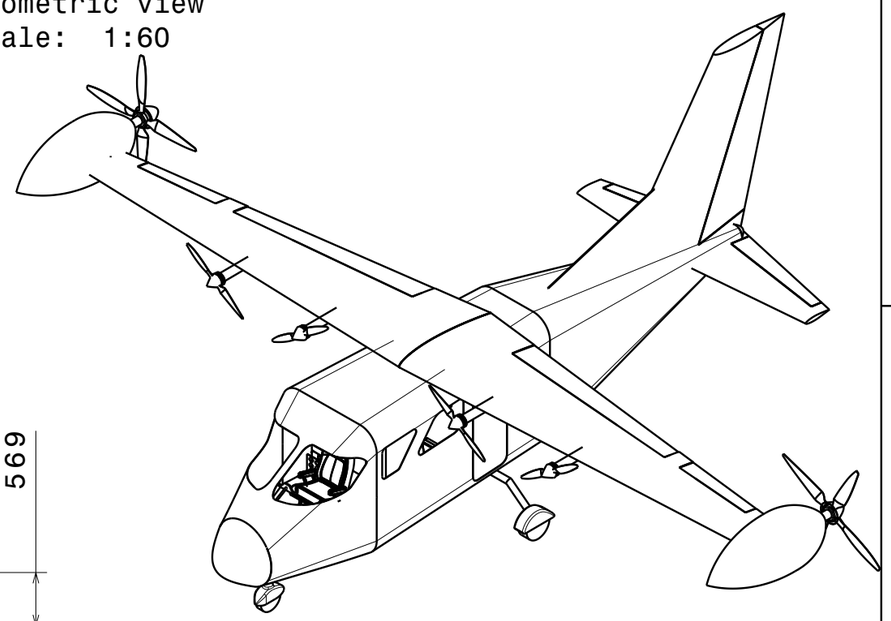

Front view
Scale: 1:60

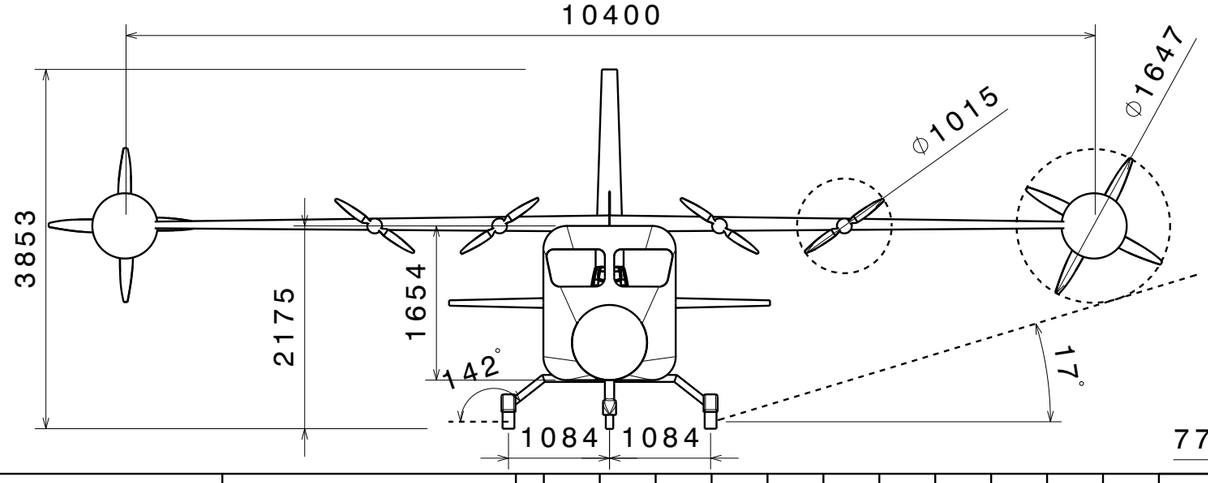

Right view
Scale: 1:60

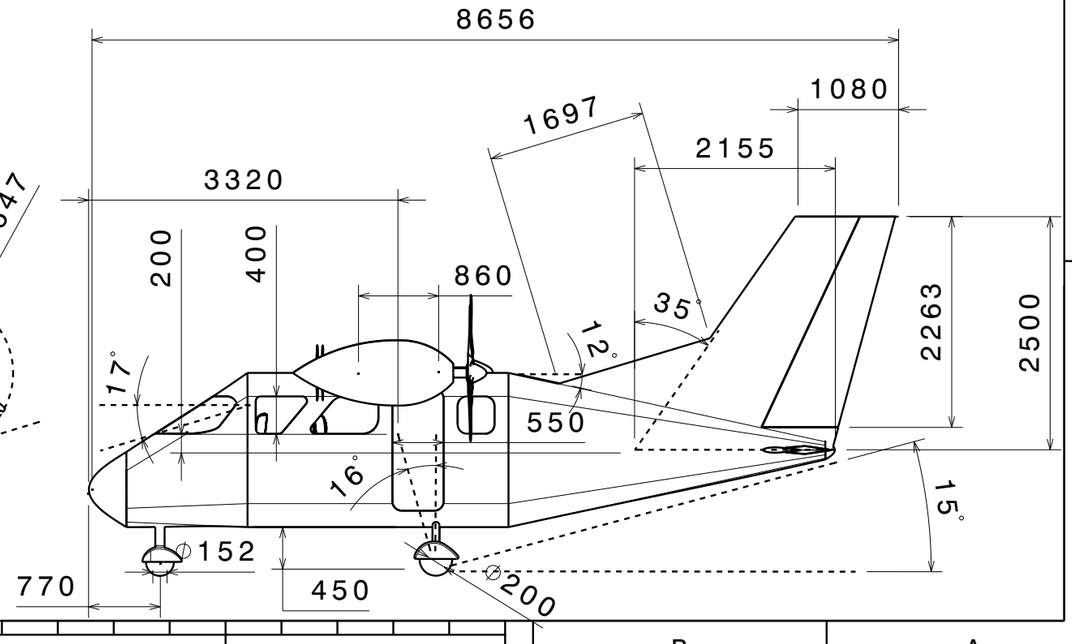

15.4. Weight breakdown

This section is dedicated to state the weight breakdown, it can be seen in Figure 15.7. The pilot is assumed to be included in and the wing is excluded from the OEW.

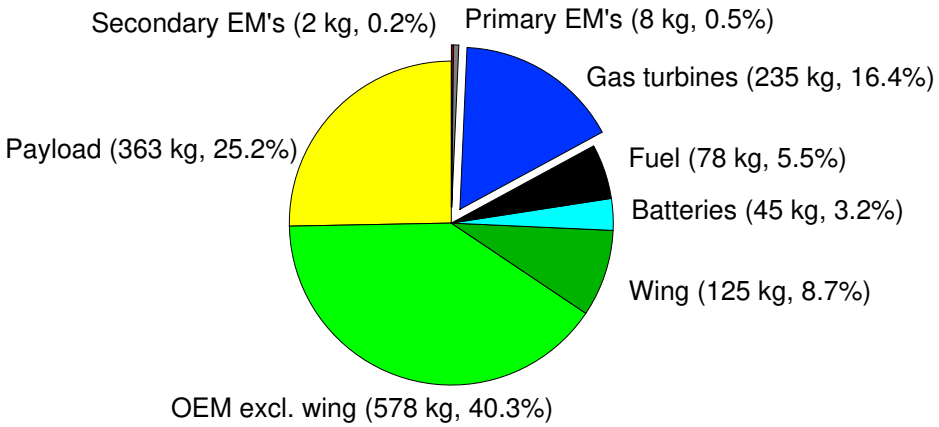

Figure 15.7: Weight breakdown

15.5. Weight & Balance

The weight and balance of the aircraft with full payload is shown in Table 15.1. All the arms are taken from the nose. In the end the total moment around that point will be divided by the mass to get the X_{CG}. The pilot is not included in this weight and balance since it was assumed that the pilot is part of the OEW. The c.g. of the OEW is thus including the pilot. In the end the X_{CG} was found to be 3.2 meters from the nose. For the zero-fuel mass, the moment and arm are added to the OEW. The same yields for the ramp mass, but then instead of payload the fuel is added. The center of gravity of the OEW can be found in Subsection 14.3.1 and Figure 14.3.

Table 15.1: Weight and balance of the aircraft with full payload

Payload Computations				**Mass and balance computations**		
Crew and passengers	**Arm [m]**	**Mass [kg]**	**Moment [Nm]**	**Item**	**mass [kg]**	**Moment [Nm]**
Passenger row 1 left	2.721	79.3	2116	**OEW**	993	31746
Passenger row 1 right	2.721	79.3	2116	**Payload**	363	10654
Passenger row 2 left	4.063	79.3	3160	**Zero Fuel mass**	1356	42400
Passenger row 2 right	4.063	79.3	3160	**Fuel**	79	2593
Luggage	2.242	45.3	102	**Ramp mass**	1435	44993
Total Payload		363	10654	**X_{CG} [m]**		3.2

16

Structures

In this chapter, the structural analysis of the aircraft will be shown. First, a trade-off will be made in order to decide on the best material in Section 16.1. Secondly, in Section 16.2 the wingbox shall be elaborated on. Finally, the structure of the fuselage shall be determined in Section 16.3. In order to be able to obtain the preliminary structural characteristics of the aircraft, some assumptions will be made in order to simplify solving the problems.

16.1. Materials

Since the aircraft will have to sustain strong loads, selecting the correct material is of utmost importance. Aluminum has been the go to choice for aircraft manufacturers for a long time, however, recently composites have fallen more and more into favor[1]. In this section, an analysis will be done with regards to the cost of each option. Finally, the material which has an optimal operational cost will be chosen.

The first of the considered options is a fiberglass epoxy based on the Cirrus SR22, a reference aircraft. This fiberglass epoxy has a material cost of 44 \$/kg, a yield strength of 206 MPa and a density of 1522 kg/m^3 [34]. This material is produced according to a wet lay-up molding process which combines layers of reinforced fiber with liquid resin to create a high quality laminar. Choosing this material will also reduce maintenance cost by eliminating metal fatigue and corrosion. Furthermore, much like many other composites, it has a reasonably low density. Additionally, there is also no need for fasteners.

The other material which is taken into consideration is Aluminum 6061 T-6. This is a material which commonly used in aircraft and has a material cost of 22 \$/kg. The yield stress is 241 MPa and the density is 2768 kg/m^3 [34]. Table 16.1 Shows an overview of the properties of the materials that are considered.

Table 16.1: Material properties

	σ_{yield} [MPa]	σ_{ult} [MPa]	ρ [kg/m^3]	Cost [\$/kg]
Fiberglass Epoxy	-	206	1522	44
Aluminum 6061-T6	241	290	2768	22

As can be seen in Table 16.1, aluminum performs superiorly to composites in every aspect, except for the density. Furthermore, aluminum also has a predictable failure mode because of its ductility. During strain, metals yield first,

[1]Aviation Outlook: Composites in General Aviation 2011-2020, accessed on 23-01-19, https://www.compositesworld.com/articles/aviation-outlook-composites-in-general-aviation-2011-2020

and only fail after significant additional strain. To the contrary, composites have a brittle failure mode which means that exceeding the stress limit of the material might have immediate disastrous consequences. Finally, aluminum also has a significantly lower engineering cost because of its isentropic characteristics. For example, it is much easier to perform a stress analysis for aluminum since the Von Mises criterion can be applied whereas it can not be applied for anisentropic materials such as composites[35].

On the other hand, composites have a strong cost advantage when it comes to maintainability. However, after having considered all these factors with regards to their cost in Chapter 17, it was decided that Aluminum 6061-T6 is the best material for the aircraft.

16.2. Wing Box

In this section the wing box will be designed. First, the load distribution will be obtained. Then, structural idealization with boom theory is used in order to perform the analysis as described in Megson [35]. The moments of inertia will be expressed in terms of the boom area, and chord length. Here, the chord length will vary along the wingspan as well as the boom area which will also vary along the wingspan. However, the boom area is assumed to be constant for each stiffener in the same section. For each cross section along the wingspan, the normal and shear stresses will be calculated in each boom. Afterwards, using the Von Mises stress criterion, the equation is solved for the boom area. The axis system that will be used for the wing box calculations is given in Figure 16.1. In order to give a clearer picture on the structural wing box calculations, an N2 chart has been made which can be seen in Figure 16.3. The cross section of the wing box can be found in Figure 16.2.

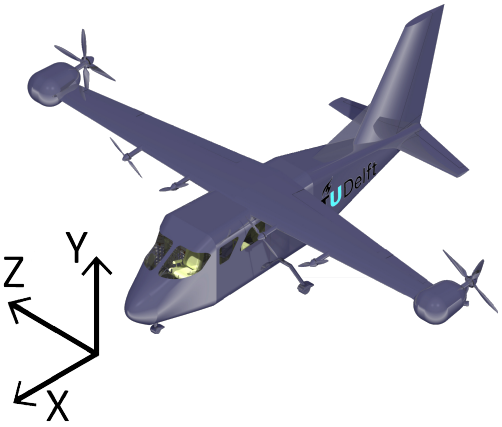

Figure 16.1: Axis System for the Wingbox Analysis

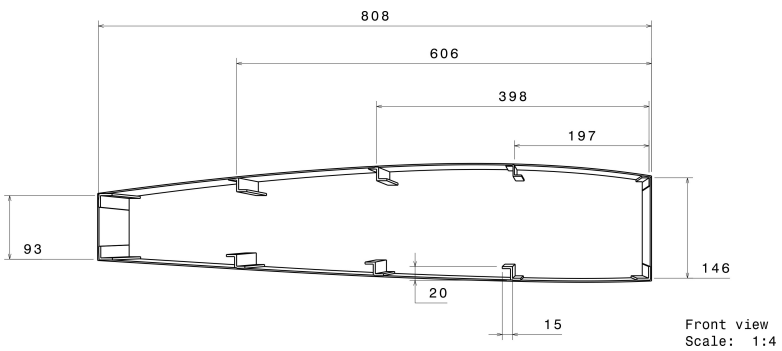

Figure 16.2: Wingbox cross section including dimensions

Initial Boom Area
X locations of booms
Y locations of booms
Enclosed Area
Skin thickness
Vertical Shear Force
Horizontal Shear Force
Bending moment around the X-axis
Bending moment around the Y-axis

Centroid Calculations	X Y					
	Inertia Calculations	Ixx Iyy Ixy	Ixx Iyy Ixy	Ixx Iyy Ixy		
		Shear Calculations			τxy	
			Torsion Calculations		τxy	
				Normal Stress Calculations	σz	
Boom Area					Von Mises Calculations	Boom Area
						Stiffener Calculations

Stiffener Area

Figure 16.3: N2 Chart of Wingbox Calculations

16.2.1. Assumptions & Load Distributions

During the structural analysis of the wing box a number of forces will have to be considered. The forces taken into consideration occur at the ultimate load factor of 4.4. In order to simplify the analysis, some assumptions will be made. First of all, as can be seen in Figure 15.7, the estimated wing weight equals less than ten percent of the lift, which is very small when compared to the final vertical force. Therefore, this force is neglected. Furthermore, the moment around the x-axis caused by the engine is neglected as well. Additionally, the drag acting on the wing is also neglected. Finally, the weight of the electric engines is neglected as well.

The loads for the lift are obtained from XFLR5, as are the loads for the torque. The loads caused by the weight and thrust of the engine are obtained from the engine characteristics Section 10.4.

This results in the free body diagrams shown in Figure 16.4 and Figure 16.5. Using these free body diagrams, two moment distributions and two shear distributions were obtained. These distributions were obtained after a discretization in order to eventually enable a numerical solution.

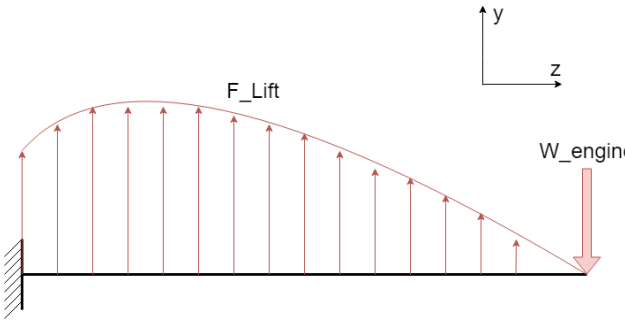

Figure 16.4: Free Body Diagram YZ Plane

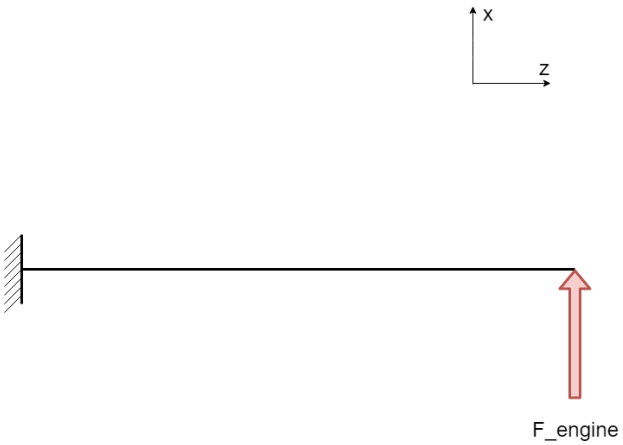

Figure 16.5: Free Body Diagram XZ Plane

With the loading distributions known, the shear force distributions are obtained as can be seen in Figure 16.6 and Figure 16.7. Evidently, the shear force distribution is X-direction is a simple horizontal line since only one force was considered. Subsequently, the bending moment distributions can be obtained as seen in Figure 16.8 and Figure 16.9.

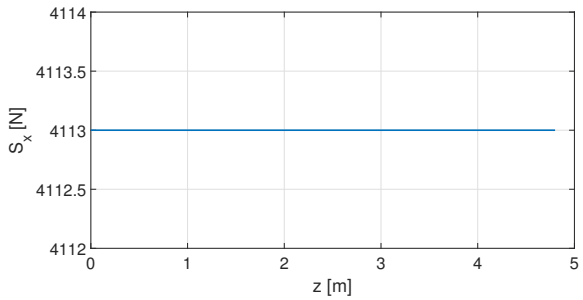

Figure 16.6: Shear force in X-direction

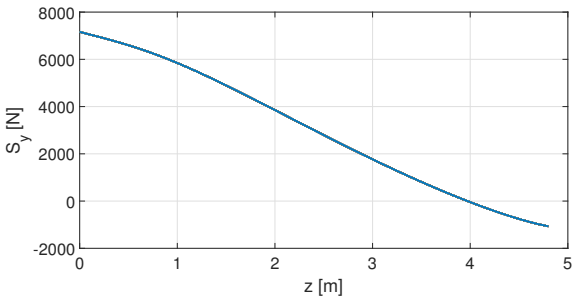

Figure 16.7: Shear Force in Y-direction

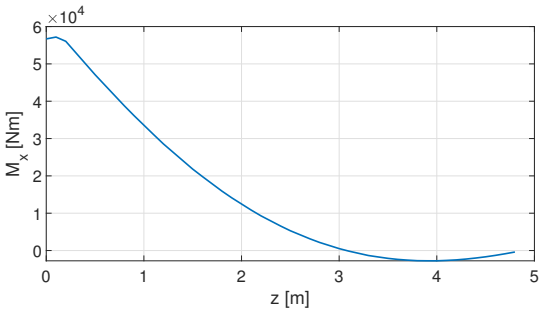

Figure 16.8: Bending Moment around the X-axis

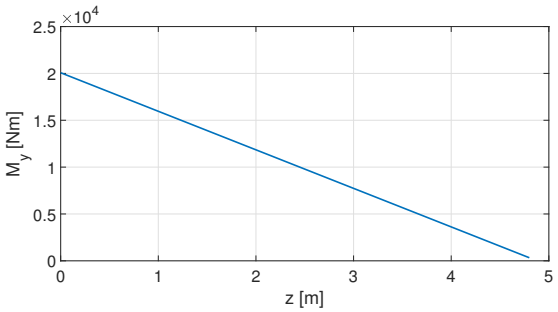

Figure 16.9: Bending Moment around the Y-axis

16.2.2. Wing Box Geometry

With the distributions known, the wing box geometry now has to be obtained in order to calculate the normal and shear stresses. In order to do so, it is assumed that the skin thickness is 0.5 mm. Preferably, the wing box should be strong enough to sustain all loads, while having as little mass as possible. In order to solve this problem, it is assumed that the wing box is idealized, with booms carrying normal stresses and webs carrying shear stresses as can be seen in figure Figure 16.2. However, it is not assumed that the wing box is symmetric along the y-axis, nor is it symmetric along the x-axis. This will complicate the calculation a bit, but not to an unmanageable extent. A further complication

will be that the wing box will taper, which will mean decreasing moments of inertia along the wingspan. The moments of inertia of the wing box are obtained as a function of the chord length and boom area as shown in Equation 16.2, Equation 16.1 and Equation 16.3. These moments of inertia are obtained as a function of the chord length and boom area.

$$I_{yy} = \Sigma_i^{10} A * x(i)^2 \quad (16.1) \qquad I_{xx} = \Sigma_i^{10} A * y(i)^2 \quad (16.2) \qquad I_{xy} = \Sigma_i^{10} A * x(i)y(i) \quad (16.3)$$

$$\sigma_z = \frac{(M_x I_{yy} - M_y I_{xy})y + (M_y I_{xx} - M_x I_{xy})x}{I_{xx} I_{yy} - I_{xy}^2} \quad (16.4)$$

$$q_s = -\frac{S_y I_{yy} - S_x I_{xy}}{I_{xx} I_{yy} - Ixy^2} \int_0^s tyds - \frac{S_x I_{xx} - S_y I_{xy}}{I_{xx} I_{yy} - Ixy^2} \int_0^s txds + q_{s0} \quad (16.5)$$

$$T = 2A_{encl} q \quad (16.6) \qquad \tau = \frac{q}{t} \quad (16.7) \qquad \sigma_{yield} = \sqrt{\sigma_z^2 + 3\tau_{xy}^2} \quad (16.8)$$

16.2.3. Stress analysis

The normal stress can be obtained from Equation 16.4, whereas the shear stress can be obtained from Equation 16.5. Finally, the shear stress due to torsion can be obtained from Equation 16.6. These three stresses are a function of the local chord length and the boom area. With the three stress forms known, the Von Mises stress analysis can now be applied according to Equation 16.8. With the material yield stress known, the required minimum boom area can be obtained for each chord length along the wing. This required boom area as a function of the span wise chord length can be found in Figure 16.10.

From the required boom area, the required stiffener area can be calculated according to the formula for the boom area as given in Equation 16.9. Applying this formula to every required span wise boom area gives the needed span wise stiffener area. Then the maximum value from these stiffener areas is chosen as the the stiffener area which is to be used in the aircraft. The required stiffener area for each part on the wingspan can be seen in Figure 16.11. From this figure, it is obtained that the stiffener area will be 772 mm^2 for all stiffeners across the entire wingspan.

$$A_{stiffener} = B_A - \frac{t_d b}{6}(2 + \frac{\sigma_1}{\sigma_2}) \quad (16.9)$$

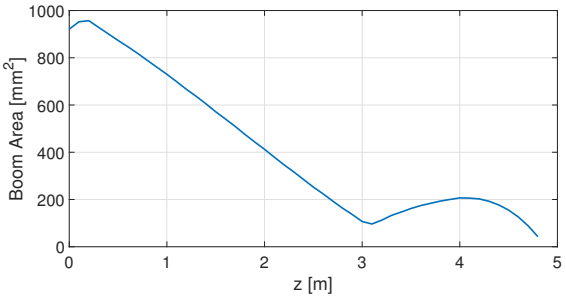

Figure 16.10: Required Boom Area along the wingspan

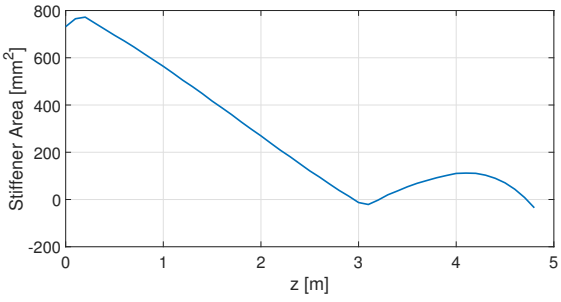

Figure 16.11: Required Stiffener Area along the wingspan

16.2.4. Verification

In order to verify the calculations, a finite element model is constructed with CATIA V5. This finite element model shows the stress through the wing box, as shown in Figure 16.12. The loads over the wing are derived from the aerodynamic loads computed in the Chapter 12 .This figure accurately verifies the previous calculations considering that the highest stresses occur near the root. If an even closer look is taken at Figure 16.12, it can be seen that at roughly 80% along the wingspan, a small bump in peak stress can be seen. This accurately verifies the results shown in Figure 16.11.

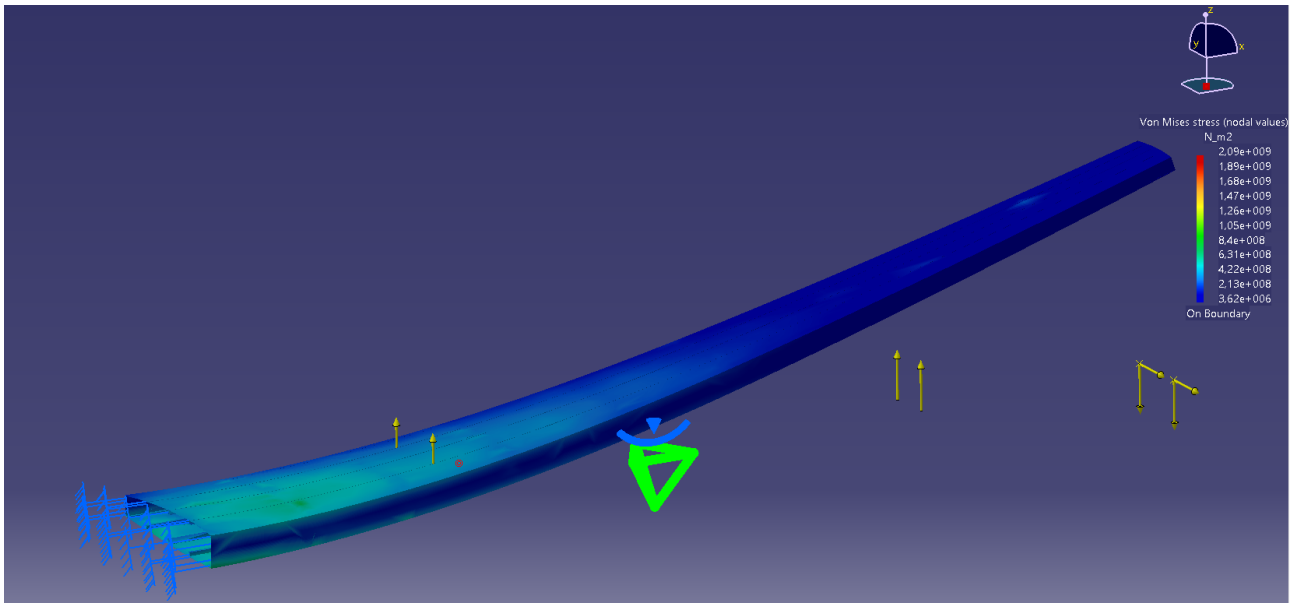

Figure 16.12: Finite Element Analysis for the wing box stress

16.2.5. Rib Spacing & Fuel Tank

The function of a rib is to carry loads from the skin to the spars and stringers, as well as to keep the shape of the airfoil. In order to suffice these rib requirements, a rib spacing of 50 cm was chosen based on reference aircraft.[2]

In order to obtain a fuel tank geometry, an analysis was made to check if the fuel tanks would fit into the wing box. The volume of the wing box was obtained through computer assisted design and turned out to be 0.5 m^3. The density of AVGAS 100LL was found to be 718 kg/m^3 [3]. Then with that density and the total fuel needed, the estimated fuel tank volume turned out to be 0.35 m^3. Which suffices the approximated wing box volume of 0.5 m^3.

16.3. Fuselage

The analysis of the fuselage was carried out in a similar way as for the wing box. The alternate steps taken are elaborated in the sections below.

[2]Cessna Maintenance Manual, accessed on 23-01-19,https://www.redskyventures.org/doc/cessna-maintenance-manuals/CessnaSingle_1996on_structural_repair_MM_SESR04.pdf

[3]SHELL AVGAS 100LL PISTON ENGINE AIRCRAFT FUEL, accessed on 22-01-19, https://www.shell.com.au/motorists/shell-fuels/sds-tds/_jcr_content/par/textimage_278c.stream/1519809888867/1fd2a443b48ce24dec1b995f7c5e6fd8e4f675f2c6923b0031e3e6eac4d1ee6a/avgas-100ll-pds.pdf

16.3.1. Loads

The ultimate load case of 4.4 during the positive stall is again used for computing the loads over the fuselage. The weights of every component of the aircraft contributing to the MTOW is accounted for and modelled as an equally distributed load developed over the fuselage, in the x-direction. These weight loads evidently act in the opposite direction to the lift force due to the wing.

Unlike the wing box, the fuselage is not hinged onto a surface. Therefore, to solve the statically in-determinant problem, the fuselage loads are solved by separating the design into two different sections from the center of gravity. A cut is made at the point of center of gravity and the two sides are solved individually. The results are then appended to one another to define the overall loads on the fuselage. The bending moment and shear loading diagrams are determined and can be seen in the Figure 16.13 Figure 16.14 respectively. The maximum bending loads on the fuselage is seen where the lift is acting (approximately). Also, the shear force changes its sign at that very point when the forces go from negative to positive force.

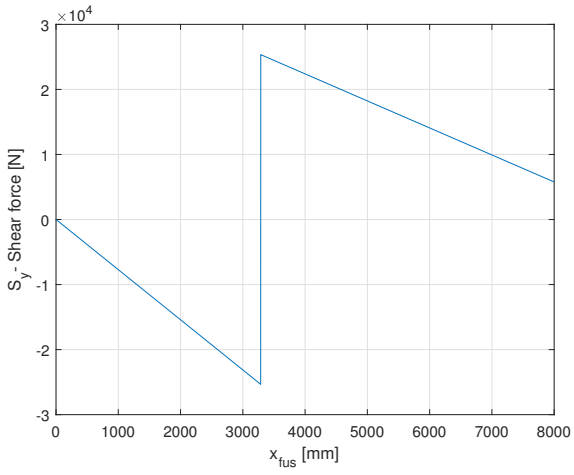

Figure 16.13: Shear force in negative y direction along the fuselage

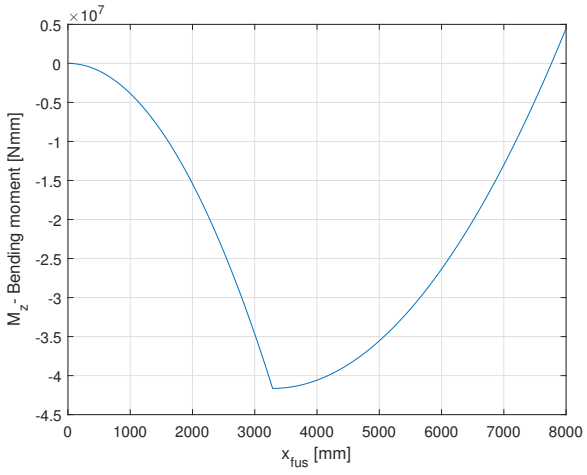

Figure 16.14: Bending moment along the fuselage

16.3.2. Idealization of the Fuselage & Assumptions

With the obtained loading diagrams the fuselage was then divided discreetly into 8000 cross-sections along the x-axis by taking steps of 1 mm starting from the nose of the fuselage to the tail. The fuselage is divided in 3 different parts, the nose, the cabin and the tail. In order to analyze the stress distribution along the fuselage, the cross sections were idealized according to the boom method. Stringers and parts of skin were represented as point masses called booms, each having an area, a moment of inertia represented by a Steiner term and a mass. Having defined the geometry of the entire fuselage and of each cross-section, the following assumptions were made to carry out the calculations for the stresses:

- The fuselage shape was simplified into 3 sections, nose cone and tail cone with the appropriate respective dimensions, and a thin cuboid for the cabin.
- Square cross-sectional fuselage is considered instead of curved edges.

- Each section is assumed symmetric in x- and y- directions.
- Boom areas and skin thickness are assumed constant in each cross section.
- Booms are evenly spaced around the cross sections, in a symmetrical manner as seen.
- Only a vertical resultant shear force and bending moment along z-axis is assumed to be acting at the centroid of every cross section along the fuselage.
- Any other loads over the structure is assumed to be negligible.
- Cut-outs are neglected while computing the stresses.

These assumptions were made to simplify the calculations and were assumed not to affect the results to a significant extent.

16.3.3. Stress Analysis

The course of analyzing the stresses, allow to understand the effects that aerodynamic loads have over the structures. The positioning and the amount of stress at a section, ultimately helps to design the components that support the structures. The stringers and the skin thickness is analyzed from this process. After multiple iterations, an optimum design is culminated. A brief description of the process is given below.

At every cross section along the fuselage, the shear and normal stress analysis was performed. The different loads and the different dimension of the fuselage in every section resulted in varying distributed stresses. Although the stresses would be spread out, for simplification, a constant thickness of the skin was assumed. Also, the stringer size was assumed to be constant [35].

It was first necessary to calculate the second moment of inertia for every cross-section. Since, they are symmetric and only have a vertical shear force and bending moment along the z-axis acting at the centroid, only I_{zz} needed to be considered. It was calculated with the following formula Equation 16.10 [35] where "i" denotes the boom number, y the distance between the boom and the centroid of that particular cross section, and A the area of the boom.

$$I_{xx} = \sum_{n=1}^{20} A(i) * y(i)^2 \tag{16.10}$$

The next step was to calculate the shear flow along the cross-section walls. According to the idealization of, a cut was made between boom 3 and 4, at the horizontal location where the shear force passes through the shear centre. It is known that the maximum shear stress in the cross section is on the centroid of the side walls and the minimum on the bottom and top walls when the shear force is acting vertically in the cross-section [36]. Therefore, the cut is made where the minimum stress would be found. Since, the total shear flow at the position where load acts is equal to zero and the loads act at the centroid, meaning no shear flow due to torsion will have to be added in the subsequent calculations. Using the following formula Equation 16.11[35], the base shear flow is calculated from boom to boom

in every cross section along the walls of every 8000 cross sections. The calculated maximum shear flow (horizontal to centroid) for every cross-section was then divided by the thickness of the skin to obtain the maximum shear stress. This will be further used to analyze the Von Mises stresses.

$$q_{s_i} = -\frac{S_y}{I_{zz}} \cdot A(i) \cdot y(i) + q_{s_{i-1}} \tag{16.11}$$

For the normal stresses, the bending moment around the z-axis was considered. The formula for normal stress is defined by Equation 16.12. According to which, the maximum normal stress would be at the farthest away from the centroid in the vertical direction (due to y). Naturally the minimum would be horizontal to the centroid. The maximum normal bending stress for each cross-section was calculated for each cross-section.

$$\sigma_x = \frac{M_z}{I_{zz}} \cdot y \tag{16.12}$$

Once the maximum shear and normal stress distribution was found at every cross-section along the entire fuselage, the yield stress was estimated at every location with the Von Mises criterion Equation 16.8.

16.3.4. Frames

The frames along the fuselage is designed to maintain the shape of the fuselage and carry a certain amount of loads from the skin. Its function is very much similar to ribs in the wing box. Furthermore, the positioning of the ribs were considered from a reference aircraft and the positioning of the doors, windows and tail positions.

16.3.5. Results

The maximum shear flow is found to be located exactly in the middle of the vertical flanges while the minimum (equal to zero) is located at the mid point of the horizontal flanges where the cut was made. For the normal stress due to bending, the minimum stress is located at the mid point of the vertical flange of the fuselage and the maximum is experienced on the top and bottom flanges. The top flanges however develops tension and the bottom compression. This is due to the moment M_z acting on the centroid in the positive z direction. Since these results only apply to the idealization that was assumed at the beginning of the section, the following observations can be made:

- No cut outs sections are introduced at the location where windows, doors and junctions should be present. These cut outs would affect the stress distribution along certain panels and would very likely be linked to the highest stress concentrations, for example at window edges and door flanges.
- The boom area is constant. This is not efficient and the stringer area should be optimized by increasing at locations of high stresses and decreasing at locations of minimal stresses. Similar with the skin thickness
- The loads acting on the fuselage are culminated and assumed to be a constant distributed loads, which creates a undisturbed stress flow calculation, however, with proper weight distribution, accurate stress analysis can be generated and eventually a complex design of stringers and skin could be obtained.

Finally, the boom areas were iterated to satisfy the Von mises criterion to achieve the most efficient values for the structure. The final structural components can be seen in the Figure 16.15.

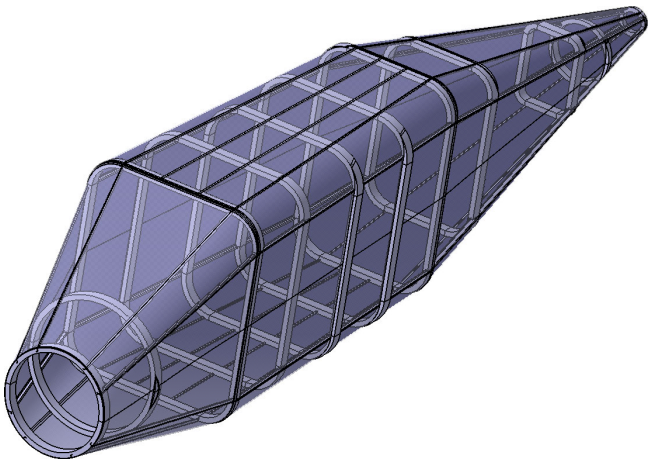

Figure 16.15: Skeleton of structural components of fuselage.

17

Cost Analysis

This chapter will be divided to give the development cost (Section 17.1 and operational cost (Section 17.2 for three different materials. Throughout this section different models will be used to calculate the cost for three different types of configuration with regards to the material. These being an aircraft which has a body consisting of composites versus aluminum. Or as a third option, a fuselage that consist out of aluminum and a composite wing. To account for the different types of materials the OEW has been adjusted to account for the difference in density between the composite choice of fiberglass/epoxy and the aluminum choice of 6061 T-6.

17.1. Development Cost

The development cost analysis was performed with the use of the DAPCA-IV (development and procurement cost of aircraft) method, developed by the RAND corporation as described by Gudmundsson [22]. This method estimates the costs for engineering, tooling, manufacturing labor and material, development support and flight testing aspect of the aircraft development process. This is done using statistical relations based only on basic information such as *OEW* and maximum airspeed. Finally, the DAPCA-IV model estimates the amount of units that have to be produced to break even. To account for the different type of material, the DAPCA-IV model introduces a composite factor in the cost respective cost relations.

The DAPCA-IV method first establishes a relation for the number of man-hours for different aspects of the development process. These are; engineering, tooling, and manufacturing man-hours. The relations for these values are based on structural aspects in addition to the complexity and type of certification of the aircraft as given in Table 17.1. The number of man-hours are then multiplied with the respective labor rates for each category. These rates were taken from the DAPCA-IV model with an adjustment for inflation.

Table 17.1: Man-Labor hours per single produced aircraft

Man-Labor	Hour rates ($/Hr)	Aluminium (hrs)	Aluminium body Composite wing (hrs)	Composite (hrs)
Engineering	102	283	292	356
Tooling	68	246	255	315
Manufacturing	59	2043	2117	2645

The accumulated cost of the engineering and tooling in addition to the cost of flight testing and development cost is attributed as the total cost to certify. This is then added to the cost of the manufacturing labor, quality control, and materials/equipment. These values are found in table Table 17.2.

Table 17.2: Development cost in the thousands USD for a single unit

Cost analysis	Aluminium	Aluminium body Composite wing	Composite
Certification	109	112	136
Manufacturing	280	290	363
Quality control	36.4	39.3	70.8
Material	28.5	27.4	19

Next the cost of the external components are added. These are the components that are purchased from other manufacturers and consist of the avionics, power train and landing gear. The Cirrus SR22 was used as a reference for the avionics. Based on estimations received from an air taxi company named Fly Aeolus that employs these types of aircraft, the used avionics had a cost price of 70,000 USD. The power train cost distribution can be found in Table 10.2. For the cost of the external components the DAPCA-IV model introduces an external quality discount factor (QDT). This factor adjusts the price based on an experience effectiveness adjustment factor. Meaning that due to a learning curve the total number of units produced can be doubled with a drop in price. This is assuming that the external components are purchased in bulk. This QDT is added since the DAPCA-IV model is based on a 5 year development frame. These values are shown in table Table 17.3.

Table 17.3: External components cost analysis in the thousands USD

Cost analysis	Without QDF	With QDF
Fixed landing gear discount	-7.5	-7.1
Power train	150.2	63.1
Avionics	70	29.4

Based on the production of 300 units in 5 years, a complete cost analysis is presented in Table 17.5. Assuming a liability insurance factor of twelve percent suggested by the DAPCA-IV model to simulate the aircraft market in the USA, a minimum selling price per unit is estimated. Additionally the DAPCA-IV model estimates the required units to break even by dividing the certification cost by the subtraction of the minimum selling price with the variable cost of producing one unit.

Table 17.4: Break even analysis in the thousands USD

Cost analysis	Aluminium	Aluminium body composite wing	Composite
Total cost to produce	665.5	680.9	800.6
Manufacturers liability insurance	61.8	63.7	78.1
minimum selling price	727.4	744.7	878.7
Units to breakeven in 5 years	199	199	199

In graph Figure 17.1 the fixed plus variable cost are compared to prices from reference aircraft. This is done to give a overview of the amount of units it would take to break even if the price of the reference aircraft was considered. With the current price set by the liability insurance factor of 12 percent the amount of units to break even is 170. Thus in terms of development cost the innovative hybrid model is competitive in the currently defined market.

Table 17.5: Reference aircraft selling price used in break even analysis

	Price USD
Cessna 206	665000
Cirrus Sr22	862900
Tecnam P2006	597000
Piper PA46	917000

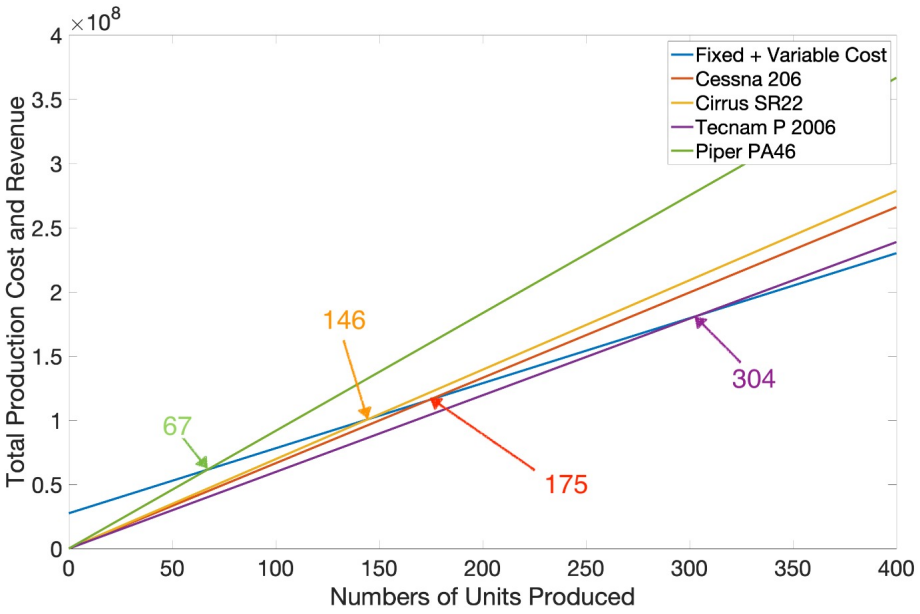

Figure 17.1: Break-even analysis for certification and manufacturing with prices of reference aircraft

17.2. Operational Cost

The operating cost is computed using the methodology described by Stoll and Veble Mikić [37]. This method includes relations for advanced concepts such as a hybrid aircraft. Relations that were found to be applicable to the hybrid configuration were taken from the RAND-IV model since this is a more elaborate method.

The operational cost is the sum of the costs for battery overhaul, electricity, engine overhaul, fuel, depreciation aircraft, crew, maintenance, interest, insurance and landing fees. The operational cost will take into account a average flight time per year of 1906 hrs. This was based on the required mission profile [1] and assuming the aircraft completes one operation every day of the year.

The fuel type that is used to run the primary engines will be Avgas. Based on global fuel index the price of Avgas fuel per gallon is 5.41 $ gallon [3]. A minimum of 0.10 $ KW-hr was considered for the cost of electricity and 250 USD per KW-hr battery pack overhaul cost for every 1000 cycles [1]. The aircraft depreciation, cost of pilot and landing fees are assumed from the article by Stoll and Veble Mikić [37].

The power train consists of an electrical and fuel driven component. For the electrical part, the battery overhual cost is a representation of the complete electrical cost. For the tip mounted fuel engines an overhual cost was calculated through the DAPCA-IV model. For the maintenance cost of the aircraft there is a difference in cost based on the type

[3] Jet fuel index muni, accessed on 23-01-19, `https://www.indexmundi.com/commodities/?commodity=jet-fuel`

of material. As can be seen in table Table 17.6 there is a difference in maintenance cost for the type of material choices. A complete composite aircraft will fare better in regards to corrosion and fatigue, which will come as a benefit in the cost of maintenance. The Stoll model gives a relation for advanced concepts. A full composite body is assumed to be a advanced concept in comparison to a full metal body.

The cost of depreciation is the highest for the composite model as this is a direct relation between the aircraft price and the depreciation period[37] which is the same logic applied to the insurance and interest rates.

The cost of the aluminum aircraft is the highest compared the other material configurations. This is due to the higher weight that is associated with the aluminum material. However this operational cost is well below the cost tabulated for the Cirrus Sr22 as given in the market analysis Chapter 7 being about 350 USD. Additionally, this operating cost approximation was presented to a the air taxi company Flight Aeoles who believed the cost to be competitive in the European market.

Table 17.6: Operational cost in USD per hour

Operational cost	Aluminium ($)	Aluminium body composite wing ($)	Composite ($)
Battery Overhaul	2.7	2.7	2.7
Electricity	1.21	1.21	1.21
Engine Overhaul	20	20	20
Fuel	31	28	21
Depreciation	24	24	29
Interest	22	23	27
Pilot	42	42	42
Maintenance	120	105	115
Insurance	4.6	4.4	5.6
Landing	13.27	12.76	7.33
Cost /hr	282	275	262

As was explained in Chapter 16, both aluminum and carbon/epoxy adhere to the structural needs imposed on the aircraft. The deciding factor on the use of material then came down to the cost. With regards to the cost analysis seen in table Table 17.5, to break even in 5 years would take the same amount of units for all three material configurations. However looking at the cost to produce an aircraft unit differs by a hundred thousands USD. This is a significant amount considering the little return that is seen in the operational cost for the composite aircraft. In order to remain competitive with the current air taxi market, as explained in the Chapter 7, the choice is to go with the aluminum material for the entire aircraft due to the low development cost.

17.3. Sensitivity study

A sensitivity study is conducted on the leading input variables of the cost analysis to give an overview of how the final outputs are affected. A 10 percent decrease is considered for airspeed and flight time as well as switching from 4 passengers to 5 passengers. Looking at the change in parameters in table Table 17.7, the most significance change comes in the change of payload. This result is in line with the big cost difference between the three material configurations. Weight seems to be the leading parameter in this design and should be considered in a future redesign. The operational cost gives a suspiciously small change. When validating the resulting cost values with reference aircraft,

the operating cost is similar. However, with this sensitivity check, an additional cost estimation method should be considered since this is an innovative hybrid model.

Table 17.7: Sensitivity analysis parameters

	Development Cost	**operational cost**
$\mathbf{V_{Cruise}}$	-5%	-1%
Flight time	-	2%
Payload	10%	3%

18

Aircraft Production and Operations

This chapter will discuss the production and operation of the aircraft. Section 18.1 elaborates on the manufacturing, assembly and integration of the aircraft and its components. Next, Section 18.2 will discuss how throughout the design phase, special attention has been given to reliability, availability, maintainability and safety to ensure that were not overlooked. Following on from this, Section 18.3 will discuss what group support is necessary at an airfield in order to be able to operate the aircraft at that airfield.

18.1. Manufacturing, Assembly, Integration Plan

In order to produce the aircraft sub-components and assemble them into a finished product, a "modular assembly line" will be used. This production system is similar to the fishbone assembly line system where the main structure will be moving along a predetermined path and have components added to its initial structure until the aircraft is complete. However, in the modular production system, employees work in cell-like structures, with tooling and machinery specific to their station and sub-component. Only the product moves through the assembly line, the cells are specialized in one specific task and repeat it as many times as needed. This is done to maximize efficiency by reducing "learning-time" and increasing customization and flexibility in design as changes can be done at module / cell level.

The main sub-components that will be linked to the main assembly line and structure will be the following 7 : fuselage, wings, powerplant, landing gear, empennage, nose/cockpit, interior and seating. These would follow a "just in time" process which increases efficiency and decreases waste when considering the assembly of large complex and expensive products. It also reduces the risk of ordering too many parts than necessary at a time and having to rent additional facilities for storage. Taking example on the Boeing 777 production process in Figure 18.1. The following diagram in figure Figure 18.1 shows the main assembly line and its sub-assemblies in a U-shaped layout.

One main facility will be used for the moving assembly of the aircraft and the storing of parts. Most sub-assemblies will be produced on-site however certain components such as engines, landing gears, wings and empennage will have to be processed in other more specialized facilities and brought to the main assembly line through specialized transport. In order to maintain the whole structure's stability and safety during the moving assembly while maintaining accuracy in its positioning, a multitude of jigs, fixtures and tugs will be used to support the employees in their work.

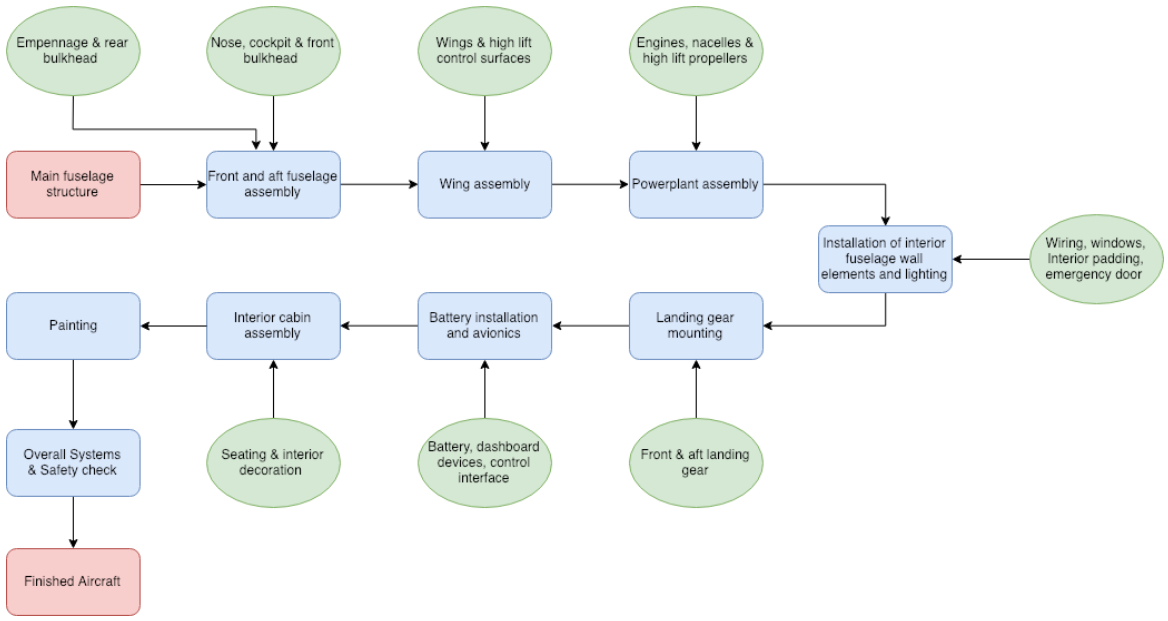

Figure 18.1: Assembly line diagram for the "Chauffeair" aircraft - Main processes (blue), sub assemblies (green), initial/final products (red)

18.2. Reliability, Availability, Maintainability and Safety Characteristics

The Reliability, Availability, Maintainability and Safety (RAMS) Characteristics is an extremely important factor that determines if an operator is willing to fly an aircraft. An aircraft with excellent RAMS characteristics will ensure that the design can function optimally and that the aircraft operating costs can be minimized. Considering that reliability, availability, maintainability and safety are all interconnected, these characteristics must be considered both individually as well as a group to determine how they impact each other. Even though the design of the aircraft is still in the preliminary phase, Subsection 18.2.1 to Subsection 18.2.4 will discuss how each characteristic is considered during the design process and operational life.

18.2.1. Reliability

The reliability of an aircraft is an important parameter to determine the operational profitability of an aircraft. Higher reliability will mean that the aircraft will not face as much (unexpected) down time when undergoing maintenance. Reliability flow diagrams will give insight into which subsystems are crucial to achieve the required functionality of the aircraft. Where necessary, redundancies should be implemented to ensure that the failure of a part or subsystem does not directly result in the plane becoming inoperable.

18.2.2. Maintainability

When it is easy to maintain an aircraft, it will have to spend less time being maintained. Hence, it can fly for more hours, meaning it is available to complete more revenue flights. This goes for both accounted and unaccounted maintenance which may be necessary throughout the aircraft's life cycle. Special attention should be given to avoiding unplanned maintenance as this is very expensive, considering the aircraft cannot operate its planned mission. The risk of having to complete unscheduled maintenance can be mitigated by scheduling frequent and thorough maintenance

checks. These could be planned when the aircraft is inoperable, e.g. throughout the night, to ensure that no valuable operational time is lost. Furthermore, the ease of maintenance and the aircraft maintainability as a whole should be considered throughout the whole design process. Significant attention should be given to this when placing and designing subsystems as well as the ability to inspect and repair certain parts without too much trouble. As an example, if a part has a low reliability or should be replaced frequently, it should be replaced with a different part which is more reliable, or be made easily accessible such that the maintenance does not take a long.

18.2.3. Availability

The availability of an aircraft is directly related to its reliability and maintainability. A reliable and easily maintainable aircraft will have a higher aircraft availability which is an important parameter to operational profitability [38]. Therefore, to increase the operational profitability, it is important to design for a reliable, maintainable aircraft and pay extra attention to this throughout the design phase.

18.2.4. Safety

Safety is a top priority within the aviation industry and therefore it is extremely important that the aircraft can and will operate safely throughout it's whole operational life. Operators will not be interested in an unsafe aircraft and hence top priority must be given to the safety aspect of the aircraft. All potential risks and hazards should be identified and mitigated and all crucial subsystems should be designed to be either fail safe of safe life. As an example, the actuators are designed to be fail safe. They are powered through the low voltage battery and should this battery fail, they will still receiver power to operate from the high voltage battery through the DC converter. Chapter 6 explains further how risks are identified and mitigated. Lastly, procedures shall be in place such that throughout the complete operational life, the aircraft will not operate in any unsafe condition. These procedures will be explained during the pilot training and will be explained in the flight manual in order to ensure that pilots are fully aware of the flight conditions that the aircraft is designed for.

18.3. Operations & Logistic Concept Description

As was mention in section Chapter 7, one of the main advantages of this aircraft it that is can fly to many small airfields where a larger aircraft cannot operate. Most small air fields will not have an extensive availability of group support equipment. As a result, the aircraft is designed in such a way that only a very small scale of ground support is necessary to ensure the operation. Much of the ground support that can be used, is not necessary. An overview of the ground support is shown in Figure 18.2, where a distinction is made between necessary ground support and optional ground support. As an example, a follow-me vehicle can be used to guide the aircraft to its designated parking space. It is not necessary however as the pilot can also navigate to the parking space himself. The same goes for the passenger shuttle which may be used to transport the passengers to the terminal, if there is a terminal at all. If a passenger shuttle is unavailable, the passengers can just walk to the aircraft. A maintenance vehicle or facility must also only be present if the aircraft must undergo maintenance. It is however crucial that fueling facilities are present as the aircraft needs

enough fuel to perform its next leg. It must be noted that both the AvGas should be refueled. Finally, a service vehicle is also optional as it is not necessary to clean the plane before its next leg which is why this is also considered optional.

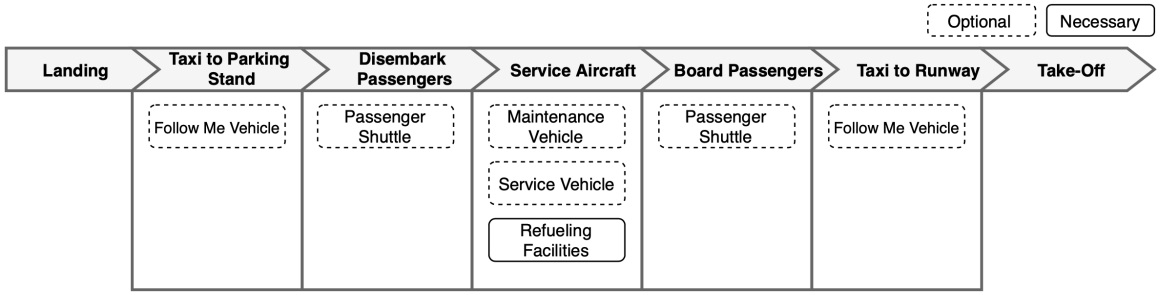

Figure 18.2: Operations Overview

19

Post-DSE Activities

The future steps for the team is planned out of the project. The development of the project after the DSE is completed is discussed in this chapter.

19.1. Project Design & Development Logic

The project design & development logic lays out the plan after the preliminary design of the aircraft is completed during DSE. Figure 19.1 illustrates this plan systematically from this design phase until the aircraft is in operation.

The first phase, illustrated in blue, shows the completion of the final design of the aircraft. This includes, for example, the detailed CAD drawings, securing funding from investors and arranging contracts for outsourcing parts of the production phase. The outsourcing would contain, among others, the internal combustion engine(s) and avionics. The production phase in illustrated in yellow and contains all associated activities like outsourcing and in-house production. Then, in parallel to, and in series with the production, the testing and certification takes place. Individual components and sections of the aircraft shall be tested in parallel with the rest of the production, whereas the full aircraft can only be tested and certified after the production phase is fully finished. This section is illustrated in green. Finally, when the detailed design, production and certification is finished, the deployment of the aircraft is set into action which is shown in red.

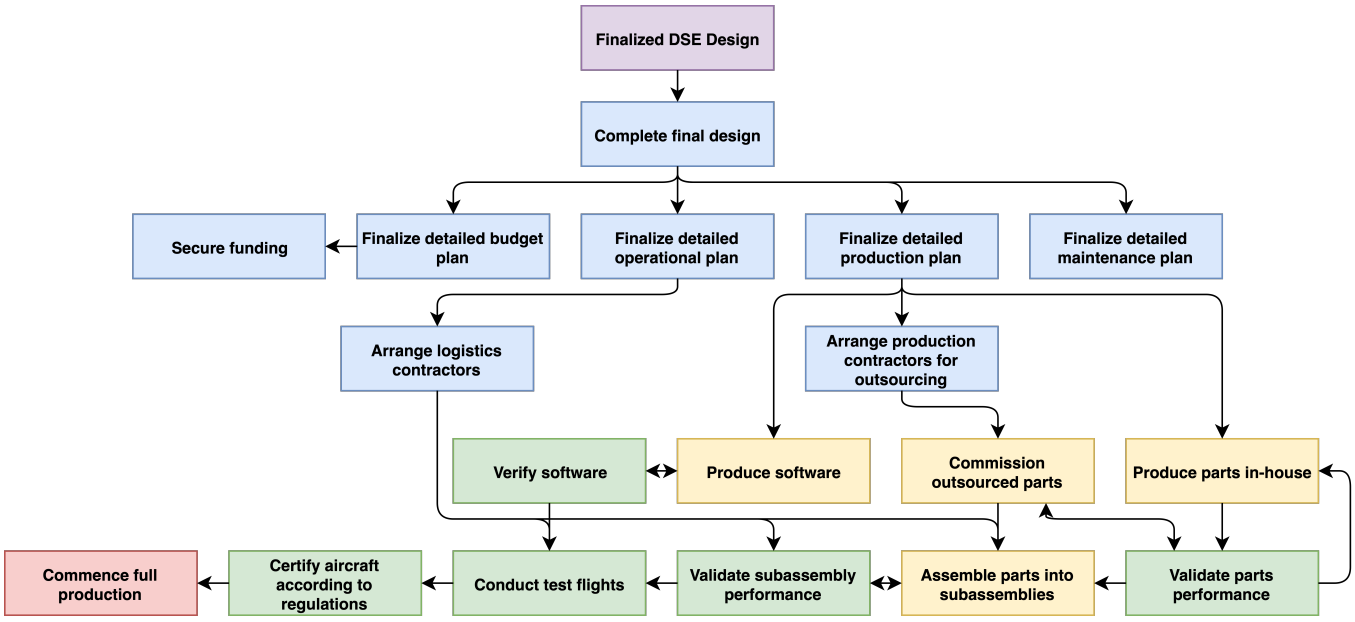

Figure 19.1: Design and development flowchart

19.2. Gantt Chart

In the Gantt chart shown in figure 19.2, the timeline for the rest of the project is shown. It shows the complete duration of the project from Preliminary Design to the provision of End-of-Life solutions for when an aircraft will be phased out at the end of their operational life. The phases shown in blue are part of the design phase, the phase in orange is the certification and production phase, the phases in green are the phases related to the operational life of the aircraft and the phases in brown is the phase linked with the end-of-life support and the end of the operational life of the aircraft. At this phase, it is unsure when these last three phases will end so hence no final year is shown.

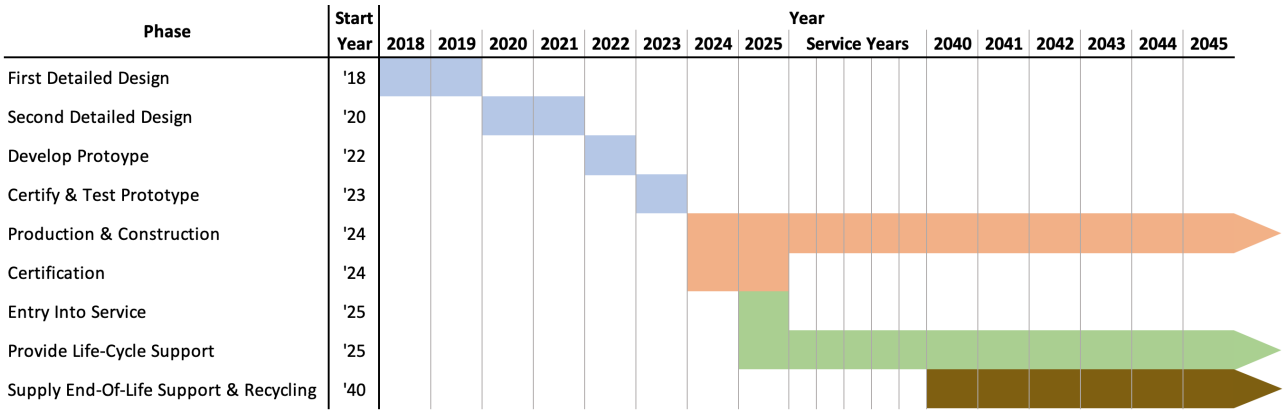

Figure 19.2: Post-DSE Gantt Chart

19.3. Recommendations

Recommendations for further analysis on subjects that were out of the scope at this stage should also be considered. Firstly on the two requirements that were not investigated, but also on subjects like noise by vibrations and component interaction, piloting the aircraft in poor visual conditions, the possibility of flying pilotless, a pressurized cabin and a more sophisticated cost analysis are interesting subjects for further investigation. For structures, a more elaborate analysis and designing must be carried out while designing for ribs, frames, cut-outs, longerons and other structural components of tails.

20

Compliance Matrix

Table 20.1: Compliance matrix

Requirement	Achieved	Notes		Achieved	Notes
THA-DES-GEN-01	✓		THA-REG-PER-01	✓	
THA-DES-GEN-02	✓		THA-REG-PER-02	✓	
THA-DES-GEN-03	✓		THA-REG-PER-03	✓	
THA-DES-GEN-04	✓		THA-REG-PER-04	×	Accelerated turning
THA-DES-GEN-05	✓				flight is not considered
THA-DES-SIZ-01	✓		THA-REG-PER-05	✓	
THA-DES-SIZ-02	✓		THA-REG-PER-06	✓	
THA-DES-REF-01	✓		THA-REG-PER-07	✓	
THA-DES-REF-02	✓		THA-REG-PWR-01	✓	
THA-DES-REF-03	✓		THA-REG-PWR-02	✓	
THA-CON-SAF-01	✓		THA-REG-PWR-03	✓	
THA-CON-CST-01	✓		THA-REG-PWR-04	✓	
THA-CON-LEG-01	✓		THA-REG-PWR-05	✓	
THA-CON-LEG-02	✓		THA-REG-DEC-01	✓	
THA-CON-SCH-01	***D***		THA-REG-DEC-02	✓	
THA-CON-SCH-02	***D***		THA-REG-DEC-03	✓	
THA-CON-RIS-01	✓		THA-REG-DEC-04	✓	
THA-CON-SUS-01	✓		THA-REG-DEC05	×	Aeroelasticity is not considered

Legend:

✓ = Requirement has been met.

× = Requirement has not been met.

D = Can only be shown through demonstrated flight.

21

Conclusion

The Chauffeair thin-haul hybrid aircraft and air taxi provides commuters with a convenient and quick way to get from A to B on low-volume routes or to hard-to-reach destinations, whilst allowing operators to fly at minimal operating costs.

After settling on a design lead by requirements and through technological and market analysis, a four passenger aircraft was designed with a range of 463km and an operating cost of 283USD per hour. The most prominent feature that distinct this aircraft from other aircraft is the hybrid powertrain configuration that enables the aircraft to be competitive in its market segment. Due to the multiple benefits of the parallel-serial hybrid powertrain offers, a 20% higher fuel efficiency is seen when compared to a similarly sized aircraft. The benefits that lead to this efficiency increase are best obtained if the propulsion divided is into a primary and secondary group.

The primary propulsion group consists of two pusher configurations with counter-rotating tip-mounted reciprocating engines. These propulsors decrease induced drag by rotating in opposite direction of the wing-tip vortices. The main benefit of the secondary propulsion group comes from allowing distributed propulsors to be mounted on the leading edge. This enables a higher L/D by increasing the dynamic pressure behind said propulsors. Combined with high lift devices in the airflow, this yields significantly increased lift during takeoff and landing operations, making a higher wing loading possible. Another benefit is the interaction between the primary and secondary propulsion group by gearbox-mounted motor-alternators. During takeoff and landing these devices are used to co-drive the primary propellers and thereby decreasing load on the reciprocating engines. This, in turn, is beneficial to noise, emissions and wear-and-tear on the primary engines during these operations. During cruise, these devices are used to charge the batteries of the secondary propulsion system. Alleviating the need of recharging at airfields, whilst maintaining the benefit of a higher efficiency.

Besides the innovative powertrain the aircraft boasts superior comfort due to favorable noise characteristics from the motors, as well as ample leg room in the cabin. The noise from the main engines, the biggest contributor to noise, is 69dBA during cruise and 85dBA during takeoff.

It is concluded that the aircraft satisfies all but two requirements, not necessarily because the aircraft would not be able to meet them, but because the two requirements were not investigated accurately. The two requirements in question are **THA-REG-PER-04** and **THA-REG-DEC-05** regarding flight performance and construction, respectively.

A

Work Distribution

	Technical	Reporting
Executive Summary		Thomas, Roel , Haroun, Sumant
Introduction		Ruben
Project Objectives		Olivier
Functional Logic Diagrams		
Functional Flow diagram	Roel, Ruben	Roel, Ruben
Functional Breakdown Structure	Roel, Ruben	Roel, Ruben
Requirement Analysis		
Mission Profile		Roel, Olivier
General Requirements		Roel, Olivier
Sub-System Requirements		Roel, Stan
Sustainability & Development Strategy		Ruben
Risk Assessment		
Risk	Terence, Ruben	Ruben
Risk Map	Ruben	Ruben
Risk Mitigation	Ruben	Ruben
Market Analysis		
Air Taxi Market Segmentation	Thomas,Terence	Thomas, Terence
Scheduled Thin-Haul & Air Taxi Vehicle Market	Thomas, Terence	Thomas, Terence
Future Market Prediction	Thomas, Terence	Thomas, Terence
Summary of Trade-Off		
Synopsis of Previous Trade-Off	Haroun	Haroun
Additions to the Design		Haroun
Design Code & Logic		
Design Code	Martin, Olivier, Pieter, Stan, Roel, Thomas	Martin
Sensivity Analysis	Terence, Martin	Martin
Design Point Selection	Martin	Martin
Parameter Summary		Roel
Powertrain		
Primary Propulsion Group	Olivier	Olivier
Secondary Propulsion Group	Olivier	Olivier
Non-Propelling Group	Olivier	Olivier
Power Requirement	Olivier	Olivier
Powertrain Components	Olivier	Olivier
Safety Measures	Olivier	Olivier
Noise and Environmental Characteristics	Olivier, Ruben	Olivier, Ruben
Retractable Propellers	Stan	Stan
Aircraft Hardware & Software Architecture		
Hardware Architecture	Olivier	Olivier
Software Architecture	Olivier	Olivier
Electrical Architecture	Olivier	Olivier
Data Handling Diagram	Ruben	Ruben
Communication Flow Diagram	Ruben	Ruben

Aerodynamic Analysis		
Airfoil Selection	Robel, Stan	Robel, Stan
3D Aerodynamics Model	Robel, Stan	Robel
Drag Estimation	Robel, Stan, Olivier	Robel, Stan
High Lift Devices	Pieter, Roel	Roel, Stan
Performance Analysis		
Payload Range Diagram	Pieter, Roel, Martin	Roel, Martin
Flight Envelope	Roel, Martin	Roel, Martin
Velocities	Roel	Roel
Take-off and Landing	Roel, Ruben	Roel
Climb & Descent	Roel	Roel
Turning	Roel	Roel
Reference & Sizing Mission Analysis	Roel	Roel
Performance Summary	Roel, Ruben	Roel
Performance Verification & Validation	Thomas, Roel	Roel
Control & Stability		
Control Surface Actuation	Olivier	Olivier
Aileron Design	Haroun	Haroun
Horizontal Tail	Martin, Sumant	Martin, Sumant
Landing Gear Position	Martin, Terence	Terence,Stan, Martin
Vertical Tail Sizing	Haroun	Haroun, Stan
Dynamic Stability	Martin, Ruben	Martin
Aircraft Geometry		
Internal Layout	Ruben,Stan	Ruben,Stan
3 Dimensional Aircraft	Stan	Stan
2D Drawings	Stan	Stan
Weight Breakdown	Stan, Martin	Stan, Martin
Weight and Balance	Roel	Roel
Structures		
Materials	Pieter, Terence	Pieter
Wing Box	Pieter, Roel	Pieter
Fuselage	Sumant, Haroun, Thomas	Sumant, Thomas, Stan
Verification	Sumant, Thomas	
Cost Analysis		
Development Cost	Terence, Robel	Terence
Operational Cost	Terence, Robel	Terence
Sensitivity Study	Terence	Terence
Aircraft Production & Operation		
Manufacturing, Assembly, Integration plan	Thomas, Ruben	Thomas, Ruben
Rams Characteristics	Ruben	Ruben
Operations and Logistic Concept Description	Olivier, Ruben	Olivier, Ruben
Post-DSE Activities		
Project Design and Development Logic		Olivier
Gannt Chart		Ruben
Recommendations		Olivier
Compliance Matrix		Haroun
Conclusion		Olivier

Bibliography

[1] Vos R. *Project Guide Design Synthesis Exercise: Design of a Thin-Haul Transport and Air Taxi.* Delft University of Technology, 2018.

[2] Group III Fall DSE 2018-2019. *Thin-Haul Transport Aircraft: Baseline Report.* Delft University of Technology, 2018.

[3] Group III Fall DSE 2018-2019. *Thin-Haul Transport Aircraft: Midterm Report.* Delft University of Technology, 2018.

[4] Group III Fall DSE 2018-2019. *Thin-Haul Transport Aircraft: Project Plan.* Delft University of Technology, 2018.

[5] Thurber M. *Pilot Report: M600, Piper's Best Performer.* Aviation International News Online, 2016.

[6] European Aviation Safety Agency. *Extra EA 400 Type-Certificate Data Sheet.* 2012. Online; Accessed on November 21, 2018.

[7] Beechcraft Berlin. *Bonanza G36 Product Analysis.* 2008.

[8] Columbia Aircraft. *Pilot's Operating Handbook and FAA Approved Airplane Flight Manual, Columbia 400.* 2007.

[9] De Vries R., Brown M., and Vos R. A Preliminary Sizing Method for Hybrid-Electric Aircraft Including Aero-Propulsive Interaction Effects. In *Aviation Technology, Integration, and Operations Conference*, Atlanta, GA, June 2018.

[10] Sinnige, T. *Aerodynamic and Aeroacoustic Interaction Effects for Tip-Mounted Propellers: An Experimental Study.* PhD thesis, Delft University of Technology, The Netherlands, 2018.

[11] Raymer D. P. *Aircraft Design: A Conceptual Approach.* AIAA, Washington, DC, 1989.

[12] Aircraft Thermal/Acoustic Insulation Materials Functions and Requirements. `https://www.fire.tc.faa.gov/pdf/insulate.pdf`. Online; accessed on (January 22, 2019).

[13] European Aviation Safety Agency. Design of a Hybrid-Electric Propulsion System for Light Aircraft, 2011. Online; accessed on (January 22, 2019).

[14] Litherland B. L., Patterson M. D., Derlaga J. M., and Borer N. K. A Method for Designing Conforming Folding Propellers. Hampton, VA, January 2019. NASA Langley Research Center.

[15] Sadraey M. *Aircraft Design: A Systems Engineering Approach.* John Wiley and Sons, Ltd., Chichester, West Sussex, UK, 2012.

[16] Patterson, M. D., and German B. J. Simplified Aerodynamics Models to Predict the Effects of Upstream Propellers on Wing Lift. In *53rd AIAA Aerospace Sciences Meeting*, Kissimmee, FL, January 2015.

[17] Miranda L. R., and Brennan J. E. Aerodynamic Effects of Wing-Tip Mounted Propellers and Turbines. In *4th Applied Aerodynamics Conference*, June 1986.

[18] Nootebos S. *Aerodynamic Analysis and Optimisation of Wingtip-Mounted Pusher Propellers.* Master's Thesis, Delft University of Technology, The Netherlands, 2018.

[19] Roskam J. *Airplane Design, Part VI: Preliminary Calculation of Aerodynamic Thrust and Power Characteristics.* DARcorporation, Lawrence, KS, 1987.

[20] Torenbeek E. *Synthesis of Subsonic Airplane Design.* Kluwer Academic Publisher, Norwell, MA, 1982.

[21] Ruijgrok G. J. J. *Elements of Airplane Performance.* Delft Academic Press, The Netherlands, 2009.

[22] Gudmundsson S. *General Aviation Aircraft Design.* Butterworth-Heinemann, Oxford, England, UK, 2014.

[23] Jayaram S. A New Fast Converging Kalman Filter for Sensor Fault Detection and Isolation. Vol. 30(No. 3), 2010.

[24] Falkena W. *Investigation of Practical Flight Control Systems for Small Aircraft.* Ph.D. Dissertation, Delft University of Technology, The Netherlands, 2012.

[25] Roskam J. *Airplane Design, Part V: Component Weight Estimation.* DARcorporation, Lawrence, KS, 1985.

[26] Roskam J. *Airplane Design, Part IV: Layout Design of Landing Gear and Systems.* DARcorporation, Lawrence, KS, 1986.

[27] Mulder J. A., Van Staveren W. H. J. J., Van der Vaart J. C., De Weerdt E., De Visser C. C., In 't Veld A. C., and Mooij E. Lecture Notes AE3202 Flight Dynamics, 2013.

[28] Roskam J. *Airplane Design, Part II: Preliminary Configuration Design and Integration of the Propulsion System.* DARcorporation, Lawrence, KS, 1985.

[29] Scholz D. Aircraft Design, 2015.

[30] La Rocca G. Requirement Analysis and Design Principles for A/C Stability and Control. 2018.

[31] Nicolosi F., Ciliberti D., Della Vecchia P., and Corcione S. Aerodynamic Design Guidelines of an Aircraft Dorsal Fin Through Numerical and Experimental Analyses. 2016.

[32] Nelson R. C. *Flight Stability and Automatic Control.* McGraw-Hill, New York, 2nd edition, 1998.

[33] Dassault Systèmes. Computer-Aided Three-Dimensional Interactive Application, CATIA V5.

[34] Verhagen W. *Materials Selection in Mechanical Design.* Butterworth-Heinemann, Oxford, England, UK, 4th edition, 2001.

[35] Megson T. H. G. *Aircraft Structures for Engineering Students.* Butterworth-Heinemann, Oxford, England, UK, 4th edition, 2007.

[36] Hibbeler R. C. *Mechanics of Materials.* Butterworth-Heinemann, Oxford, England, UK, 10th edition, 2014.

[37] Stoll, A., and Veble Mikić, G. Design Studies of Thin-Haul Commuter Aircraft with Distributed Electric Propulsion. In *Aviation Technology, Integration, and Operations Conference*, Washington, DC, June 2016.

[38] IATA. *Aircraft Operational Availability.* 2018.